Biophotonics Targeting Pharmaceutical Challenges

Focusing on photopharmaceutical and antimicrobial delivery studies

HANNA CAMILLE THOMSEN

UNIVERSITY OF GOTHENBURG

Department of Chemistry and Molecular Biology
University of Gothenburg
2018

DOCTORAL THESIS
Submitted for fulfilment of the requirements for the degree of Doctor of Philosophy in Biophysics

Biophotonics Targeting Pharmaceutical Challenges

Focusing on photopharmaceutical and antimicrobial delivery studies

HANNA CAMILLE THOMSEN

ISBN: 978-91-7833-055-3 [Print]

ISBN: 978-7833-056-0 [Electronic]
Available online at: http://hdl.handle.net/2077/56327

Cover Art:

Microscopy images of a *Staphylococcus epidermidis* biofilm incubated with a fluorescein-labelled γ-cyclodextrin (paper V). Images were taken to evaluate subcellular localization of the cyclodextrin compound within individual bacterial cells. Imaging performed with dual excitation wavelength and dual emission channels. Channels were assigned colors post-imaging (blue corresponds to cyclodextrin and pink corresponds to FM4-64 membrane staining of bacteria).

Biomedical Photonics Group

Department of Chemistry and Molecular Biology

University of Gothenburg

SE-412 96 Göteborg

Sweden

Printed by BrandFactory AB

Gothenburg, Sweden 2018

To mom.

Thank you for teaching me to see only opportunity.

Abstract

The study of the interaction between light and biological matter, called *biophotonics*, contributes to our understanding of biological systems - from subcellular compartments up to the human organ system. Herein, light is employed as a tool to understand delivery of novel photopharmaceutical and antimicrobial systems to bacteria, cells, and tissue.

The first part of this thesis (papers I and II) focuses on production of toxic species via photoactivation of a compound, both in cells and tissue, using two photon excitation (2PE). 2PE studies using near infrared excitation (NIR) afford deeper light penetrations depths in tissue. Novel methods for fluorescence reporting were developed to monitor penetration and localization of compounds, and *via* spectral signal from Förster resonance energy transfer (FRET) to monitor release in real-time.

Nanoparticles are becoming increasingly interesting as drug delivery systems. Multiphoton microscopy (MPM) and spectral analysis were used to evaluate particles for potential dermal drug delivery in paper III. Inherently luminescent silica particles revealed the size-dependent penetration of the particles in skin by combining *ex vivo* diffusion studies with 3D imaging and 2PE spectral detection and analysis.

The final part of this thesis (papers IV – VII) combines photoactivation with drug delivery systems to focus on the study and potential treatment of bacterial infections. Charge-functionalization of cyclodextrins (CDs) for optimal delivery to biofilms was evaluated. It was found that positively charged CDs better distribute in a *Staphylococcus epidermidis* biofilm environment. Eliminating biofilm cultures without the use of antibiotics is explored by applying phototherapy with NIR 2PE. It was demonstrated that curcumin, the active ingredient in turmeric, can be targeted to kill bacteria within 3D regions as small as 1 x 1 x 1 μm.

Taken together, this work developed biophotonics approaches for studying delivery of photopharmaceutics and antimicrobials to biological systems through application of MPM, spectral imaging, photoactivation, and development of model systems.

Keywords: Multiphoton microscopy, two photon excitation, super resolution microscopy, fluorescence imaging, drug delivery, nanoparticles, cyclodextrins, antibiotics, microbial biofilms, Staphylococcus, photodynamic inactivation

List of publications

The work presented in this thesis is based upon seven research articles, referred to as Paper I – VII:

Paper I	Confined photo-release of nitric oxide with simultaneous two-photon fluorescence tracking in a cellular system Hanna Thomsen, Nino Marino, Sabrina Conoci, Salvatore Sortino, and Marica B. Ericson *Scientific Reports* **8**, 9753 (2018)
Paper II	Monitoring the Release of a NO Photodonor from Polymer Nanoparticles via Förster Resonance Energy Transfer and Two-photon Fluorescence Imaging Claudia Conte, Aurore Fraix, Hanna Thomsen, Francesca Ungaro, Venera Cardile, Adriana C. E. Graziano, Marica B. Ericson, Fabiana Quaglia and Salvatore Sortino *Journal of Materials Chemistry B* **6,** 249-256 (2017).
Paper III	Nanoporous silica particles intercalate at stratum corneum – targeting transcutaneous drug delivery. Sabrina Valetti, Hanna Thomsen, Jitendra Wankar, Peter Falkman, Ilse Manet, Adam Feiler, Johan Engblom, and Marica B. Ericson *To be submitted to ACS Nano* (2018)
Paper IV	Delivery of cyclodextrin polymers to bacterial biofilms – An exploratory study using rhodamine labelled cyclodextrins and multiphoton microscopy Hanna Thomsen, Gabor Benkovics, Eva Fenyvesi, Anne Farewell, Milo Malanga, and Marica B. Ericson. *International Journal of Pharmaceutics* **531(2),** 650-657 (2017).
Paper V	Increased antibiotic efficacy and noninvasive diagnostic monitoring of biofilms by complexation with FITC—tagged cysteamine-substituted cyclodextrins Hanna Thomsen, Marco Agnes, Owens Uwangue, Fabrice E. Graf, Konstantina Yannakopoulou, Anne Farewell, and Marica B. Ericson *Manuscript* (2018)

Paper VI Spatially confined photoinactivation of bacteria towards novel treatment and mechanistic understanding of biofilm growth
Hanna Thomsen, Jeemol James, Anne Farewell, and Marica B. Ericson
Proc. SPIE Proc, **10498**, *1049825* (2018)

Paper VII Exploring photoinactivation of microbial biofilms using laser scanning microscopy and confined 2-photon excitation
Hanna Thomsen, Fabrice Graf, Anne Farwell, and Marica B. Ericson
Journal of Biophotonics, **doi: /10.1002/jbio.201800018** (2018)

Contribution report

The contributions by the author (HT) to the appended papers have been the following:

Paper I	Performed data presented in manuscript, analyzed data with MBE. Planned project with MBE based on the compound synthesis and previous paper by SS. Drafted manuscript together with MBE.
Paper II	Planned, performed, and analyzed skin penetration studies, performed 1PE and 2PE spectral data, and performed/analyzed imaging data. Collected images selected as part of the journal cover story.
Paper III	Performed and analyzed spectral and imaging data, performed MPM imaging with SV. Helped in writing spectral and MPM portion of manuscript together with MBE.
Paper IV	Designed and planned project together with MBE. Performed and analyzed spectral, biological, and imaging data. Compounds created by GB, MM, and EF. Drafted manuscript with MBE.
Paper V	Planned project together with AF, MBE, KY, and MA. Performed and analyzed spectral and imaging data. Drafted manuscript. Corresponding author.
Paper VI	Planned project, performed and analyzed spectral and imaging data. Wrote conference proceedings.
Paper VII	Planned project, performed and analyzed spectral, biological, and imaging data. Drafted manuscript. Corresponding author.

Publications not included in this thesis:

Electronic transition moments of 6-methyl isoxanthopterin-a fluorescent analogue of the nucleic acid base guanine
Julia R. Widom, Dmitrij Rappoport, Alejandro Perdomo-Ortiz, Hanna Thomsen, Neil P. Johnson, Peter H. von Hippel, Alan Aspuru-Guzik, and Andrew H. Marcus.
Nucleic Acids Res **41(2),** 995-1004 (2013)

Exploring plasmonic coupling as a stimuli responsive contrast mechanism in multiphoton microscopy
Marica B. Ericson, Hanna Thomsen, Jeemol James, Vladimir Kirejev, Daniel Aili, Antonio Vargas-Berenguel
Proc. SPIE Proc, **10509**, *1050907* (2018)

Optimizing Ti:Sapphire laser for quantitative biomedical imaging
Jeemol James, Hanna Thomsen, Dag Hanstorp, Felipe Ademir Aleman Hernandez, Sebastian Rothe, Jonas Enger, Marica B. Ericson
Proc. SPIE Proc, **10498**, *1049824* (2018)

Abbreviations

PDT	Photodynamic Therapy
MPM	Multiphoton Microscopy
NIR	Near-infrared
ISC	Intersystem Crossing
FRET	Förster Resonance Energy Transfer
BFP	Blue Fluorescent Protein
SYTO9	Green Fluorescent Nucleic Acid Stain
PI	Propidium Iodide
CLSM	Confocal laser scanning microscopy
2PE	Two-photon Excitation
TPA	Two-photon Absorption
1PE	One-photon Excitation
MPM	Multiphoton Microscopy
TPM	Two-photon Microscopy
NA	Numerical Aperture
SR-SIM	Super-resolution Structured Illumination Microscopy
PALM	Photoactivation localization microscopy
STED	Stimulated Emission Depletion
EPS	Extracellular Polymeric Substances
S. epidermidis	*Staphylococcus epidermidis*
IMD	Implanted Medical Device
PS	Photosensitizer
ROS	Reactive Oxygen Species
PDI	Photodynamic Inactivation
NO	Nitric Oxide
CD	Cyclodextrin
PBS	Phosphate Buffered Saline
TSB	Tryptic Soy Broth
CPA	Cupferron-anthracene (Paper I)
HPγCD	Hydroxypropyl-γ-cyclodextrin
UV	Ultra-violet
FITC	Fluorescein

Symbols

λ	Wavelength
μ	Micron
$h\nu$	Photon
S_1 / S_2	Singlet excited state
T_1	Triplet excited state
τ	Lifetime
r	Molecular distance
$k_{T(}r)$	Rate of energy transfer
R_0	Förster distance
F/FI	Fluorescence intensity
O_2	Molecular oxygen
$^1O_2$	Singlet oxygen
e^-	Electron
$HO^{\cdot}$	Hydroxyl radical
H_2O_2	Hydrogen peroxide
Ø	Diameter
M	Molar
J	Joules (energy dosage)
z	Depth location in a biological sample

Contents

Chapter 1. Introduction

1 Introduction

Light interaction with biological systems enables us to not only see within microscopically small organisms *i.e.* microscopy images of cells and bacteria, but also influence physiological mechanisms, and even treat disease through light application, such as the clinical treatment "photodynamic therapy (PDT)" [1, 2]. The beauty of light as a tool to image, characterize, and treat lies in the non-invasive nature of light itself *i.e.* near-infrared light (NIR) to image deeper into tissue and the high precision and spatial control of light delivery [3-5]. In this thesis, light interaction with biology was used to aid in the development of new pharmaceutics and novel treatment within the framework of a European research consortium. In the Marie Curie International Training Network (ITN), "CyclonHIT," my goal has been to characterize the photopharmaceutical compounds created by the network in biological systems, using non-invasive biophotonics analysis techniques.

The photodynamic process applied in light therapy is a wide-reaching treatment modality in which light sources are used to excite and promote release of toxic compounds from an external or endogenous photoactivatable compound with the goal of treating disease [6]. This is well documented for cells and tumors [7], although current translational methods face challenges from damaging light sources such as UV and blue-light irradiation, as well as difficulties in pharmaceutical delivery [8]. Phototherapy for treatment of antimicrobial resistant infections is also a growing field in itself; antimicrobial resistance has been named one of the most important health threats of the 21st century by the World Health Organization [9]. Photodynamic inactivation of bacteria (PDI) is an attractive approach for treatment due to the ability to use photoactivatable compounds to overcome systemic drug side effects, resistance development, and long-term treatment plans of traditional antibiotic approaches [10, 11] . Similar restrictions apply to PDI; delivery of pharmaceuticals and novel antimicrobial systems is not only an obstacle in drug design, but also difficult to monitor or measure in live systems.

The process by which photoactivatable and antimicrobial compounds are used for therapeutic treatments requires an understanding of the mechanistic process by which the compound reacts with its environment, *e.g.* where the compound localizes in the biological target (cells, bacteria, skin, etc), how it interacts with

the environment, and the mode of action or mechanism by which it acts as a toxic agent.

Herein, photoactivatable compounds, both novel [12, 13] and natural [14, 15] were investigated using techniques of biophotonics. Non-invasive bioimaging, using two photon excitation (2PE) and spectral analysis enabled penetration, localization, and activity studies of the compounds *in vitro* and in real-time.

The primary aim of this research was to develop and optimize light-based methods for studying photopharmaceuticals and new antimicrobial delivery systems, but the biological system being studied varies throughout the papers presented. The papers progress from studies in single cancer cells using already established PDT techniques (paper I), to multiphoton microscopy (MPM) imaging and spectral characterization within the more complex human skin system using novel luminescent and photoactivatable nanoparticles (papers II and III). In the final stages, PDT, MPM imaging, and spectral analysis were combined to present novel methods for understanding drug delivery in a complex 3D infectious bacterial system. Lastly, in paper VII, PDI techniques were applied to bacteria, and were shown to be effective using non-invasive NIR two photon excitation (2PE) against biofilms for the first time.

The structure of this thesis is as follows: chapter 2 introduces the background needed to understand the biophotonics techniques applied in this research (2.1); from the fundamental rules of fluorescence and photoactivation to the microscopy tools applied. Chapter 2 also introduces the three primary pharmaceutical challenges addressed (2.2) with a focus on the global problem of antibiotic resistance, and difficulties surrounding pharmaceutical development. In chapter 3 the scientific objectives of each paper are described by introducing the primary research question addressed. Chapter 4 establishes the methods used in papers I – VII. Following this, the highlights of each paper are presented in chapter 5, and chapter 6 and 7 give a brief conclusion of the primary findings of this work and an outlook on what more could be done in the future.

Chapter 2. Background

2 Background

2.1 Biophotonics

Light as a tool is an elegant, non-invasive option for scientific exploration of the nano- and microscopic-world. Exploitation of light for scientific research, photonics, applied to the study of biological systems, leads to the field of *biophotonics* [16]. This section covers fundamentals of light spectroscopy and microscopy and principles of light excitation for applied research and experimental treatments.

2.1.1 Photoexcitation and fluorescence

The process of photoexcitation and subsequent fluorescence emission is illustrated by the Jablonski diagram in figure 1. Fluorescence refers to the process by which certain molecules, fluorophores, absorb a photon of a specific energy from a lamp or laser light source, and go through a series of photochemical processes which in turn lead to emission of another photon of lower energy; this photon produces the fluorescent signal seen in spectroscopy or microscopy. Figure 1 demonstrates the molecular interactions onset by the absorption of photons, and different potential processes that can be taken by the molecule.

Upon absorption, the molecule enters an excited singlet electronic state (S_1 or S_2). This excited state exists for a finite period (referred to as the excited state lifetime, τ), then the fluorophore loses energy through internal conversion; conformational changes and interactions with the surrounding environment aid in this loss of energy and relaxation to the lowest vibrational energy state of the excited state of the fluorophore. At this point, a photon can be released producing a fluorescent signal [17].

Alternatively, the fluorophore can be quenched, a process in which the energy is lost through energy transfer, complex-formation, or collisions with other molecules or environment.

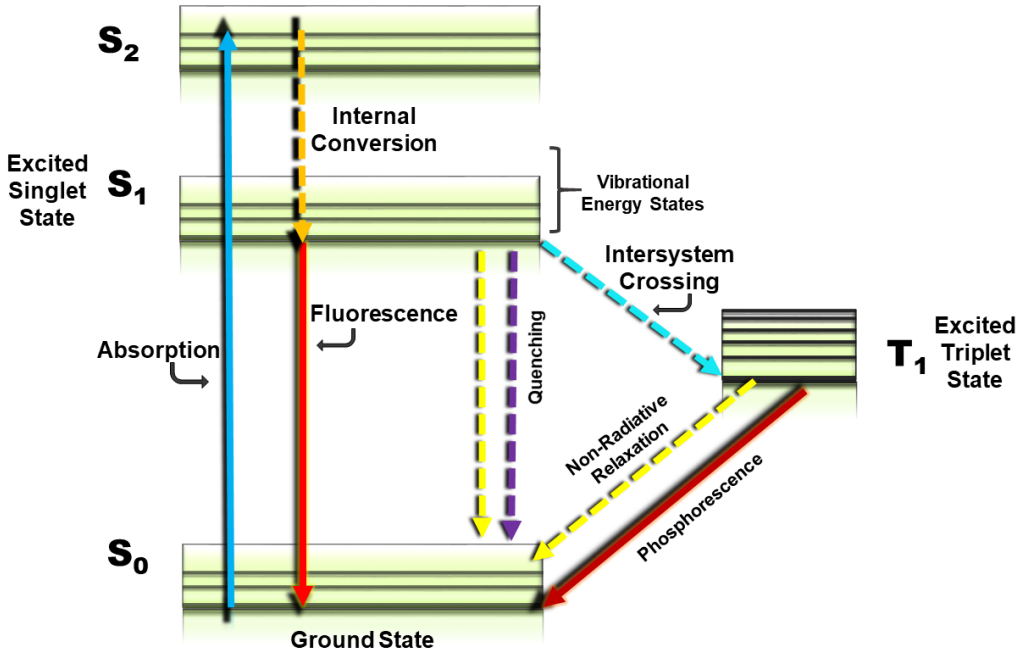

Figure 1. Jablonski diagram demonstrating the basics of fluorescence. A fluorophore enters an excited state after absorption of a photon. Energy is lost, as heat dissipation, through collisions with the environment. The molecule then relaxes back to the ground state, during which a photon is released as fluorescence emission.

An additional photochemical process that can occur instead of fluorescence emission, is that of intersystem crossing (ISC), considered "forbidden" by the laws of quantum mechanics. Although ISC does still occur, it is unfavoured. During this process the molecule transitions between the singlet excited state to the triplet excited state (T_1). From this excited triplet state, the molecule can go through non-radiative relaxation in which energy is lost through environmental interaction but no fluorescence signal is produced, or it can lose energy through phosphorescence. Phosphorescence is emission of light, through emission of a photon like fluorescence, but at a longer time scale. The increase in length of emission radiation is due to the unfavourable emission process from T_1 back to the singlet ground state, again through ISC [17].

In one photon excitation, the peak fluorescence emission will be at a longer wavelength than the peak fluorescence excitation, due to the stokes shift. The stokes shift refers to the energy difference between the two peaks; due to the energy of the excited state fluorophore that is dissipated as heat to the surrounding solvent molecules through collisions with the excited state fluorophore; this energy lost occurs during the lifetime of the excited state of the molecule as it enters S_1 (figure 2).

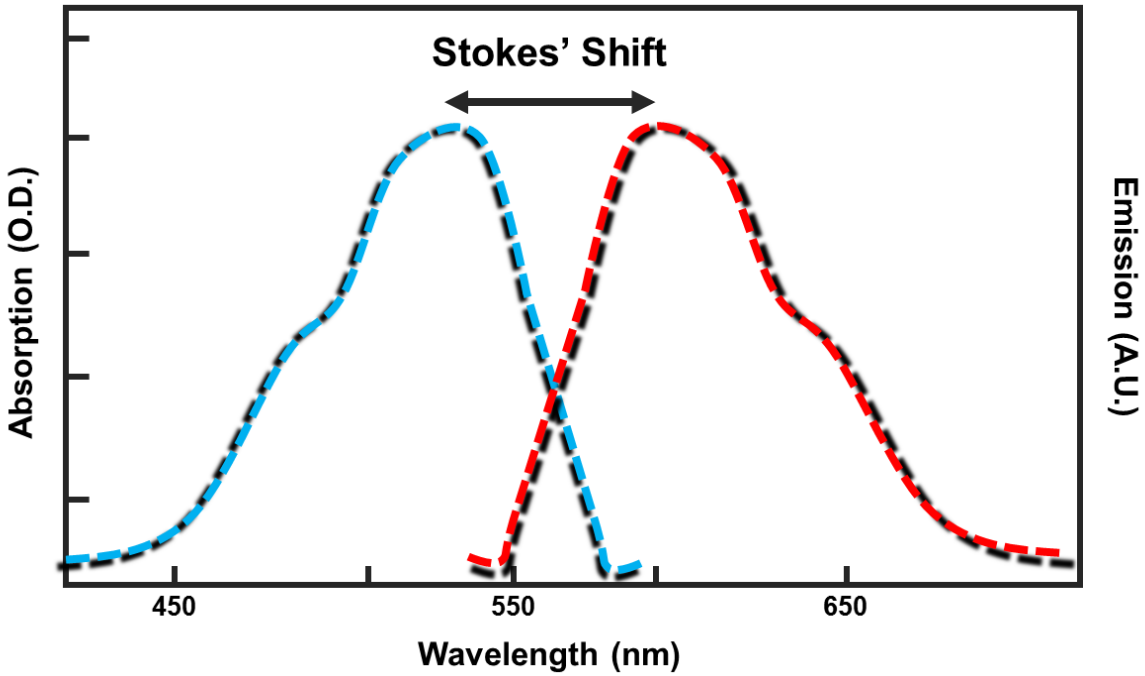

Figure 2. Upon absorption a fluorophore emits fluorescence emission at a longer wavelength due to the stokes shift, in which energy is lost during the excited state lifetime of the molecule. In one photon microscopy, emission will always be at a lower energy (longer wavelength) than excitation.

Not all molecules will return to a relaxed excited state and emit fluorescence; some can undergo processes such as quenching (in which fluorescence is not emitted due to an alternate transfer of the excited state energy), förster resonance energy transfer (FRET), in which energy will be transferred to another molecule (described in 2.1.6), or other energy processes.

Fluorescence is a principle theme in all work presented in this thesis; every project was based on the use of fluorescence emission from compounds – although capture, analysis, technique, and materials used for fluorescence signal vary from papers I-VII.

2.1.2 Fluorescent dyes

Many biological materials contain endogenous fluorescence, referred to as autofluorescence, in which biological structures naturally emit light due to absorbing properties of cell organelles, such as mitochondria and lysosomes. The most common molecules causing autofluorescence in cells are nicotinamide adenine dinucleotide phosphate (NADPH) and flavins, as well as fluorescent signal due to collagen and elastin in the extracellular matrix of cells [18, 19]. To visualize biological material that does not contain autofluorescent molecules, or does not have high enough natural emission to analyse spectral signal, an exogenous fluorescent dye can be added [20, 21].

Three primary types of fluorescent dyes are used in this research; (i) Organic dyes, employed for tracking of compounds in biological systems – anthracene, rhodamine, and fluorescein were chemically linked to molecules and tracked in cells, bacteria, and skin in papers I, II, IV, and V. (ii) Molecular probes, used as indicators of cell health or for staining of lipids and derivatives, in bacterial studies in papers V – VII and (iii) Biological fluorophores, including green fluorescent protein (GFP), blue fluorescent protein (BFP), and red fluorescent protein (dsRED), which can be used to modify bacteria to inherently express fluorescence [22, 23].

The primary molecular probes used in this research were nucleic acid stains SYTO9 and Propidium Iodide (PI) (papers IV- VII). These dyes provided viability staining of bacterial cultures. SYTO9 is a cell-permeant stain that increases in fluorescence upon binding to nucleic acids of intact, living cells. PI is not permeant to live cells so it is used to detect “dead” (membrane compromised) cells [24]. The use of SYTO9 and PI combined is often referred to as a “LIVE/DEAD” staining.

The lipophilic molecular probe FM4-64 was used in papers V- VII to selectively label the membrane of bacterial cells for detection of individual bacterial with high resolution microscopy. FM4-64 dyes are nontoxic to cells and non-fluorescent when in aqueous media. Upon insertion into the membrane they present a deep-red fluorescence (emission maximum = 734 nm) [25].

2.1.3 Laser scanning fluorescence microscopy

Fluorescence microscopy provides an approach for studying living and fixed cells with high sensitivity, unique labelling, and specificity [26]. By exploiting fluorescence properties of materials and biological samples, visualization and analysis of biological systems, such as cells and subcellular compartments, and dynamic events therein, can be understood [27, 28]. In laser scanning fluorescence microscopy, the sample is illuminated at a small focal volume and scanned point-by-point, enabling detection of 3D volumes at higher resolution, with less overall light damage to the biological sample [29].

Illustrated in figure 3 is a schematic diagram of a confocal laser scanning fluorescent microscope (CLSM). A laser excitation source is used for illumination with a specific wavelength and is sent through an illumination pinhole. This light then reflects from the surface of a dichroic mirror and passes through the microscope objective, and is scanned across the sample in a defined focal plane [30].

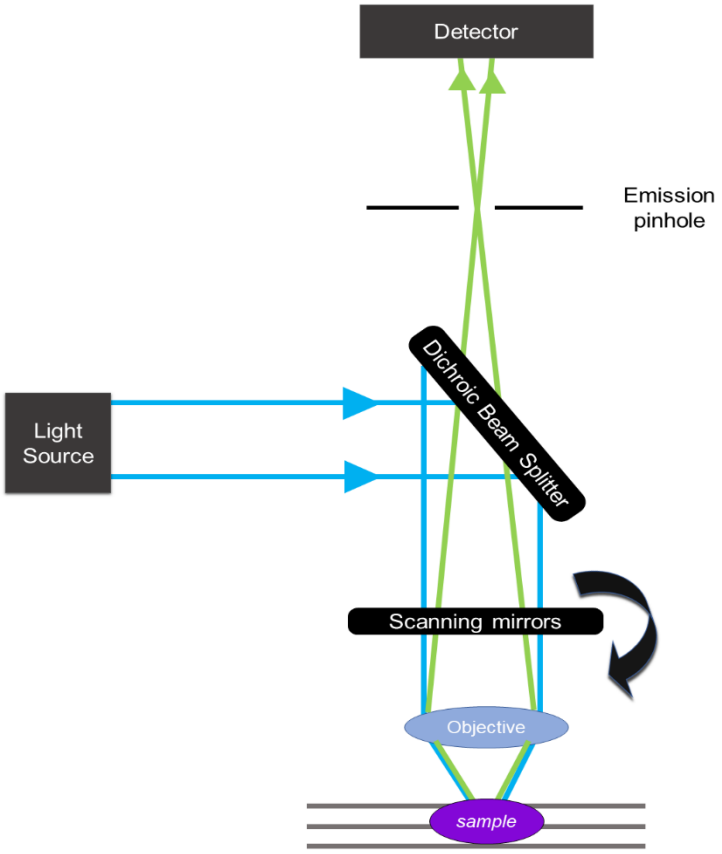

Figure 3. Schematic illustration of the fundamentals of a laser scanning confocal fluorescent microscope. Light emitted from the sample passes through a “pinhole” that blocks out-of-focus light, before being collected by the detector. Scanning of the excitation light across the sample enables collection of an image one point at a time. Redrawn from [30].

Fluorescence emission from the sample is collected by the microscope objective and passes through the dichroic mirror (the mirror works by reflecting the

excitation wavelength from the light source but transmitting the emission wavelength from the sample). The light emitted by points on the sample are focused as a confocal point at the detector pinhole aperture; the fluorescence emission that occurs above and below the focal plane is not confocal with the pinhole and thus not detected and does not contribute to the final image [31].

A photomultiplier tube, tuned for different fluorescent wavelengths, amplifies the signal detected and is then converted to a digital signal for further processing in the specific software used for the system.

Alternative to a CLSM, laser scanning fluorescence microscopy can be achieved without the use of excitation and emission pinhole apertures by employing a more focused excitation light point source, as will be described in the next section.

2.1.4 Multiphoton microscopy

Multiphoton microscopy (MPM) is a form of laser-scanning microscopy that uses a 'nonlinear' excitation process; in which the fluorescent signal produced is not linearly dependent on the intensity of incident light, in contrast to conventional optical imaging. In this research, two photon excitation / microscopy (2PE / 2PM) is primarily used for biological imaging so this section will focus on the fundamentals of 2PE, but it should be noted that other nonlinear imaging techniques are equally useful in this field, such as second harmonic generation (SHG), ideal for imaging collagen [32], or three photon excitation, which can image as deep at 700 μm into brain tissue [33].

2PE takes advantage of two-photon absorption (TPA) as first described by Maria Goeppert-Mayer in 1931 [34], in which two photons of light are absorbed with lower energy than what would be required to excite a molecule with one photon absorption, illustrated in figure 4. The energy of a photon is inversely proportional to its wavelength; the two photons absorbed in a singular event must have wavelengths double of that required for traditional one-photon excitation (1PE). Emitted light produced by TPA is higher in energy than the excitation light, thus the ability to excite fluorescence at higher energy using lower energy near-infrared (NIR) light enables laser microscopy at a less damaging and higher-penetrating optical window [4, 5, 35, 36].

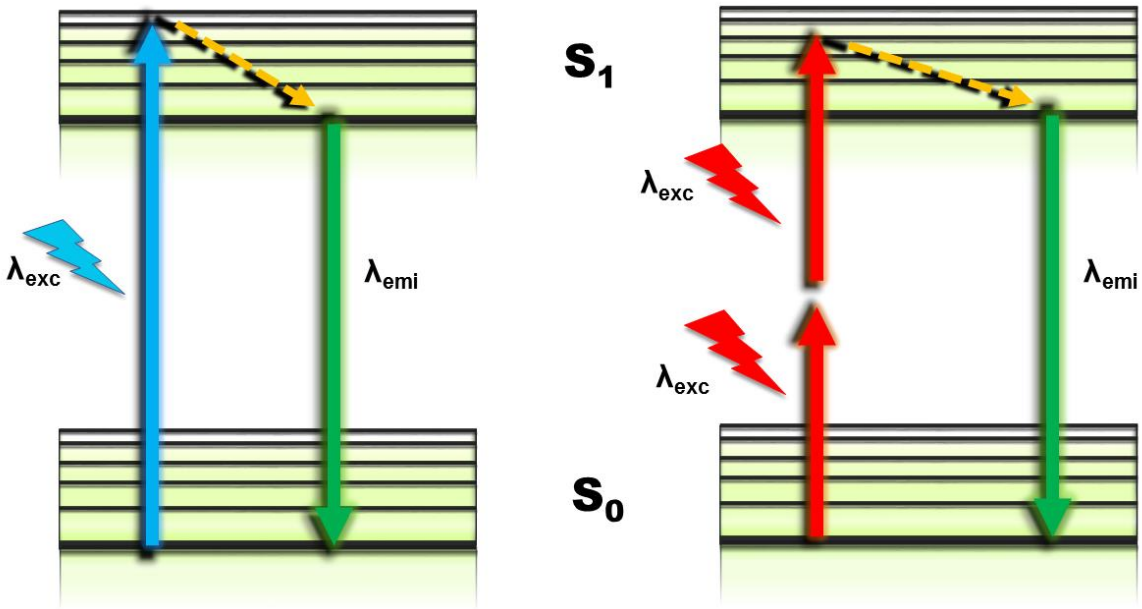

Figure 4. Jablonski diagram of one-photon (1PE) and two-photon excitation (2PE). 1PE occurs upon absorption of a single photon. 2PE requires that two photons of lower energy are absorbed through an intermediate state. A vibrational relaxation occurs from the higher energy level of the excited state to the lowest energy level prior to the fluorescence emission process. Fluorescence emission occurs at the same wavelength for both 1PE and 2PE.

MPM overcomes standard drawbacks of other traditional microscopy techniques such as photobleaching and phototoxicity [37], which at high laser power, is a problem in the imaging of live samples. Furthermore, MPM provides a significant advantage in the imaging of thick specimens, such as tissue, as excitation with NIR light enables further reach of the beam path due to reduced absorption of light and reduced scattering of excitation and emission photons [38].

2PE requires nearly simultaneous absorption of two photons. The probability of a TPA event is a quadratic function of the excitation intensity. Because of this quadratic relationship; 2PE occurs only at the focal point where the photon density is high enough for two photons to absorb in the same instant, thus producing localized excitation with no need of a pinhole to block background light. This can be seen illustrated in figure 5, where the primary differences in the optical setup of MPM versus confocal (as described in section 2.1.3) are shown.

To perform MPM, specific adjustments to a standard optical configuration are required. MPM requires the use of a mode-locked laser; pulses generated from this laser are at a higher power, which can produce the required photon density

for a 2PE [39]. Although overall, the average power output of the laser remains relatively low [40]. Objectives, used to focus the beam into the sample, with high numerical aperture (NA) are required for optimal collection efficiency; with water or oil immersion objectives being preferred [41].

MPM provides advantage in imaging of scattering biological samples due to the decreased absorption of longer wavelengths and reduced scattering of the sample,

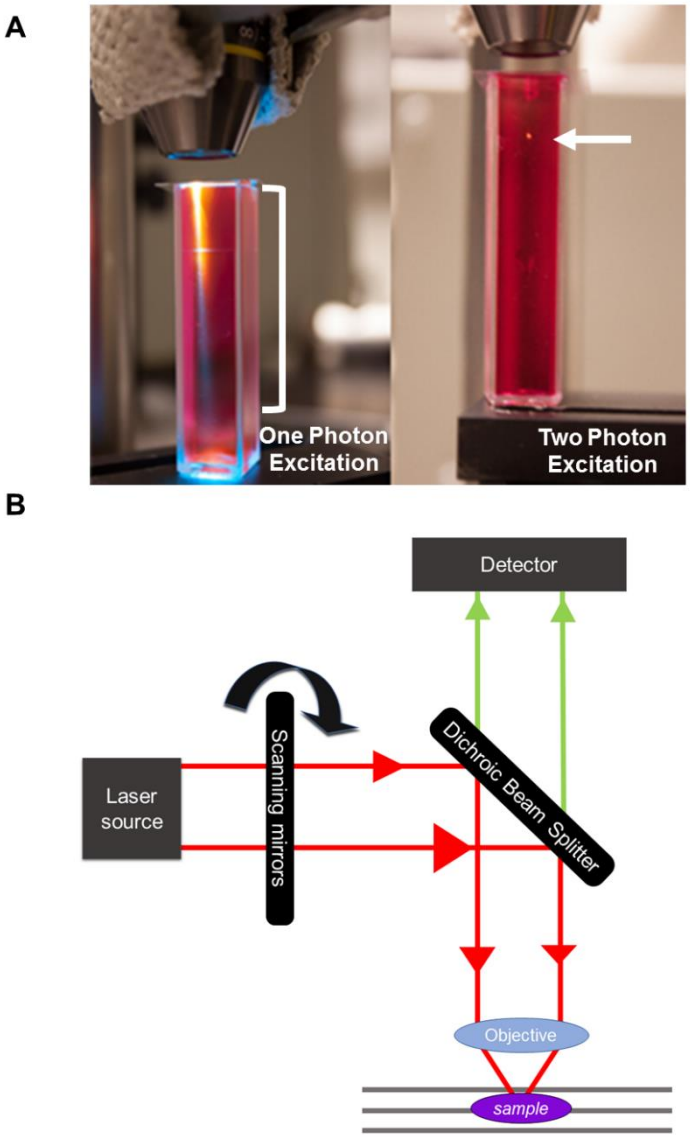

Figure 5. (A) One-photon vs two-photon excitation demonstrated by liquid solution in a quartz cuvette. Photos kindly provided by Johan Borglin. (B) Simplified illustration of the fundamental configuration of a multiphoton microscope.

as demonstrated by MPM images vs. wide-field images of bacterial biofilms in figure 6. Reduce absorption by biological materials such as water and blood leads to deeper penetration depths in tissue [42]; for example, MPM has been used to image skin up to 200 µm in depth [43]. This technique has become a valuable

tool in the life sciences and can be seen applied to a variety of other optically dense material, including bacterial communities [44-48].

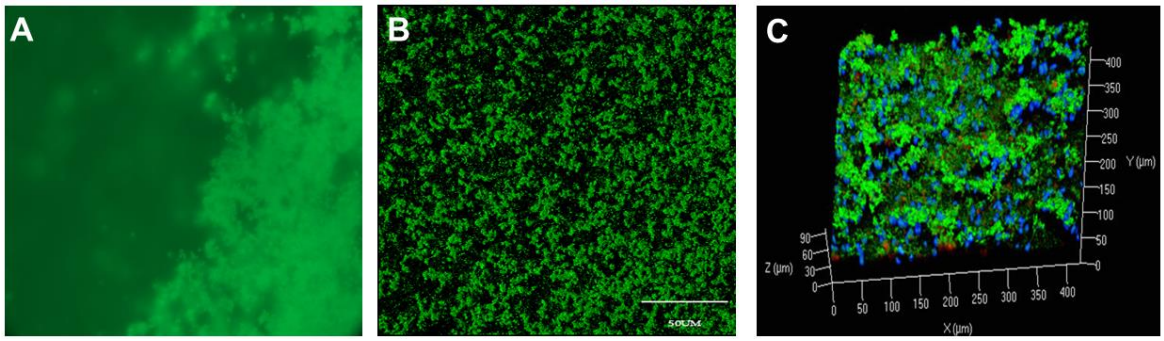

Figure 6. (A) Wide-field fluorescence microscopy image of SYTO9 stained *S. epidermidis* biofilm, (B) Two photon microscopy (TPM) image of SYTO9 stained *S. epidermidis* biofilm, collected in a 3D z-stack, z-slices reconstructed to show topological features from z view, (C) TPM image of SYTO9 stained *S. epidermidis* biofilm incubated with a blue-fluorescent nanoparticle, collected in 3D z-stack, z-slices reconstructed to 3D boxed image to visualize the entire structure of biofilm community.

2.1.5 Super resolution microscopy

Imaging of subcellular localization within bacteria requires better spatial resolution than what is achievable by standard microscopy. The standard resolution limit of fluorescence microscopy has been set by the diffraction-limited resolution theory by Ernst Abbe, shown below, where NA is the objective numerical aperture and λ is wavelength of illumination, restricts resolution at ideal conditions to approximately 200-300 nm [49].

$$\text{Abbe Resolution}_{x,y} = \lambda / 2NA$$

Super resolution microscopy is an umbrella term describing several new techniques that overcome the traditional diffraction barrier. Two techniques were explored in papers V-VII; super resolution structured illumination (SR-SIM) and Airyscan imaging (figure 7). These techniques were used to understand the subcellular localization of compounds within individual bacterial cells.

SR-SIM is a wide field technique in which a sinusoidal pattern of light is used to illuminate the sample; and Fourier transformations are used to transform information collected from imaging into mathematical functions which, through computation, can provide fine details in terms of frequencies. Further computation transforms these details to be visible in real space again, thus providing a super resolution image [50, 51]. This technique was used briefly using a commercial system with help from the Center for Cellular Imaging at Sahlgrenska Academy, but the technique itself was not explored in detail in this research. SR-SIM required longer imaging times and higher laser power than what was most suitable for the live biological samples used in this research, thus Airyscan imaging was used for the continuation of the work.

Although the Airyscan technique does not reach the same resolution as the other super resolution techniques (i.e. PALM, STED, refer to [52] for a thorough review) the subcellular localization of a compound in bacteria could be measured, *i.e.* the technique was robust enough for the scientific questions in papers V – VII. To describe the Airyscan technique requires a short background in collection methods of confocal microscopy:

In traditional confocal laser scanning microscopy, as described in section 2.1.3, a pinhole is placed to the image conjugated plan (figure 3 in 2.1.3); fluorescence emission light is sent through a pinhole, and the resultant diffraction pattern of the light is known as the “airy disk”, a bright central circular disk surrounded by rings with decreasing intensity at increasing distance (figure 7) [53].

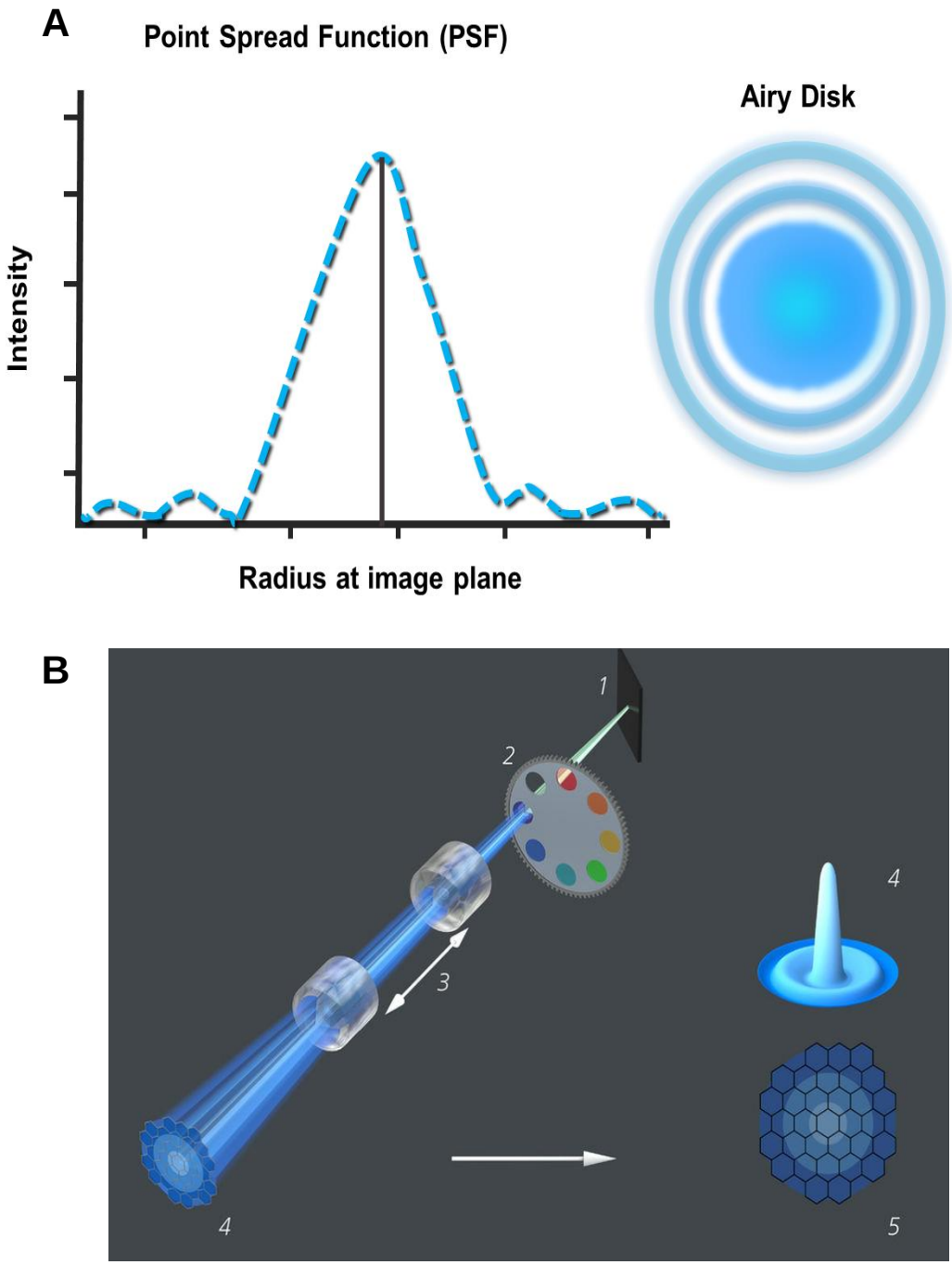

Figure 7. (A) The point spread function, the diffraction pattern of light emitted from a point source, shown as an intensity distribution relative to the radius of the concentric rings of the diffraction pattern when viewed in the x-y plane, shown by the "airy disk." (B) Illustration of the airyscan detection technique. The Airyscan detector array (5) is placed in a conjugate plane relative to the excitation spot, generated fluorescence is sent through an emission filter (2) and zoom optics (3) project a chosen number of airy unit (AU) orders; the resultant airy disk pattern (4) is projected onto the detector array where each of the detector elements acts as its own small pinhole with information of the point source position. Reprinted with permission from [54].

With the use of a pinhole, the most intense central point of the airy disk is detected while the lower intensity outer regions are rejected, thus out-of-focus light emitted from the sample will be rejected and not imaged.

A smaller pinhole results in higher resolution as the signal detected can be better localized to the point source emission (the fluorophore in the sample), but with a reduction in pinhole also comes a reduction in light detection efficiency, as less light will be collected through the pinhole. This leads to an increase in signal-to-noise ratio, thus poorer quality images. Using the Airyscan technique, the traditional pinhole in confocal microscopy is replaced with a concentrically-arranged hexagonal detector array consisting of 32 single detector elements each acting as a pinhole (figure 7). The confocal pinhole remains open so the entire airy disc is collected, while the signal collected by the individual detector elements is reconstructed (post-imaging) to produce an image [54].

2.1.6 Förster resonance energy transfer

Förster resonance energy transfer (FRET) is a process in which energy is transferred between a donor (D) molecule and an acceptor (A) molecule through non-radiative interaction. For FRET to occur, the emission spectrum of the donor molecule should overlap with the absorption spectrum of the acceptor molecule (figure 8), and D-A should be within a specific distance of each other. This distance is a distance known for specific FRET pairs of D-A, thus FRET signal can be used to calculate the distance between two known molecules [17]. The rate of FRET depends on the spectral overlap of D-A, quantum yield of the donor, and orientation of the D-A transition dipole. This technique has become valuable for the study of, for example, protein-protein interactions in cellular environments [55, 56].

An important distinction in understanding FRET is that there is no photon emission involved in the resonance energy transfer described. Theoretically, FRET relies on the concept that an oscillating dipole can undergo energy

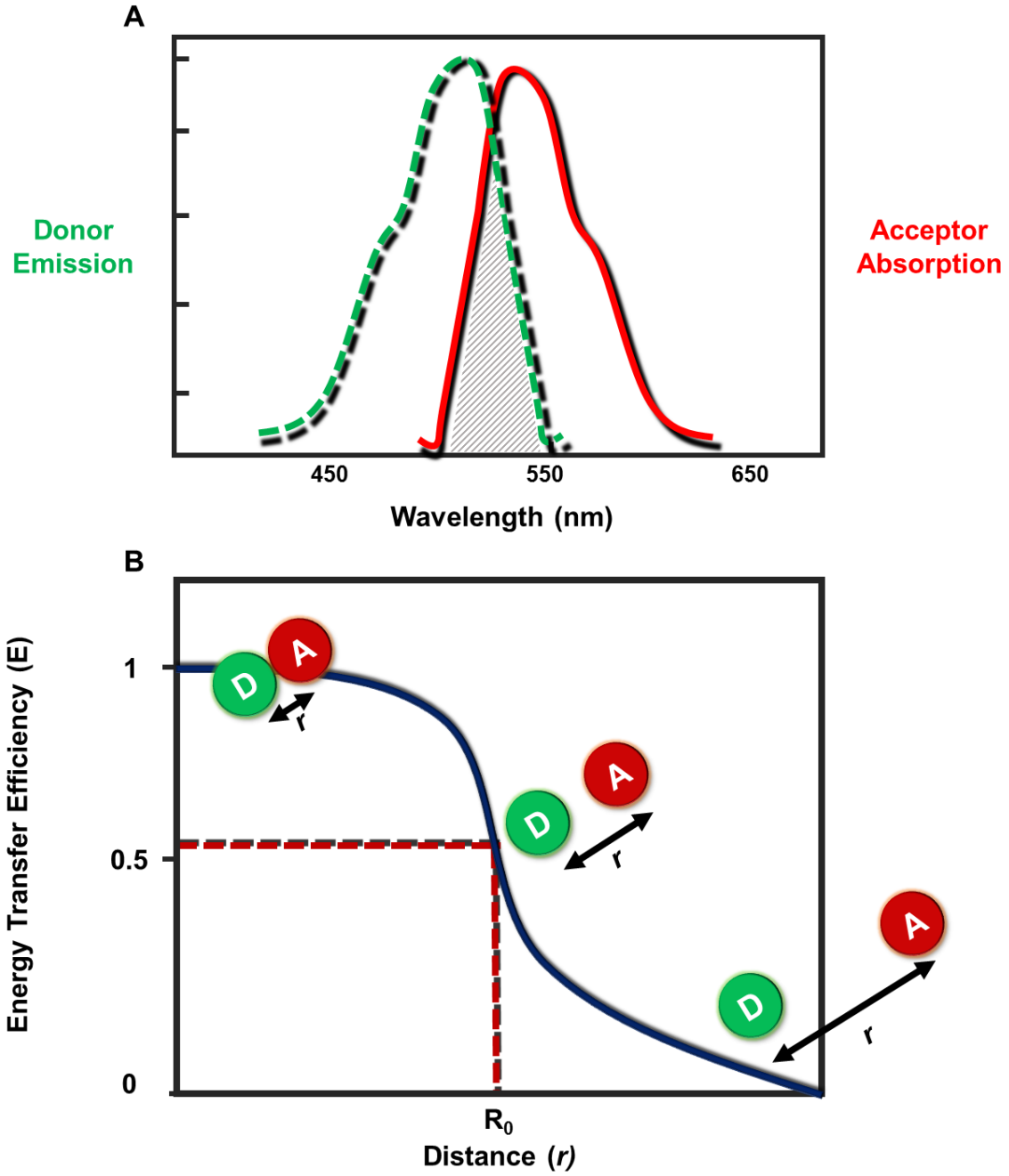

Figure 8. (A) A förster resonance energy transfer molecular pair (FRET) must have an overlap between donor emission and acceptor absorption spectra. (B) The energy transfer efficiency in a FRET process decreases with increasing distance between donor and acceptor molecule.

exchange with another dipole with similar resonance frequency, i.e. "coupled oscillators" [57].

In experimentation, FRET can be described in rate of energy transfer ($k_T(r)$), in which transfer rate is written as a function of the distance *r* between D-A, shown in equation 1.

$$k_T(r) = (1 / \tau_D) (R_0 / r)^6 \quad \text{(eqn 1)}$$

To calculate $k_T(r)$ with this equation the distance between D-A at which E_{FRET} is at 50%, R_0 ("Förster distance"), must be known, as well τ_D, the decay time of the donor in the absence of the acceptor.

As energy transfer rate depends on the decay rate of the donor, energy transfer will be efficient if the transfer rate is much faster than decay rate. The efficiency of energy transfer (E_{FRET}) is described by the fraction of photons absorbed by the donor that are transferred to the acceptor, given by equation 2.

$$E = k_T(r) / (\tau_D^{-1} + k_T(r)) \quad \text{(eqn 2)}$$

Combining equations 1 and 2 gives E_{FRET} and demonstrates the dependence of transfer efficiency on the distance of D-A when the distance is near R_0.

$$E = R_0^6 / (R_0^6 + r^6) \quad \text{(eqn 3)}$$

In the experimental settings in this research (paper II), the exact distance of D-A was not measured, rather transfer efficiency was observed to qualitatively assess whether D-A remained linked or had separated. In this case, relative fluorescence intensity of the donor in absence of the acceptor (F_D) and presence of acceptor (F_{DA}) could be used (equation 4).

$$E = 1 - (F_{DA} / F_D) \quad \text{(eqn 4)}$$

FRET signal by 2PE spectra and TPM imaging in human skin was performed in paper II.

2.2 Pharmaceutical challenges

In this section, the three major challenges in current medical research explored in this thesis are described: antimicrobial resistance, cancer and light therapy applied to skin cancer, and drug delivery to tissue.

2.2.1 Bacterial biofilms & antibiotic resistance

Antibiotic resistance has become a global concern; the US Centers for Disease Control and Prevention (CDC) have declared multiple resistant bacteria to be an urgent threat with the emergence of resistant bacteria being declared a "crisis" [58]; the World Health Organization has named antibiotic resistance one of the most important threats of the 21st century [9]. The work presented in this thesis was performed under the framework of a Marie Curie ITN project with the focus "*nanocarriers for the delivery of antimicrobial agents to fight resistance mechanisms*." My role was to develop and apply methods to characterize the compounds produced by the consortium, targeting antimicrobial resistance.

The field of antibiotic resistance mechanisms is a huge research field in itself; and although pertinent, is not addressed in this research. The reader is referred to literature sources for background of antibiotic resistance evolution and mechanisms [59-61].

This thesis focuses on visualization and drug delivery studies to *biofilms* – a bacterial mode of growth in which bacteria adhere to a surface and form a colony, rather than existing as planktonic (individual) cells (figure 9) [62].

Bacterial biofilm cultures exist in an aggregate format on the surface of wounds, catheters, medical implants, and throughout nature. Covered in a protective exopolysaccharide matrix, biofilms can survive through particularly harsh environmental conditions. Fluid channels and heterogeneity within the biofilm allow for flow of nutrients and protection of low-lying dormant "persister" cells to survive attack from antibiotic treatment [63-65].

Drug delivery to biofilms is a unique pharmaceutical challenge owing to the complex structural and physiological characteristics of a biofilm. The extracellular polymeric substances (EPS) produced by biofilms consists of compounds that can sequester external compounds, such as applied drugs [66, 67]. Deactivation of antibiotics in a biofilm can cause retarded penetration, as well as charged agents in the EPS and matrix, preventing the drug from reaching all bacteria, and this can differ between antibiotics and bacteria [68-70].

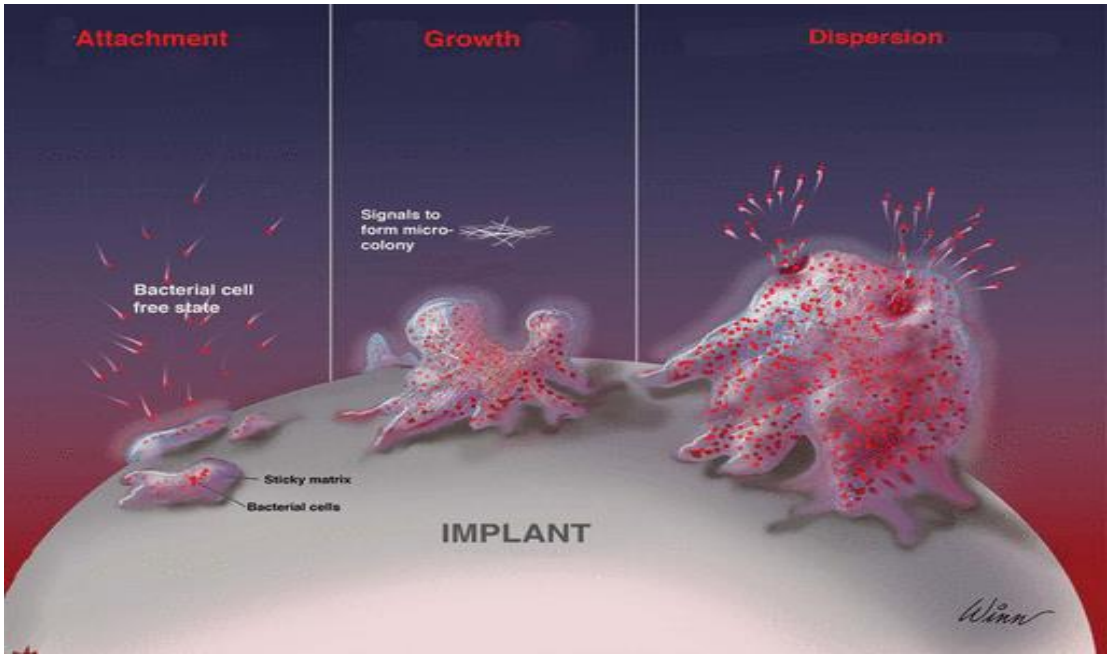

Figure 9. Biofilms form through adherence of bacteria and are a common cause of chronic infections. Bacteria first adhere to a surface via initial colonization through physical forces or appendages. Cell signaling mechanisms are used to stimulate production of the extracellular matrix. Mature biofilms consist of water and waste channels found throughout a heterogeneous and highly complicated structure in which bacteria can detach and return to planktonic form of growth. Image reprinted with permission from Centre for Biofilm Engineering.

Many clinically problematic biofilms are a result of growth on tissue and implanted medical devices (IMDs) caused by *Staphylococcus epidermidis* [71]. *S. epidermidis* can cause severe complications [72-74] and is often found as mature biofilms in skin wounds, ulcers, and burns as the bacterium itself is found naturally on human skin [75, 76]. *S. epidermidis* was the primary strain of bacteria explored in this research.

Visualization of biofilms presents a unique challenge; the heterogenous and 3D structure of biofilms represents layers of bacteria with varying metabolic activity, and thus varying interactions with drug compounds. Traditional microscopy does not provide the resolution, optical sectioning, or spectral detection needed to separate interactions within different depth of a biofilm (which can grow more than 100 µm in depth in the *in vitro* model used in this research). It is this complication in drug delivery studies to biofilms that is addressed through this work; novel methods for both analyzing drug delivery and potential experimental treatment are presented to address this gap in the field of biofilm research.

2.2.2 Photopharmaceutics

2.2.2.1 Photodynamic action

Photodynamic action refers to the induction of a light reaction with a compound, in which oxygen is consumed, causing a therapeutic effect in biological systems [77]. Essentially, upon application of light to a specific compound, photochemical processes occur in the compound which cause it to release reactive oxygen species (ROS), which are harmful to cells. This process is used in the treatment *photodynamic therapy* (PDT), a method of treatment in which a photosensitizer (PS) compound is applied to an effected area and a specific wavelength of light is used to selectively activate the compound to release ROS [7, 78, 79].

The general mechanism of photodynamic processes is shown in figure 10. Like the photoexcitation process described in 2.1.1, a photon of light is absorbed by the PS, exciting the compound to S_1 and T_1 *via* intersystem crossing. From T_1; the PS can react in two primary patterns; type I or type II PDT reactions. In type I reactions the excited PS interacts directly with the substrate to form radicals *via* transfer of a hydrogen atom to the triplet state PS. The radicals produced can immediately react with oxygen to form reactive oxygen intermediates toxic to biological species [80]. Alternatively, in a type II process T_1 interacts directly

with molecular oxygen to produce singlet oxygen[1] [81], which can go on to can damage or kill cells [79, 80]

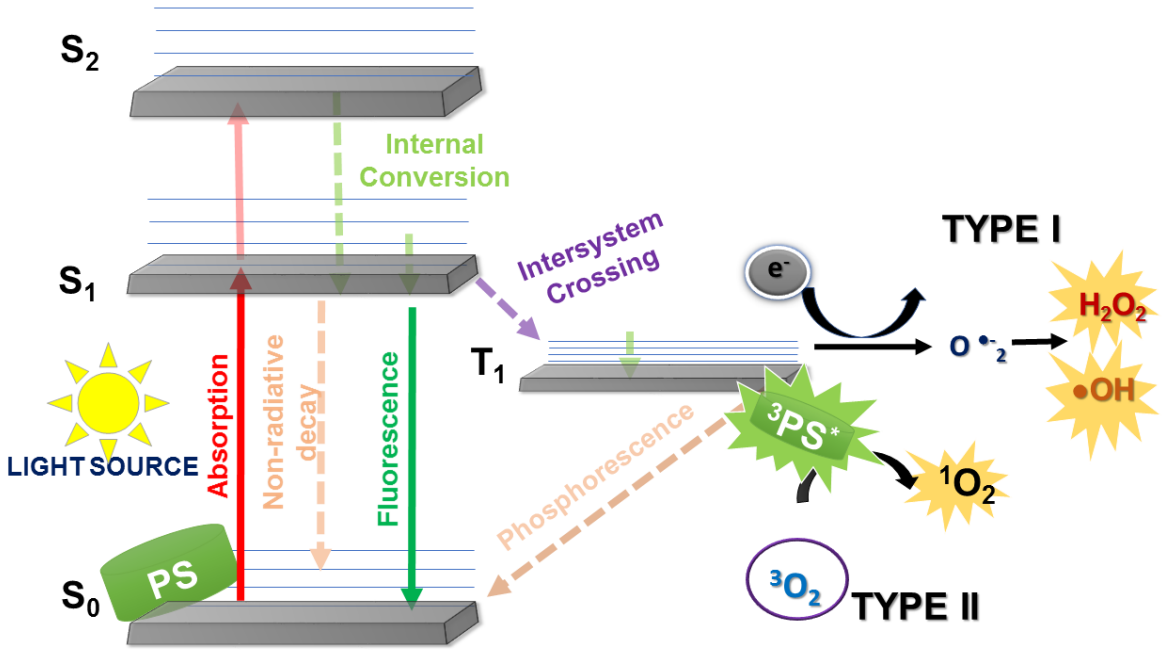

Figure 10. Schematic Jablonski diagram demonstrating the photodynamic therapy (PDT) processes. A photosensitizer (PS) absorbs a photon to be excited from the lower-energy ground state to the higher-energy singlet excited state. PS can lose energy by emitting a photon from the singlet excited state through fluorescence emission, or through non-radiative decay back to the ground state. Alternatively, as in a PDT process, the singlet state can be converted to a long-lived triplet excited state through intersystem crossing. The excited triplet state can interact with molecular oxygen to produce singlet oxygen (type II reaction) or can react with molecular oxygen by electron transfer to form superoxide radicals (type I reaction), which can go on to generate hydrogen peroxide and hydroxyl radicals.

In papers VI and VII, PDT protocol was adapted to test as a method for targeting bacterial cells within *S. epidermidis* biofilms. PDT for killing bacteria, termed *photodynamic inactivation* (PDI), has been shown to target multi-antibiotic resistant strains while avoiding development of resistance to the therapy [82].

A natural compound, curcumin, is used as the PS in these studies and is further described in the following section (2.2.2.2). Studies of curcumin have demonstrated useful anticancer, anti-inflammatory, and antibacterial effects with minimal toxicity using a biologically effective dose [83-85]. PDI with curcumin has been performed [86-91], but generally uses blue or white light, thus causing unnecessary tissue damage with limited light penetration.

[1] To describe this process in more detail requires a deviation from the aim of this thesis work, but the reader is referred to reference 81 for background on the mechanistic details of PDT reactions.

Curcumin-mediated PDI with 2PE allows for deeper tissue penetration and minimal tissue damage due to use of NIR light [92].

To date, PDI has been explored against planktonic and biofilm bacteria [10, 11, 89, 93], but has not been demonstrated with 2PE, nor has the distribution and interaction of PS in 3D biofilms (and subcellularly in single cell bacteria) been visualized. Papers VI and VII address these issues and aim to lay groundwork for further translational applications of non-invasive PDI using curcumin.

2.2.2.2 Photosensitizers

Photosensitizers (PS) used in PDT are non-toxic dyes that can undergo a type I or type II photodynamic process to produce toxic species targeting cells. The interaction of PS with cells in tissue is a key factor in effective PDT; understanding this biological interaction is critical when creating new PS or assessing a known PS for a new treatment [94, 95].

The first PS approved for clinical use, Photofrin, induces skin toxicity to the patient, lacks selectivity, and is excited by a lower wavelength (630 nm) thus less accessible in thick tissues. A wealth of new PS have been, and are continuously, being developed to address these major factors in successful PDT [96], but are often difficult to synthesize and have potentially high toxicity to humans. Natural compounds with minimal toxicity, excitable by NIR light, and producing fewer systemic side-effects are important to characterize for better PDT/PDI.

In this work, the natural compound curcumin was explored for use of PDI in a bacterial system (papers VI and VII). Curcumin is a natural dye, originating from the spice turmeric, with a broad absorption spectrum ranging from 300 – 550 nm with an excitation maximum at approximately 430 nm [97]. Curcumin has long been known for its interactive properties with biological material; and although active naturally at certain concentrations, toxicity of curcumin is enhanced by activation with light – thus leading to the use of curcumin as a PS in PDT/PDI studies [98, 99].

The exact photosensitization method by which curcumin acts has not been studied extensively but literature data has shown that curcumin takes multiple photochemical pathways; including production of singlet oxygen *via* interaction with molecular oxygen, as well as reduction of molecular oxygen to hydrogen peroxide and other radicals (figure 11) [99].

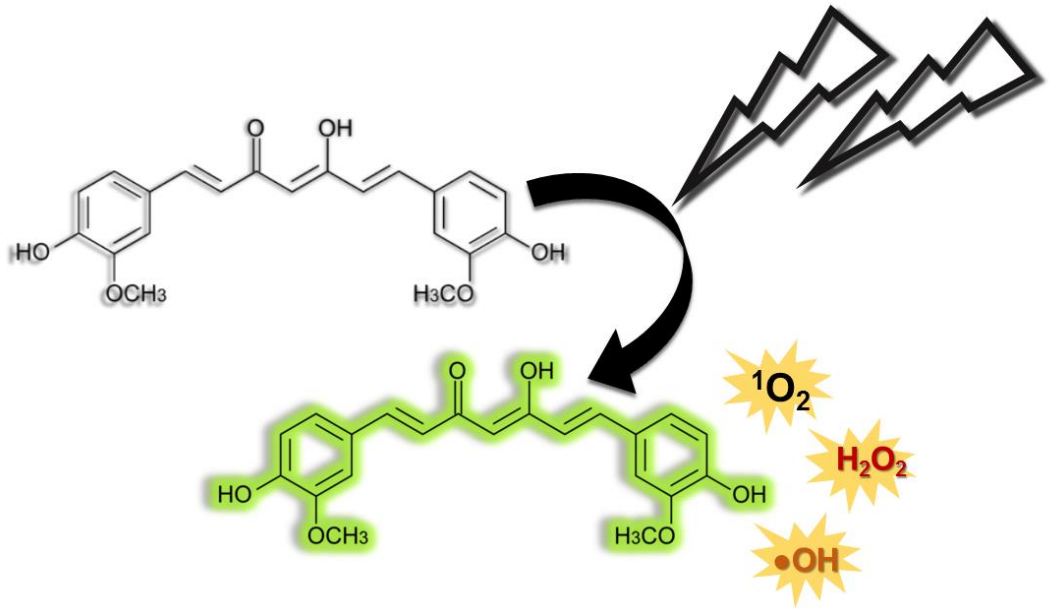

Figure 11. Upon light irradiation curcumin takes multiple photochemical pathways ending in production of singlet oxygen, as well as reduction of molecular oxygen to radicals.

The environment of curcumin, such as solvent effects, pH, and extra- or intra-cellular localization will affect its phototoxic activity. Curcumin is largely insoluble in aqueous solutions and is demonstrated to have poor bioavailability. Despite this, curcumin has shown success in *in vitro*, *in vivo*, and preclinical trials [86, 100-102]. Curcumin has a strong two-photon cross section absorption [103] and thus could be a promising 2PE PDI agent.

Subcellular localization of curcumin, as well as 2PE PDI using curcumin as a photosensitizer, were addressed in papers VI and VII. Furthermore, challenges in solubility and bioavailability of curcumin were addressed by employing complexation with a solubility enhancing compound (described in section 4.3.1).

2.2.2.4 Photoactivatable Compounds

Photoactivation can also be used to trigger release of toxic species without the need for molecular oxygen (as is needed in type II PDT), or to study cellular

processes. A photoactivatable compound is targeted to cells and a light source triggers a light-sensitive group of the compound (figure 12). In this work, photoactivation was used to trigger the release of nitric oxide (NO) (papers I and II). In addition, the compounds used herein were dual-function; release of NO was simultaneous to activation (paper I) or modification (paper II) of fluorescence, thus enabling tracking of the compound and NO release.

NO shows experimental promise as an anti-cancer, anti-bacterial, and antioxidant agent [104-108]. Ability of exogenous targeted NO to inhibit various physiological processes in cell growth and damage cancer cells, as well as de-aminate nucleoside bases and induce strand breakage in DNA, can be used to inhibit cancer cell growth [108]. Although high levels of NO present in tumor tissue has been shown to hinder tumor progression [109], both endogenous and induced NO are implicated in tumor progression [108, 110, 111], owing to its reputation as a "*double-edged sword.*"

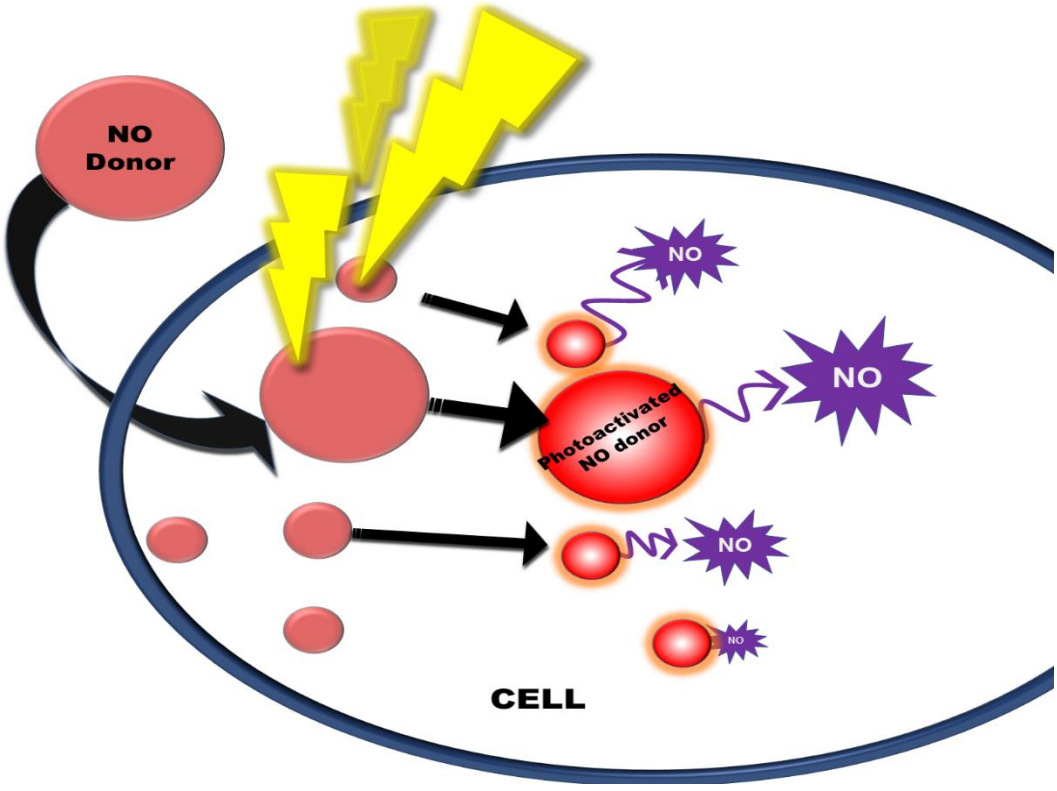

Figure 12. Nitric oxide (NO) photodonors release NO upon light irradiation. Ideally, the compound will have entered the cell prior to photoactivation and can release NO intracellularly.

Given the nature of NO to both repress and promote cancer growth or to both kill and aid in microbial infection, spatiotemporal control of NO release in targeted delivery is important. As the precise molecular action of NO is still unclear in

biological environments, there is a need for non-invasive methods to probe release and function.

Light-triggered NO release for targeted delivery presents an option for specific delivery of high concentrations to a biological site using standard PDT techniques with potential for spatial and dosage controlled release through non-invasive methods, without affecting pH, temperature, and ionic strength [112-115]. Furthermore, released NO upon photoactivation can produce cytotoxic results without the need for oxygen (as singlet oxygen production does in traditional PDT), opening the door to treatment of hypoxic conditions such as deep-seated tumors and resistant bacterial communities.

Non-invasive methods for studying NO release and targeting NO to produce cytotoxic effects in a biological system were developed and applied in papers I and II, opening possibility for future research in the field of NO targeting.

2.2.3 Drug Delivery

Advances in pharmaceutical science has led to successful treatment of many of the most common and harmful diseases and infections. Despite this, promising therapeutic compounds face difficult hurdles in targeting disease agents; many are inaccessible to the free-form of the drug compound [8]. Furthermore, physiochemical properties of the compounds can cause severe side effects at the concentration levels required for treatment, thus rendering the compound irrelevant in clinical settings [116]. In this research, various methods for improved drug delivery were explored. This section describes the fundamentals of the three major methods for drug delivery used in papers I-VII.

2.2.3.1 Topical drug delivery

Topical drug delivery overcomes limitations in oral delivery such as degradation, systemic side effects, and limited transport. The goal is to deliver active material by penetrating the outermost layer of the skin. The complex physical structure of skin makes penetration of xenobiotic compounds difficult; the primary function of the skin is acting as a barrier to the surrounding environment through complex physical and biochemical structure and function.

Skin is comprised of three layers: the epidermis (outermost layer of skin that provides the waterproof barrier), the dermis (containing connective tissue, sweat

glands, and follicles), and the subcutaneous tissue made up of fat and connective tissue (figure 13) [117, 118].

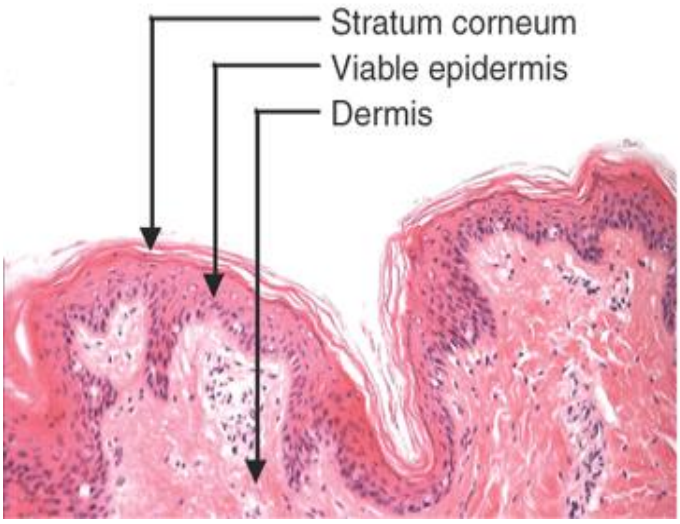

Figure 13. Histological skin structure demonstrating the three primary layers of mammalian skin. The stratum corneum, the outermost layer, is the first barrier to drug diffusion. This research focuses on imaging of drug delivery through the stratum corneum. Image used with permission from [119].

The outermost layer of the skin, the stratum corneum, approximately 20 µm thick, is the first penetration barrier encountered by drugs delivered dermally. Drug transport through the stratum corneum involves diffusion of the drug *via* the intercellular pathway, through the lipid matrix, but this pathway is not an easy feat for diffusing molecules due to solubility requirements and structural barriers [119].

Measurements of compound permeation and drug release through tissue is a fundamental step in pharmaceutical research. A standard *ex vivo* assessment is human skin models combined with percutaneous absorption studies [120, 121]. Excised human skin is obtained from plastic surgery or cadavers and is thought to maintain the stratum corneum barrier function for up to 6 months of storage [122].

In this research, penetration and localization of nanoparticle drug carriers through *ex vivo* human and murine skin tissue is explored by employing 2PM, spectral detection, and fluorescence techniques such as FRET (explained in 2.1.6). 2PE enables illumination with near infrared light, the ideal wavelength for limited absorption in skin, thus location of the diffused particles can be visualized.

Through this technique, 3D images of 100 µm in depth and more can be collected to demonstrate location of an exogenous compound within skin after application.

2.2.3.2 Cyclodextrins for drug delivery

Common challenges in pharmaceutical design are aqueous solubility [123], penetration in various biological environments [124], delivery of active agents to targeted cells [125], and degradation. An approach for improved delivery of pharmaceutical compounds – delivery that could improve solubility in biologically-relevant solution, enhance penetration through tissue/cells/etc, and block degradation – is complexation with another compound. Cyclodextrins are used extensively for this purpose due to their favorable physiochemical properties and utility as "carriers" [126, 127]. The use of CDs has been a key strategy within the CyclonHIT ITN project, thus appears in this research as a common theme.

Cyclodextrins (CDs) are chemically and physically stable cyclic oligomers of glucose, soluble in water, consisting of a hydrophobic core cavity and hydrophilic outer surface. CDs can form inclusion complexes with guest molecules, through complexation of a drug compound within the CD cavity, and can thus alter biological interaction of a guest drug molecule with its environment. The most commonly used CDs are α, γ, and β, differing in the glucopyranose units making up the CD structure, thus also differing in cavity size [128-130]. Among these, CD derivatives are often developed with altered physiochemical or biopharmaceutical properties to enhance complexation or utility. An example of this is charge functionalization of β-CDs for enhanced penetration and drug delivery in bacterial biofilms as was explored in paper IV.

As shown in figure 14, the association of free CD and drug form a drug-CD complex. The complex is maintained by a dynamic equilibrium between free drug and free CD molecules given the size of drug and size of the CD inner cavity are sufficient to form a favorable complex, while physiochemical properties of the complex are studied to determine strength of the complex itself within solution and further biological studies.

In papers V and VII, potential of CDs to increase treatment efficacy, *via* CD-complexation with known antibacterials, was studied.

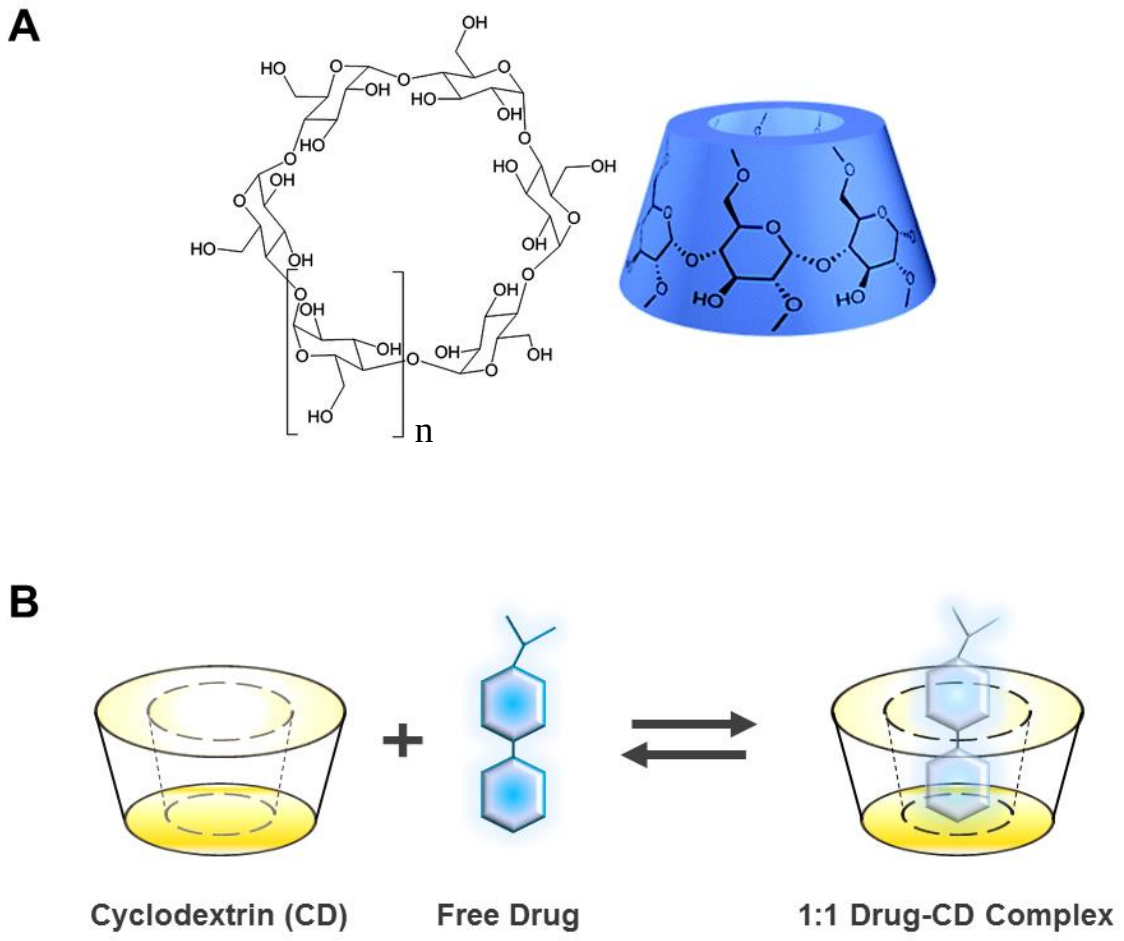

Figure 14. (A) Structure of cyclodextrins (CD); n = 1, 2, or 3 if referring to α, β, or γ – CD, respectively. Image modified with permission from [130]. In papers IV – VII β- and γ-CDs were used. (B) Drug-CD inclusion complex shown as a 1:1 drug-CD complex. The hydrophilic exterior of the CD enables water solubility while the hydrophobic inner cavity allows for inclusion of hydrophobic 'guest' molecules.

Chapter 3. Scientific Objectives

3 Scientific Objectives

The overall aim of this thesis was to develop biophotonics approaches for studying delivery of photopharmaceutics and antimicrobials to biological systems. The specific aims of each paper are described belo

Paper I	This paper aimed to demonstrate if two photon excited photorelease could be implemented in a cellular system. What causes cell toxicity in two photon excited photodynamic therapy with a nitric oxide photodonor?
Paper II	This paper aimed to track delivery of nitric oxide (NO), in a biological sample. Can förster resonance energy transfer be used to non-invasively monitor NO release with high specificity?
Paper III	The aim of my contribution was to measure and analyse the spectral characteristics of silica nanoparticles. Furthermore, to determine where the particles localize in human skin.
Paper IV	The aim of this paper was to understand how cyclodextrin based nanoparticles penetrate biofilms and how the charge of a cyclodextrin might change penetration – does neutral, negative, or positive charge produce better penetration?
Paper V	The goal of this paper was to determine if complexation with cyclodextrins can make antibiotics more effective for treating bacterial infections.
Paper VI	How can two photon excited photodynamic inactivation be implemented in a bacterial biofilm?
Paper VII	Where do photosensitizers localize in biofilms and does complexation with cyclodextrin improve efficacy of photodynamic inactivation with curcumin? A non-invasive diagnostic method for measuring treatment efficacy using two photon microscopy was presented.

Chapter 4. Methods

4 Methods

4.1 Microscopy and spectroscopy

4.1.1 Multiphoton microscopy

The MPM experiments in paper II – VII were performed using an LSM 710 NLO microscope (Carl Zeiss, Jena, Germany) equipped with a mode-locked femtosecond pulsed Mai Tai DeepSee laser tunable in the wavelength region 700-1100 nm and Plan-Apochromat 20x water-immersion objective (NA 1.0) (figure 15, left). Emission was registered with descanned (internal) detectors using fully opened pinhole, and recorded in varying channels corresponding to the fluorophores under investigation (varies throughout papers I – VII). The experiments in paper I were performed on an inverted custom built MPM (figure 15, right).

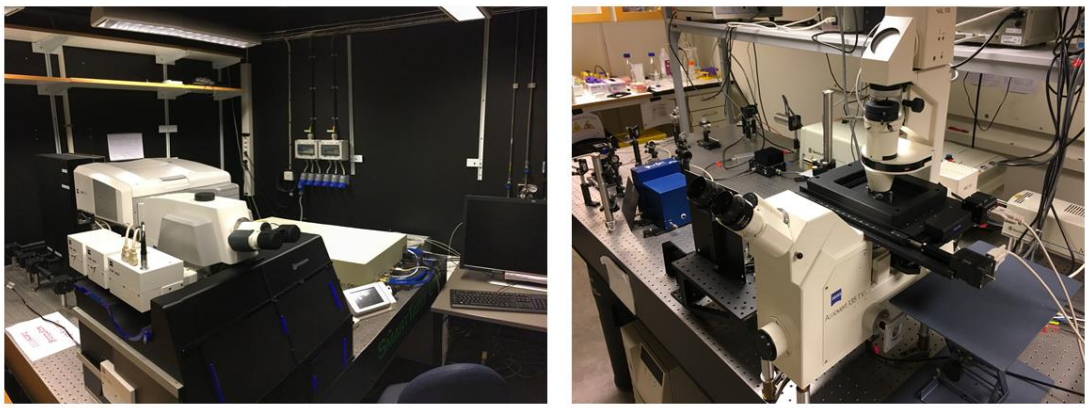

Figure 15. Two different multiphoton microscopy (MPM) setups were used in this research; a commercial system by Carl Zeiss shown on the left and the custom-built experimental setup shown on the right.

Emission spectra was acquired using the spectral detector in the emission range of 416 to 727 nm at a resolution of 10 nm. This was also performed simultaneous to imaging ("spectral imaging"), which enables separation between fluorescence signals that could otherwise present as bleed-through or signal overlap in imaging alone.

2PE photorelease was performed, in papers I, VI, and VII, by sequential scanning of a selected region with the laser throughout a pre-determined number of iterations (figure 16).

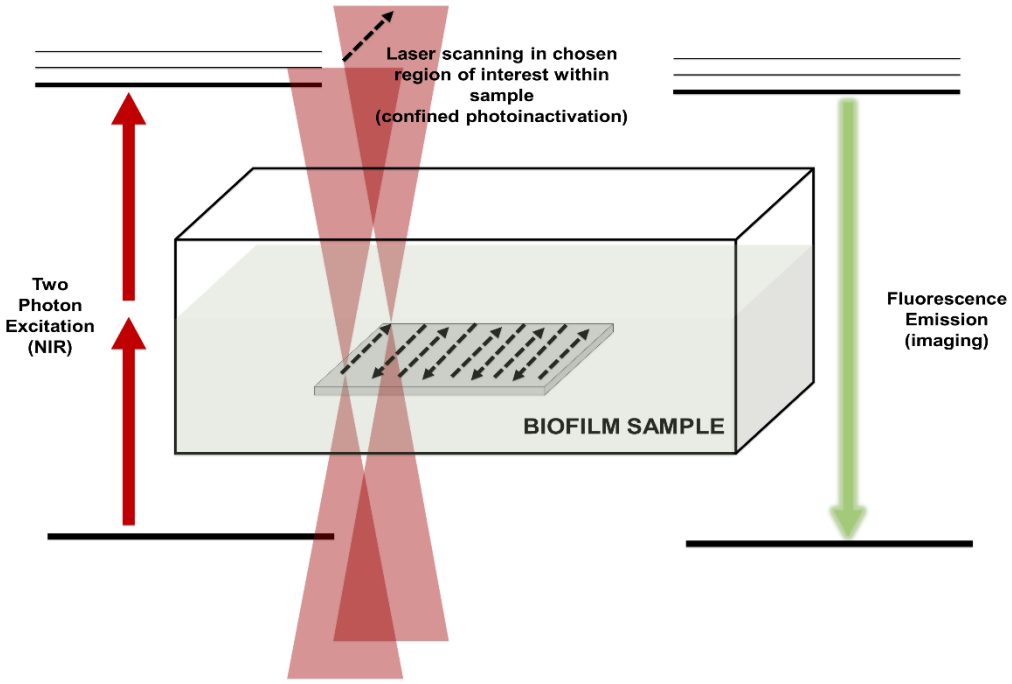

Figure 16. General principle behind two photon (2PE) photodynamic inactivation of biofilms. Laser scanning is performed with 2PE in a chosen region of interest within the sample to excite a photosensitizer.

Images were recorded prior to scanning, and in between each set of scanning iterations. The number of iterations were chosen to deliver a specific light dosage, calculated by using pixel dwell time (in µs), image size (i.e. scanning region size, in pixels), and estimated laser intensity after transmission through the objective lens (in mW). The sequence of images and resultant spectra were used to evaluate photorelease of both an NO-releasing system (paper I) and a photosensitizer system (curcumin, papers VI and VII).

Analysis of images and spectra from TPM was performed using ZEN (Carl Ziess, Jena, Germany), ImageJ (U.S. National Institutes of Health, Bethesda, Maryland), and Matlab (The MathWorks, Inc., Natick, Massachusetts, United States) software.

4.1.2 Structured illumination and Airyscan microscopy

Two different super resolution methods were explored for imaging of bacterial biofilms in this research. Super resolution of *S. epidermidis* biofilms was first performed using an ELYRA S.1 structured illumination microscope (Carl Zeiss, Jena, Germany). In paper VII, a Plan-Apochromat 63x/1.4 Oil immersion objective was used with live *S. epidermidis* biofilms grown in optical quality glass petri dishes. Biofilms were stained with FM 4-64 dye to image the membrane and

co-stained with the test compounds for the study. Two excitation lasers were used: 405 nm and 561 nm to excite curcumin and FM 4-64, respectively. Band pass filters, 570-650 nm and long-pass 750 nm were used to detect fluorescence signal in channels corresponding to curcumin and FM 4-64. Images were processed using the inherent structured illumination reconstruction in ZEN software accompanying the ELYRA microscope. Images were analysed using ZEN and ImageJ. This technique was found to be inefficient for live biofilms due to movement of the sample.

Following imaging with a SIM microscope, Airyscan confocal imaging was performed using an LSM 880 (Carl Zeiss, Jena, Germany), equipped with a 32 channel GaAsP spectral detector and Plan-Apochromat 63x/1.4 water objective. Laser excitation was split into two channels; 561 nm for excitation of the bacterial membrane stain FM4-64 used in both papers, 405 nm for curcumin excitation (paper VII), and 488 nm for FITC excitation (paper V). Detection was performed using a combination of band-pass filters; 570-620 nm with a 570 nm long-pass filter and 495-550 nm band-pass to collect fluorescence emission of FM4-64 and curcumin/FITC, respectively.

4.1 Pharmaceutical targets

4.1.1 Biofilm model

Biofilm samples were prepared using a biofilm model for *S. epidermidis* (strain ATCC 35984 / RP62A) bacteria cultured as described below, and subjected to various imaging and analysis experiments (figure 17).

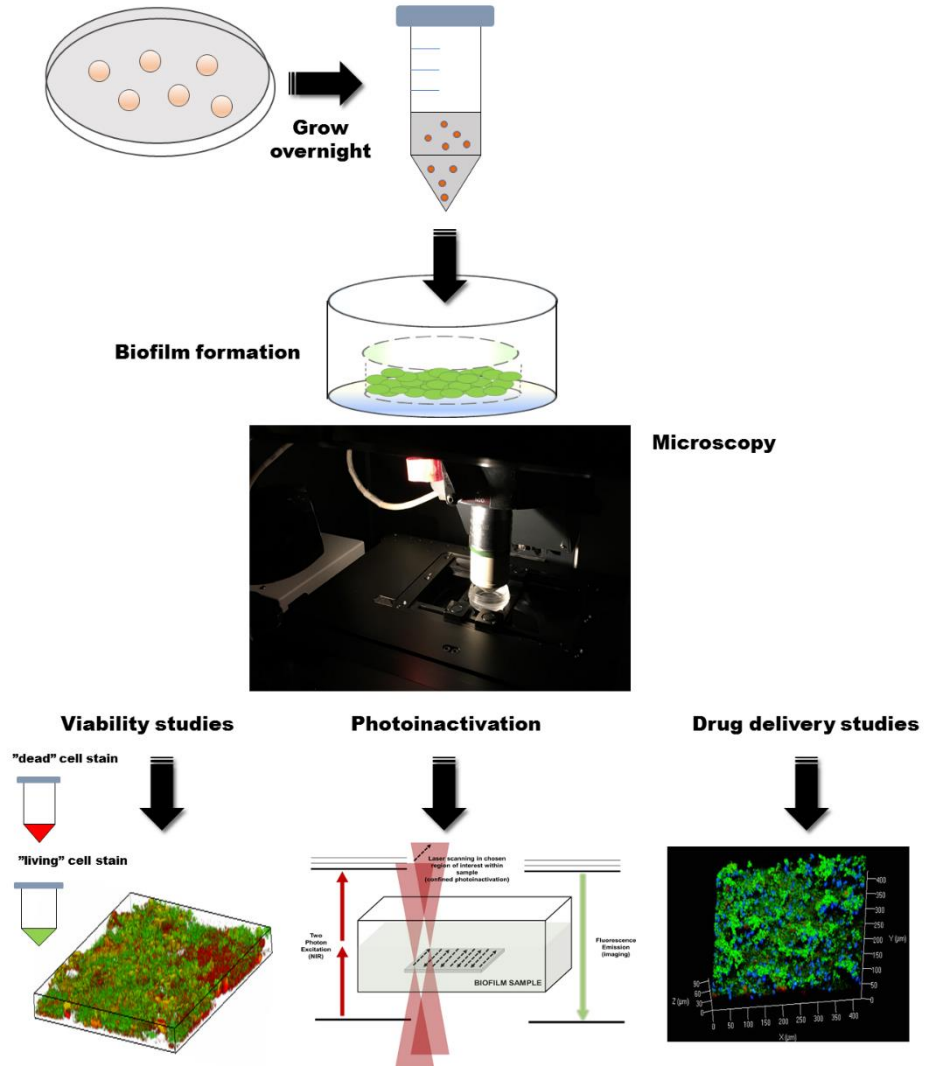

Figure 17. Experimental setup for biofilm studies. Biofilms are formed in optical quality culture dishes for 48-72 hours and studied live directly on the microscope stage. Biofilm viability can be studied using viability staining in real-time. Photoinactivation is performed using laser scanning through chosen regions of interest. Drug delivery is monitored using two photon microscopy and spectral imaging; images are collected in z-stacks to form 3D images.

Cultures were obtained from maintained subcultures in tryptic soy agar plates and grown overnight in aerobic atmosphere at 37°C. Second day overnight cultures were diluted in tryptic soy broth (TSB) to optical density O.D. ~ 0.2-.3; corresponding to ~10^8 colony-forming units per ml. Biofilm formation occurred in either pre-sterilized polycarbonate optical quality glass-bottom 3.5 cm diameter cell culture dishes (No. 1.5 glass thickness, Ibidi, LRI Instrument AB, Lund, Sweden) or pre-sterilized polycarbonate 96-well multi-well plates. Aliquots of 2 mL or 200 µL of bacterial/TSB inoculum containing approximately 10^8 cells/mL were transferred into each 3cm petri dish or 96-well plate, respectively. Biofilms were incubated under aerobic atmosphere at 37°C for an initial incubation period of 24 h to ensure attachment. After the first 24 h, liquid medium was carefully aspirated and replaced with fresh sterile TSB to remove planktonic cells. TSB was replaced every 24 h for the remainder of the incubation time of each sample.

Immediately prior to imaging or treatment with compound; biofilms were washed carefully with PBS (pH 7.4) to remove planktonic cells. During imaging, biofilms were kept in 3 mL PBS and imaged directly on the microscope stage using either a water-dip objective in an upright microscope setting (figure 17) or water/oil-immersion objective in an inverted microscope setting.

4.2.2 Eukaryotic cell culture

Human squamous cancer cell line A431 was cultured in a sterile cell culture facility. The general protocol for all cellular experiments described in this work is as follows:

A431 cells (HPA cultures, Salisbury, UK) were cultured at 2x10^5 cells per mL in full-growth minimum essential media (MEM) supplemented with 10% fetal bovine serum (FBS), 5% glutamine, and 5% non-essential amino acids (NEAA) at 37 degrees Celsius at 5% CO_2. MEM, phosphate buffered saline (PBS, pH 7.4), glutamine, NEAA, and FBS (EU approved South American origin) were obtained from Thermo Fischer Scientific, Gothenburg, Sweden. For multi-well experiments, cells were seeded in 96-well plates at 10,000 cells per well and maintained at 37°C and 5% CO_2 prior to experimentation. Cells used for imaging were seeded in tissue culture treated glass bottom petri dishes suitable for optics at 60 000 cells per mL (Ø= 3 cm, Ibidi, LRI Instruments, Lund, Sweden). Cell fixation was performed using 4% formaldehyde solution prepared in PBS (pH

7.4). Cells were washed carefully with PBS and the formaldehyde solution was added to the culture for 20 minutes at room temperature. Cells were then washed carefully twice with PBS and 2mL PBS was added to the imaging dishes for both inverted and upright microscopies.

4.2.3 Cell-based assays

Herein, two different cell viability assays were used for assessment. The basis of these assays is similar; cells are incubated with a reagent that is converted to a colored or fluorescence product by viable cells. Cells that die are not able to produce this signal, thus fluorescence readouts are proportional to the number of viable cells present in the culture (figure 18).

The MTT tetrazolium assay uses the compound MTT (3-(4,5-dimethylthiazol-2-yl)-2,5-diphenyltetrazolium bromide), which is converted into formazan, a purple product with absorbance maximum of 550-570 nm, by cells with an active metabolism. Thus, viable cells are measured by measuring absorbance of the cell culture following treatment with MTT.

The general protocol for the MTT assay used in this work is as follows: MTT substrate is diluted in aqueous cell media and added to the cell culture. After 4 hours of incubation, MTT solution is replaced with hydrochloric acid diluted in DMSO. Hydrochloric acid adjusts the pH of the solubilized formazan to provide maximum absorbance. Absorbance is then measured at the peak emission of formazan using a SpectraMax M2 Multi-mode microplate reader (Molecular Devices, Berkshire, UK). Generally, experiments are performed in replicates and statistical analysis is done using the excel data analysis toolbox.

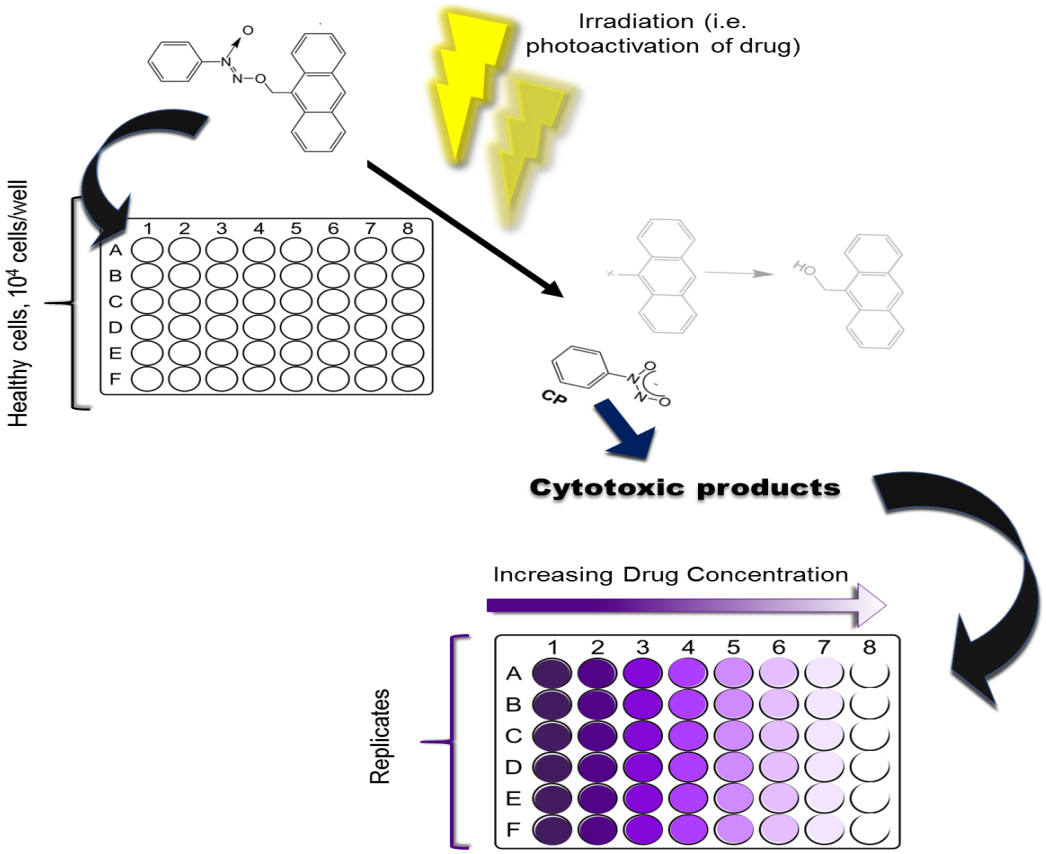

Figure 18. Application of the MTT assay. Healthy cells are cultured in 96 well plates and the drug compound is added. Light photoactivates the compound to release toxic species. Toxicity is measured with reduction of tetrazolium dye to formazan (purple), reduced by viable cells.

The resazurin reduction assay is an alternative to the MTT assay. Resazurin is a cell permeable redox indicator that monitors viable cell counts. Resazurin is soluble in physiological buffers and can be added directly to cell culture once solubilized. Cells with an active metabolism (*i.e.* viable cells) can reduce resazurin into resorufin, a fluorescent product, which can be monitored via fluorescence spectroscopy measurements.

The general protocol for the resazurin reduction assay is as follows: AlamarBlue reagent (Thermo Fisher Scientific, Stockholm, Sweden), is added to cell culture at 10% of the cell culture media volume. The cells are incubated for 4 hours with solution and either absorbance (560-570 nm) or fluorescence (590 – 600 nm) of the cells with solution is read using a SpectraMax M2 Multi-mode microplate reader. Viable cell counts are determined by analyzing absorbance vs. compound concentration as described by the manufacturer protocol.

4.2.4 Skin permeation studies

In this research, open chamber jacketed Franz diffusion cells (PermeGear, Inc., Pennsylvania, USA) were used, shown schematically in figure 19A. The donor chambers hold test compound and the receptor chamber contains a collection medium (in this research, phosphate buffered saline was used for all experiments). The outer compartment is filled with water which is circulated at 30°C constantly throughout the experiment.

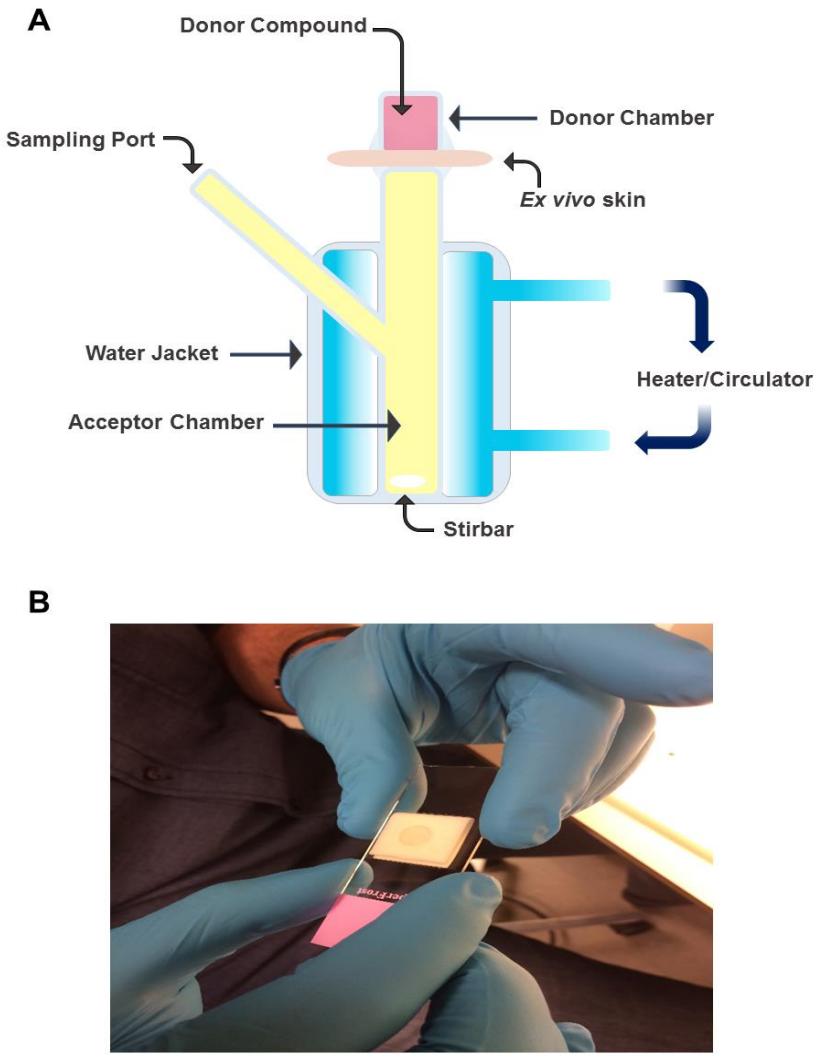

Figure 19. (A) Standard flow-through Franz diffusion cell used for skin permeation studies with *ex vivo* skin samples. Test compounds are added to the donor chamber in contact with the skin sample and PBS is added to the acceptor chamber. (B) Following incubation skin samples are removed and analyzed for biodistribution of the test compound using two photon microscopy and spectral analysis.

Cadaver skin for all experiments was obtained from Caucasian females as leftover specimens from breast reduction surgeries, through an agreement with Sahlgrenska University Hospital (Gothenburg, Sweden). Samples were

maintained at a temperature of -70° C for no longer than 6 months. Prior to experimentation, samples were thawed at room temperature, subcutaneous fat was removed using a scalpel, and samples were mounted on the chamber with the stratum corneum facing the donor chamber. Samples were kept under heat circulation for 4 – 24 hours depending on the experiment.

Following exposure samples were carefully washed with PBS and the exposed region was separated using an 8 mm biopsy punch and then mounted to a custom-made imaging chamber prepared by attaching a No. 1.5 glass cover slip (.17 mm thickness, 24 mm diameter, Bioscience Tools) to a microscopy slide *via* double-sided tape (figure 19B).

4.2 Drug delivery

4.3.1 Nitric oxide photodonors

Two novel compounds designed for photodynamic release of nitric oxide (NO) were developed by collaborators within the Marie Curie ITN project No. 608407, with the group of Salvatore Sortino at University of Catania (Catania, Italy). The compounds were then tested in biological systems as part of this thesis work.

In paper I, a dual-function NO photodonor was adapted with a fluorescent reporter, and designed to be excited by both 1PE and 2PE, such that upon release of NO, the fluorescence of the PS is activated and an increase in fluorescence intensity can be measured and directly correlated to release of NO. The previously published compound [131] (CPA, figure 20) consists of a cupferron (CP) O-alkylated with anthracene, a common fluorophore exhibiting blue (400-500nm peak) fluorescence. Prior to irradiation, the fluorescence of CPA is quenched due to charge transfer within the molecule, while upon irradiation, the anthrylmethyl carbocation and CP is released, activating a fluorescent co-product, while resultant CP spontaneously releases NO when decomposed (figure 20).

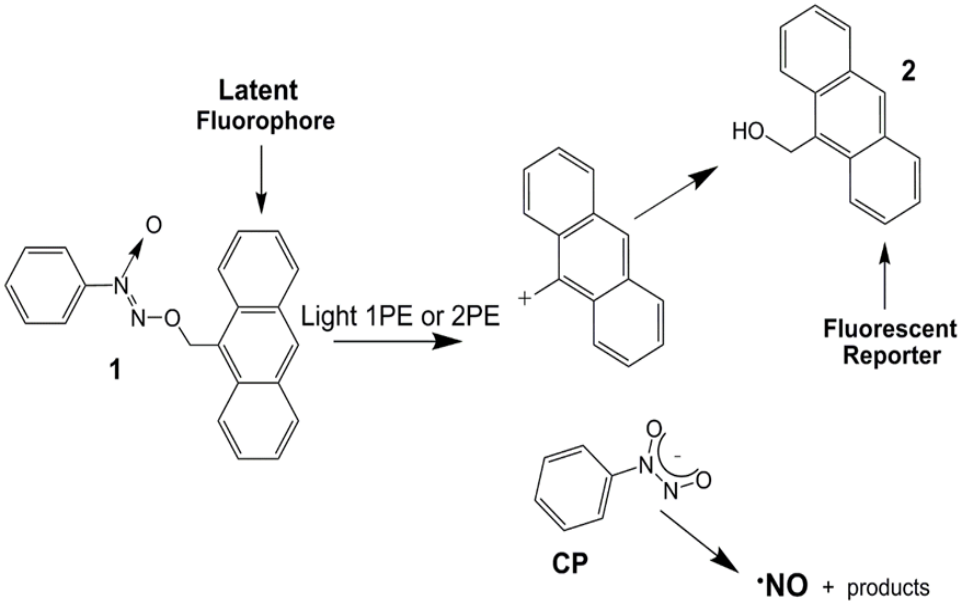

Figure 20. Cupferron-anthracene compound (CPA) employed as a nitric oxide photodonor in paper I. Cupferron *O*-alkylated with anthracene (1), upon light activation, forms two separate species; anthrylmethyl carbocation and CP. Fluorescence of 1 is quenched due to charge transfer of the intact compound, upon photoactivation, a fluorescent co-product (2) is formed and CP spontaneously decomposes to release nitric oxide (NO). Figure reprinted with permission from [13].

An alternative method for targeted NO release was demonstrated in paper II. A nanoparticle (NP) system designed to release NO with inherent fluorescence tracking *via* FRET was developed. The NPs were made of di-block poly-ε-caprolactone and polyethylene glycol copolymers covalently linked to rhodamine B. The polymeric NPs contained rhodamine in the core while a green fluorescent NO photodonor ("NBF") was trapped within (figure 21). NBF and rhodamine acted as a FRET pair, wherein excitation of NBF led to excitation and emission of rhodamine through a FRET process, with simultaneous release of NO upon excitation of NBF.

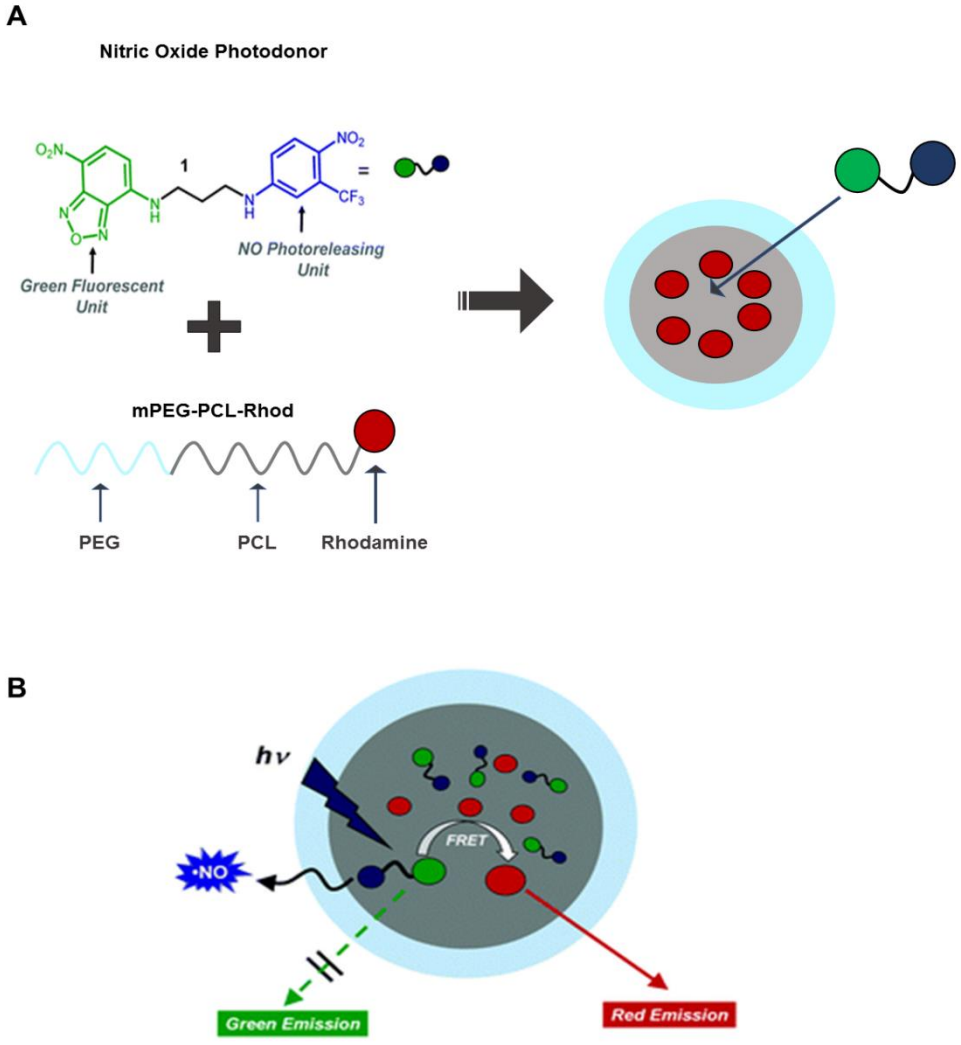

Figure 21. Di-block PEG-PCL nanoparticles used in paper II. Copolymers form a PEG core-shell structure with a hydrophobic PCL core, ideal for housing a lipophilic drug. The hydrophilic PEG shell provides solubility and stability of the NP structure, while rhodamine is covalently integrated as a fluorescent label in the di-block copolymer ("mPEG-PCL-Rhod"). An NO photodonor, consisting of an NO photoreleasing unit and green fluorescent unit, is loaded in the nanoparticle core. Figure adapted with permission from [12].

4.3.2 Cyclodextrins

Cyclodextrins for drug delivery (section 2.2.3.1) was demonstrated in a microbial biofilm in papers IV-VII. CDs shown in this work were developed by

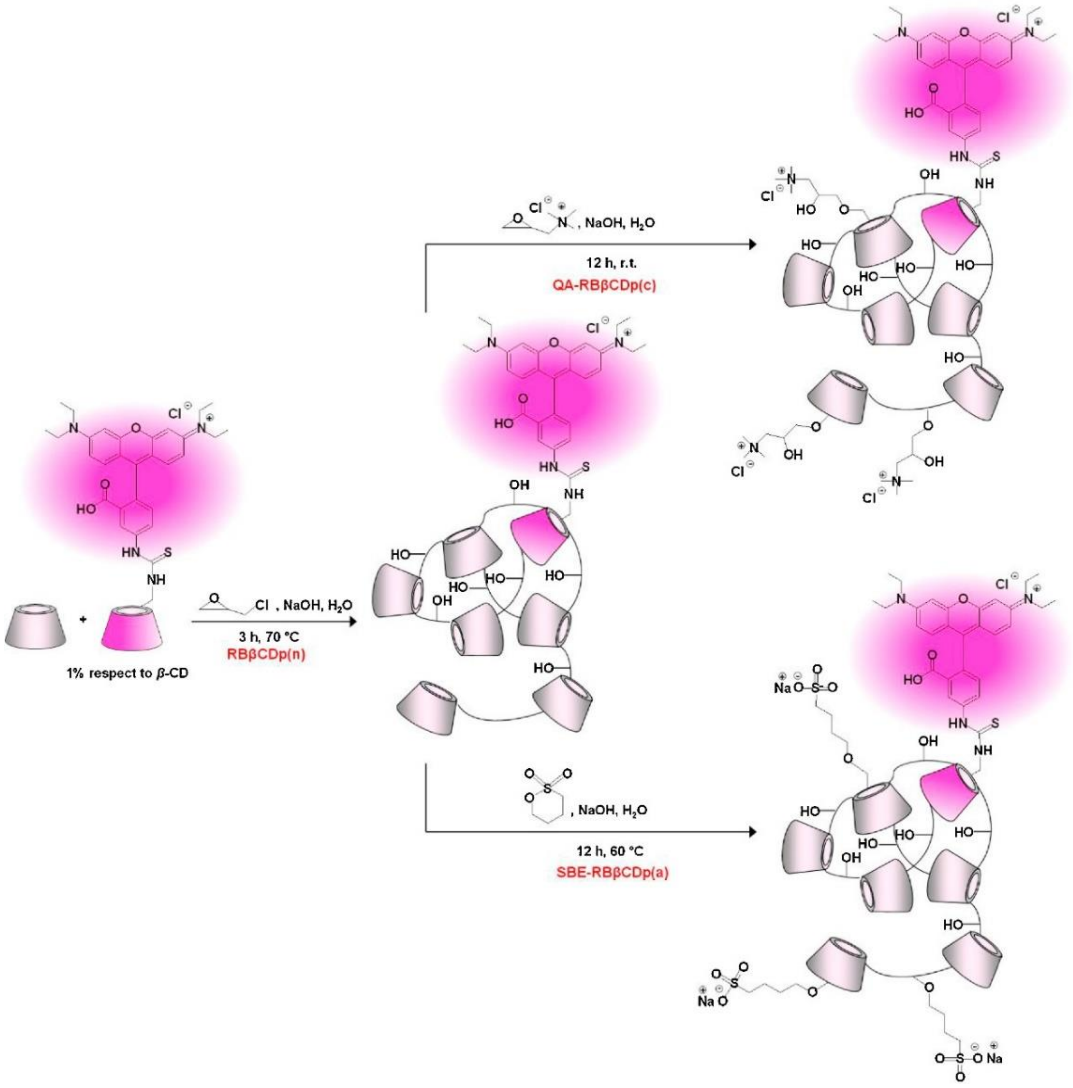

Figure 22. β-cyclodextrins functionalized with rhodamine and charged-moieties. Reprinted with permission from [15].

collaborators CycloLab (Budapest, Hungary) in papers IV, VI, and VII and the group of Konstantina Yannakopoulou at the National Center for Scientific Research Demokritos (Athens, Greece) in paper V. In paper IV, three β-cyclodextrins were labelled with rhodamine and functionalized with positive, negative, or no additional moieties. Rhodamine labelled βCD polymers (RBβCDp) were prepared via functionalization of previously prepared CD

scaffolds conjugated with rhodamine B [132, 133] as shown schematically in figure 22, described in more detail in [15].

Following paper IV, in which ideal charge functionalization of cyclodextrins for penetration into microbial biofilms was found, CDs were then loaded with antibiotics to determine if a CD-antibiotic complex would be more successful in targeting biofilm-encased bacteria than the antibiotic alone.

In paper V, previously synthesized γ-cyclodextrins were modified with positive charge and labelled with fluorescein (FITC) for fluorescence tracking [134]. Stock solutions of γ-CDs were prepared in sterile 1x PBS (pH 7.4) at a concentration of 100 µM. γCD-antibiotic complex was prepared by dissolving CD in sterile PBS and stirring to achieve dissolution at room temperature and adding antibiotic sodium salt (rifampicin or oxacillin) under stirring in a ratio of 1:1.5 (CD:antibiotic).

Lastly, in papers VI and VII, CDs were used to enhance aqueous solubility and biological penetration of curcumin (section 2.2.2.2). A curcumin-CD complex was created by combination of hydroxypropyl-γ-cyclodextrin (HPγCD) provided by CycloLab and curcumin (Sigma-Aldrich, Stockholm, Sweden). HPγCD was dissolved to a concentration of 112 g/L in 0.18 mol/L sodium hydroxide solution. Curcumin was added to a concentration of 15 g/L. The solution was agitated and after complete dissolution of curcumin, the pH wad adjusted to 6.0. Solutions were diluted from stock solution to 10 and 40 µM in PBS adjusted to pH 6.1 with HCl.

4.3.3 Nanoparticles for drug delivery

In paper III, localization of nanoporous silica particles (SPs) (sizes 440 nm, 2 µm, and 7 µm) in tissue was measured using MPM and spectral detection.

Luminescent SPs were developed by collaboration with Nanologica (Stockholm, Sweden). SPs were functionalized with carboamino groups leading to luminescent nanosized carbon dots forming within the porous SPs.

A full spectral characterization of the particles was performed. SPs were applied to skin using franz cell diffusion (section 4.2.4) and imaged using MPM (4.1.1).

SPs were sonicated prior to analysis in PBS (pH 7.4), at a concentration of 2 mg/mL. Following skin permeation studies, the mounted skin samples were imaged using emission channels corresponding to the SPs (434 – 552 nm) and autofluorescence of skin (552 – 640 nm). Ideal 2PE excitation was acquired prior

to imaging using spectral detection. 3D images were rendered using 1 µm z-stacks and analyzed using ZEN software and ImageJ.

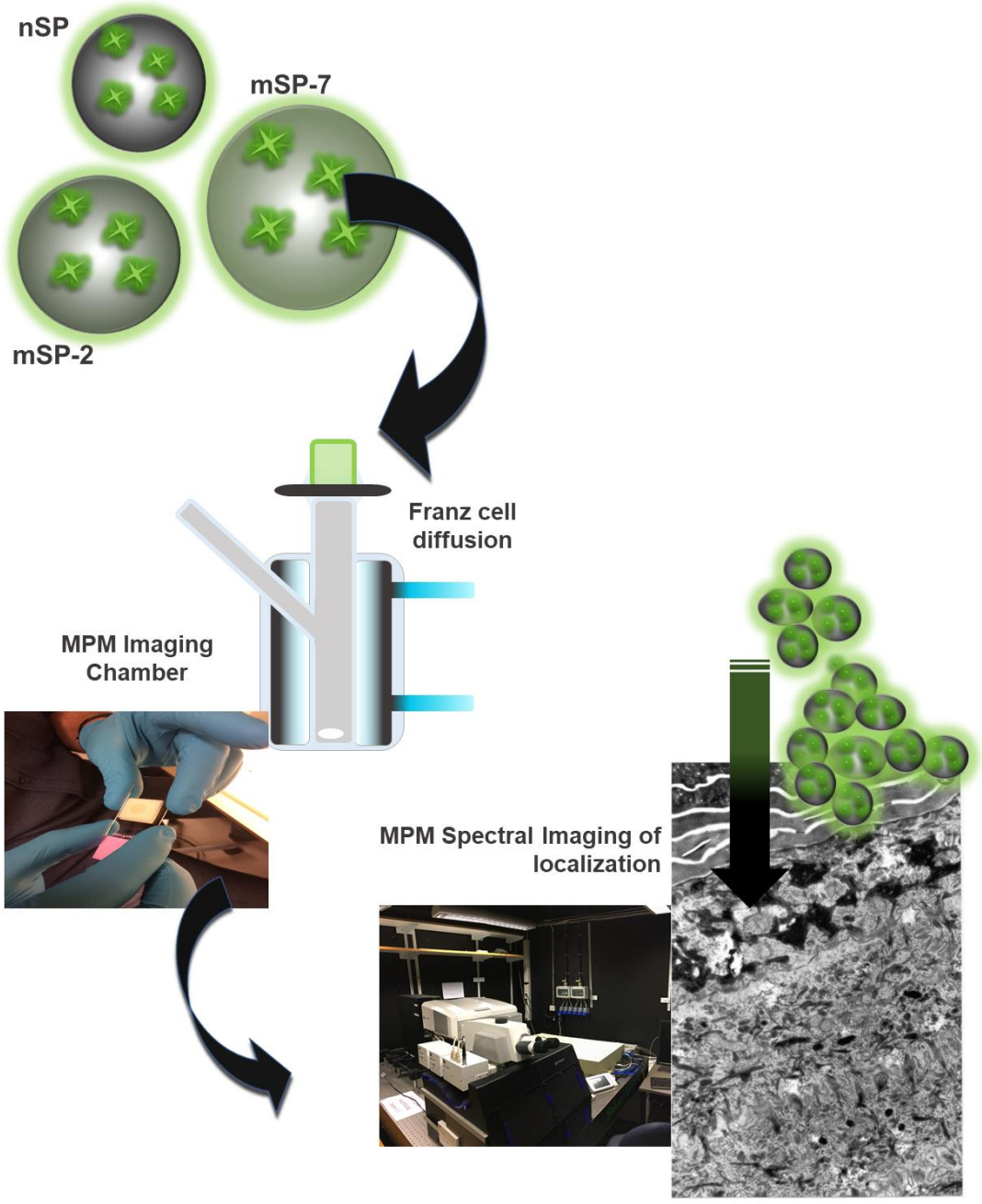

Figure 23. Study of nanoparticle localization in skin using franz cell diffusion and multiphoton microscopy.

Chapter 5. Results

5 Results

5.1 Paper I

In this project, the inherent confinement of two photon excitation (2PE) was used as a tool to demonstrate cytotoxicity, or lack thereof, of an NO-releasing PS (CPA, described in 4.3.1)

Upon irradiation with 745 nm 2PE, fluorescence emission of CPA is activated and increases with increasing light dosage as shown in figure 24. Previous spectral studies of CPA in solution confirmed release of NO at the start of light irradiation, simultaneous to increase in fluorescence intensity in 1PE [131]. Combined with the 1PE and 2PE imaging in figure 24, this indicates that NO is being produced simultaneously within the cell culture.

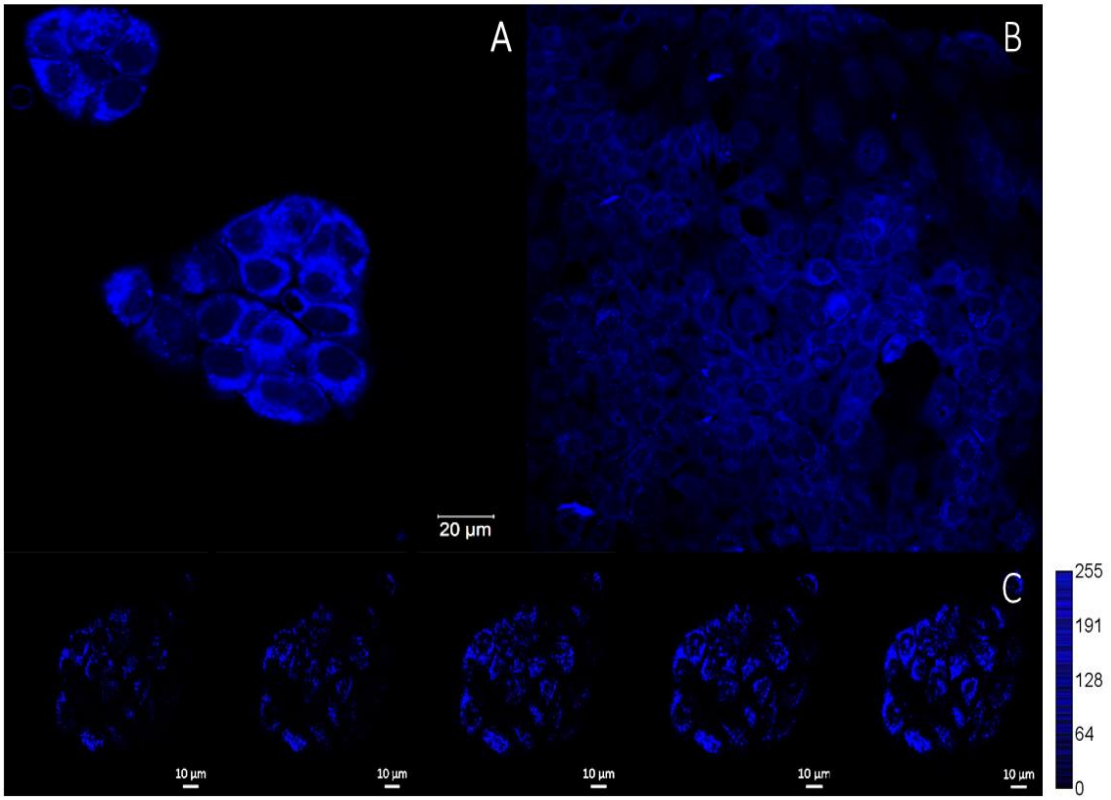

Figure 24. Two photon microscopy (TPM) and confocal images of A431 cells incubated with CPA in FBS-media for 4 hours. (A) TPM image (λexc = 745 nm), cells incubated with 5% CPA. (B) Confocal image (λexc = 405 nm), cells incubated with 20% CPA and fixed with 4% formaldehyde (in PBS). (C) Cells incubated with 5% CPA and subjected to increasing 2PE photoactivation with light doses of 0.9, 1.7, 2.6, and 4.4 J using laser power of 19 mW at the sample. Images reprinted with permission from [13].

The cytotoxicity of CPA against cancer cells with 1PE irradiation was first studied. Then, CPA was excited with 2PE light to determine if the same cytotoxicity could be produced using 2PE PDT. During this experiment, the same cytotoxicity to cells could not be reproduced using 2PE, as can be seen in figure 25B.

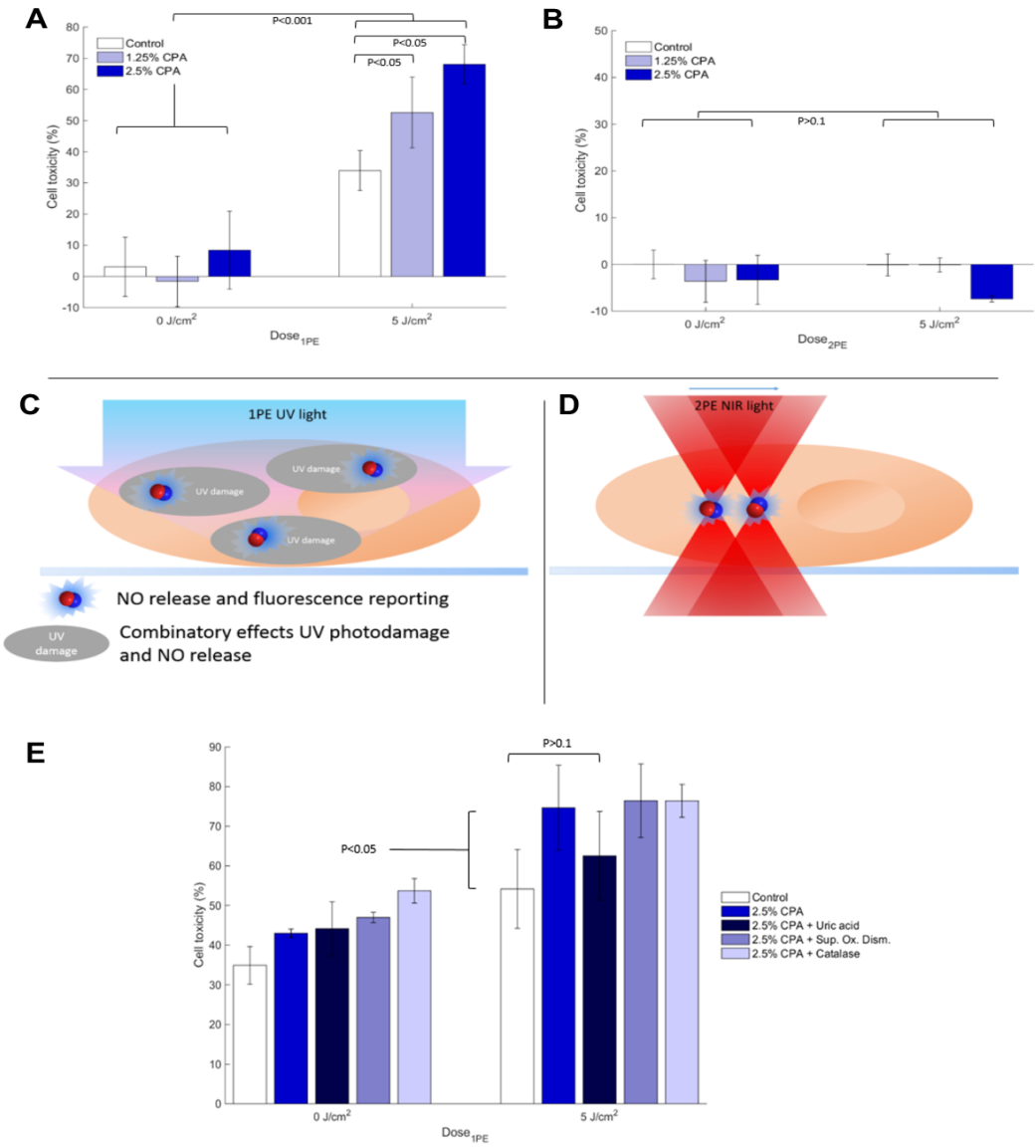

Figure 25. Cell toxicity following photoactivation of CPA in A431 cells with one-photon (1PE) or two-photon (2PE) excitation. Cells were treated with 0, 1.25, and 2.5 % CPA and irradiated with one-photon blue light at a dosage of 0 or 5 J/cm2. A) Cell toxicity with 1PE photoactivation. (B) Cell toxicity with 2PE photoactivation. (C-D) Schematic illustration of 1PE UV light irradiation vs. confined 2PE irradiation. (E) Toxicity following treatment with scavengers of peroxynitrite (uric acid), superoxide (superoxide dismutase), and hydrogen peroxide (catalase), at concentrations of 100 ug/mL in PBS. Cells were treated with 2.5% CPA or cell media only, and irradiated with 0 or 5 J/cm2 UV light. Statistical analysis performed from replicates of n=6. Error bars represent standard error of mean of replicates. Figure reprinted with permission from [13].

In the 2PE case, superoxide is not present in the same levels as 1PE; UV-irradiation produces superoxide whereas 2PE NIR does not to the same degree [135]. As it is referenced in literature that the cytotoxic effect of NO may be due to the production of peroxynitrite, through reaction of superoxide with NO [136], this led to the hypothesis that the lack of superoxide accompanying 2PE irradiation is the cause of lack of toxicity, since peroxynitrite might not be produced within the cells (figure 25).

To investigate this potential cause of cytotoxicity, cell toxicity with 2PE irradiation was measured in the presence of a peroxynitrite scavenger (with superoxide and hydrogen peroxide scavengers as controls). The results, figure 25E, show that when peroxynitrite is removed from the cells using a scavenging molecule, the viability of the cells is slightly recovered. These results are only a first investigation into this hypothesis; further experiments are needed to elucidate the mechanism.

5.2 Paper II

In this research, nanoparticles releasing NO upon irradiation with a specific wavelength of light were designed (section 4.3.1). To understand how and where NO is delivered in this scenario, the NPs were designed as a Förster resonance energy transfer (FRET) pair, such that monitoring FRET signal should be directly correlated to the release of NO.

My role in this paper was to measure spectra of the NPs in solution as well as monitor penetration of the NPs in human skin (figure 26). NPs with rhodamine core (acceptor), and with or without NBF (donor), were monitored with excitation to rhodamine or NBF only. Indication of a FRET process can be seen when rhodamine-core NPs loaded with NBF, excited at the ideal 2PE excitation of NBF; demonstrate stronger emission in the rhodamine (red) channel, rather than NBF (green) channel. While the NPs did penetrate and accumulate in skin, the design of the FRET NP system should be addressed prior to use as a FRET reporter of NO in tissue. Firstly, the images and spectral quantification confirmed that NBF appears to be released at the surface of the skin, accumulating in lines at the surface, while the rhodamine-containing core of the NPs successfully penetrate (figure 26).

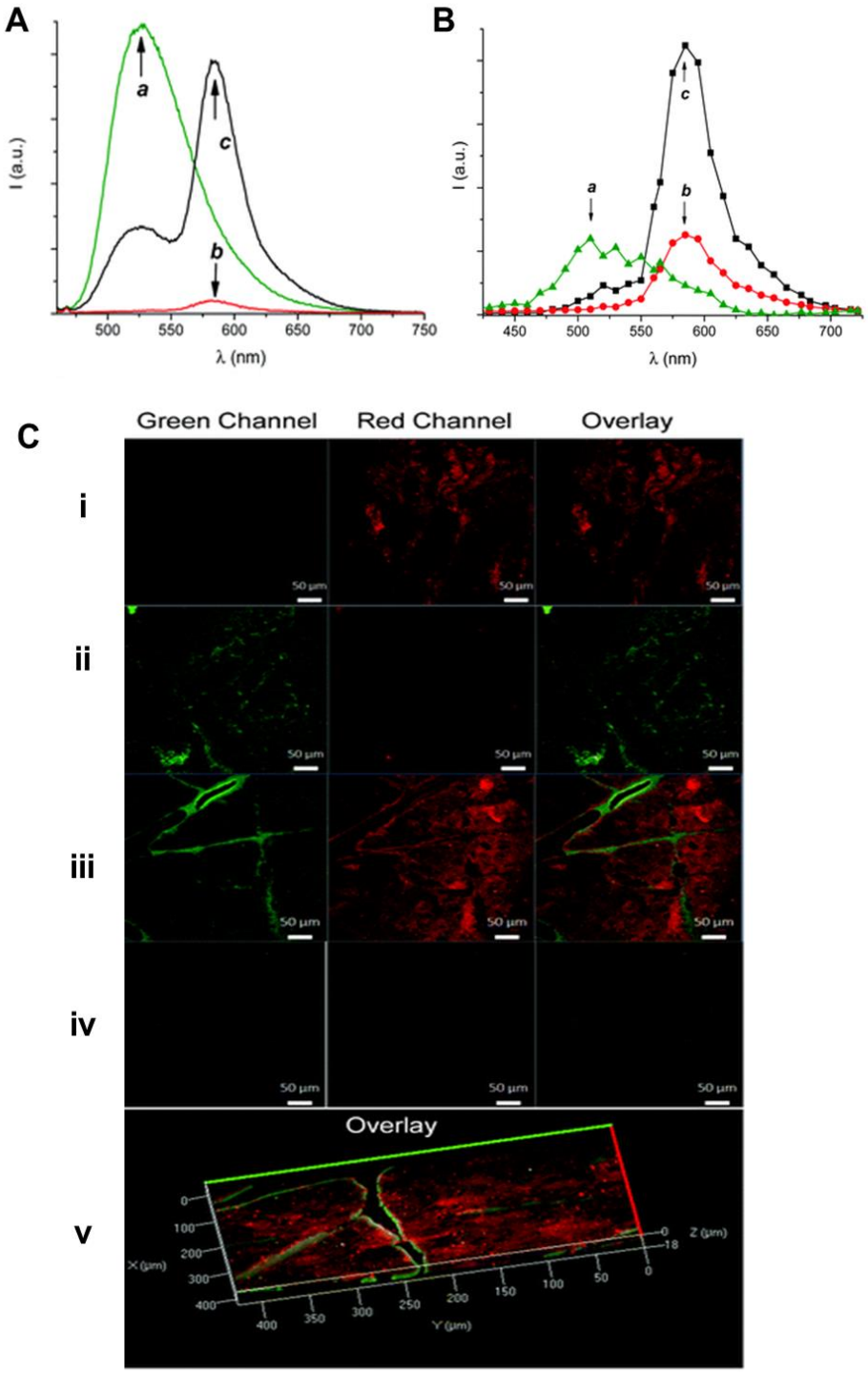

Figure 26. (A) Fluorescence emission spectra (λexc = 450 nm) of NPs with (a) NBF only (b) rhodamine only (c) rhodamine-NBF. (B) Two photon excitation fluorescence emission spectra (λexc = 900 nm) corresponding to A. (C) 2PE images of human skin samples after 24 h incubation with (i) Rhodamine-NPs (ii) NPs loaded with NBF (iii) Rhodamine-NPs with NBF and (iv) PBS only, (v) overaly 3D image. Images reproduced with permission from [12].

In addition, a FRET pair should consist of an acceptor fluorophore which is not excited by the same wavelength as a donor fluorophore (section 2.1.6). The NPs in this paper use a rhodamine-NBF pair, and while it meets this requirement with 1PE, both rhodamine and NBF are excited by the 2PE excitation wavelengths required. Thus, the fluorescence signal is not an accurate representation of FRET, and thus cannot be used as a quantifiable reporter of NO release.

Although the NP system would need to be re-evaluated for direct correlation between FRET signal and NO release, as well as full penetration into tissue, the system demonstrates, via proof-of-principle studies, a novel tool for monitoring release in optically dense tissue.

5.3 Paper III

In this paper, nanoporous silica particles ranging from 400 nm to 7 µm were developed (particles described in 4.3.3) and delivery to skin was measured using three different methods. My role in this paper comprised of performing *ex vivo* transcutaneous drug delivery studies and measuring particle location in solution and tissue.

Initial spectral analysis was performed in solution (figure 27). As seen in the figure, spectral profiles with both 1PE and 2PE were similar, confirming that the luminescent property of the particles are retained with 2PE excitation. Additionally, as it has been shown that carbon dots exhibit excitation-dependent photoluminescence that is “tunable” in the visible range [137]; the excitation-dependent luminescence emission seen provides evidence that carbon dots have formed within the particles.

Depth of penetration of the particles was shown using MPM. Resultant images from one particle, nSP (400 nm in size), are shown in the figure; nSP appears to accumulate a depth of 25 µm, whereas the larger micron size particles were visualized only to 14 µm (results shown in paper III).

To confirm that the fluorescence emission seen is a result of nSP accumulation, rather than autofluorescence from skin, spectral imaging was performed. Separate regions were selected; region 1 (R1) appears as localized nSP in the skin furrows and region 2 (R2) appears to be autofluorescence of the skin. As seen in figure 27E, peak emission from R1 is

that expected from nSP, whereas emission from R2 is a weaker signal more characteristic of skin autofluorescence.

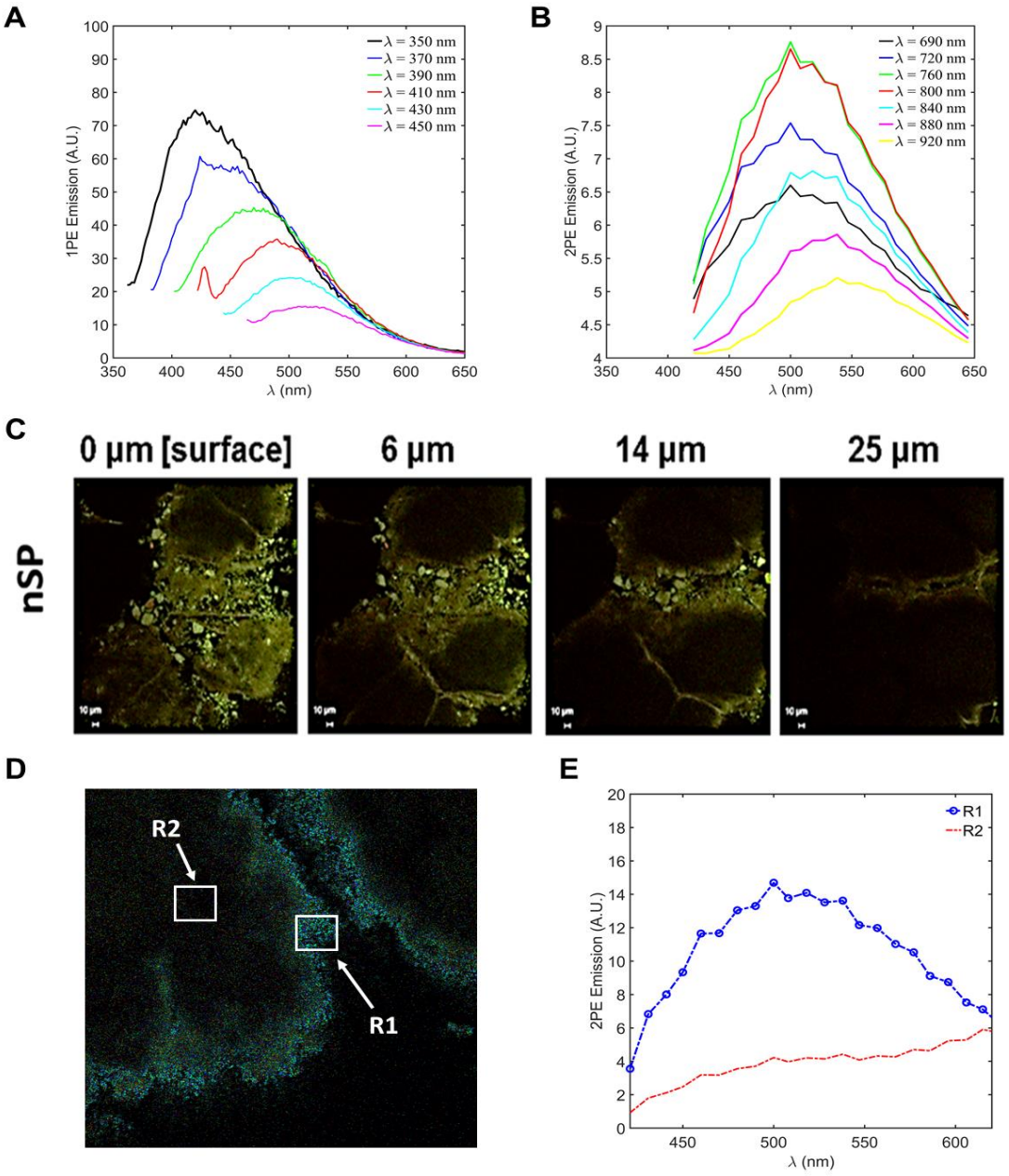

Figure 27. (A) Spectral characterization of nSP in solution (2 mg/mL in PBS) with λ_{exc} = 350 – 450 nm and (B) two photon excitation (2PE) with λ_{exc} = 690 – 920 nm. (C) Multiphoton microscopy data of porcine skin treated with nSP. Images are shown at varying tissue depth, represented in µm from the surface of the skin. nSP emission is shown in green, corresponding to 431 – 552 nm detection. Autofluorescence is shown in red, corresponding to 552 – 640 nm detection. Images are collected as z-stack images, with 1 z-stack acquired every 1 µm. Field of view of images shown corresponds to 424 x 424 x 1 µm. (D) Two photon spectral imaging data of porcine skin treated with nSP. Spectra were acquired using spectral detection in the range of 416 to 727 nm at a resolution of 10 nm. 1 z-stack, at a depth of 25 µm from the skin surface, is shown here. (E) Emission from R1 and R2 in image D, R1 corresponds to autofluorescent signal of skin while R2 corresponds to suspected nSP location. Field of view of images shown corresponds to 424 x 424 x 1 µm.

5.4 Paper IV

In this paper, MPM was used as a method for measuring penetration of an experimental drug carrier developed by a collaborating company, CycloLab (4.3.2). The research aimed to determine which charge-functionalization of the drug-carrier, a β-cyclodextrin (β-CDs) tagged with a fluorescent reporter, more efficiently penetrated a biofilm.

Both monomer and polymer β-CDs were adapted with fluorescence (rhodamine, peak emission = approx. 600 nm) and charge-functionalization and 2PE emission spectra of the entire range of β-CDs incubated with SYTO9 (peak emission = approx. 500 nm) stained *S. epidermidis* biofilms was performed (figure 28).

Interestingly, minimal fluorescence signal from the monomer β-CDs was collected throughout the biofilm structure. Whereas the polymer β-CDs show a strong emission peak with cationic charge (figure 28).

This initial experiment concluded that primarily polymer β-CDs would be monitored in the biofilms as no signal could be found for monomers. Understanding the mechanism behind the difference in both monomer vs polymer and charge requires further experimentation that was beyond the scope of this publication.

MPM images of charged and fluorescent polymer β-CDs incubated with SYTO9 stained *S. epidermidis* biofilms are shown in figure 29. Biodistribution of the β-CDs (red emission) in comparison to bacterial cells (green emission) was monitored via 3D imaging and confirmed with spectral detection, in which spectra from bacteria and β-CDs can be distinguished.

As can be seen in the figure, the cationic β-CDs are significantly more distributed throughout the biofilm compared to the others. This could suggest that CDs designed for drug delivery to biofilm cultures may be enhanced by functionalization with cationic charge but further analysis of imaging data should be performed to confirm the findings.

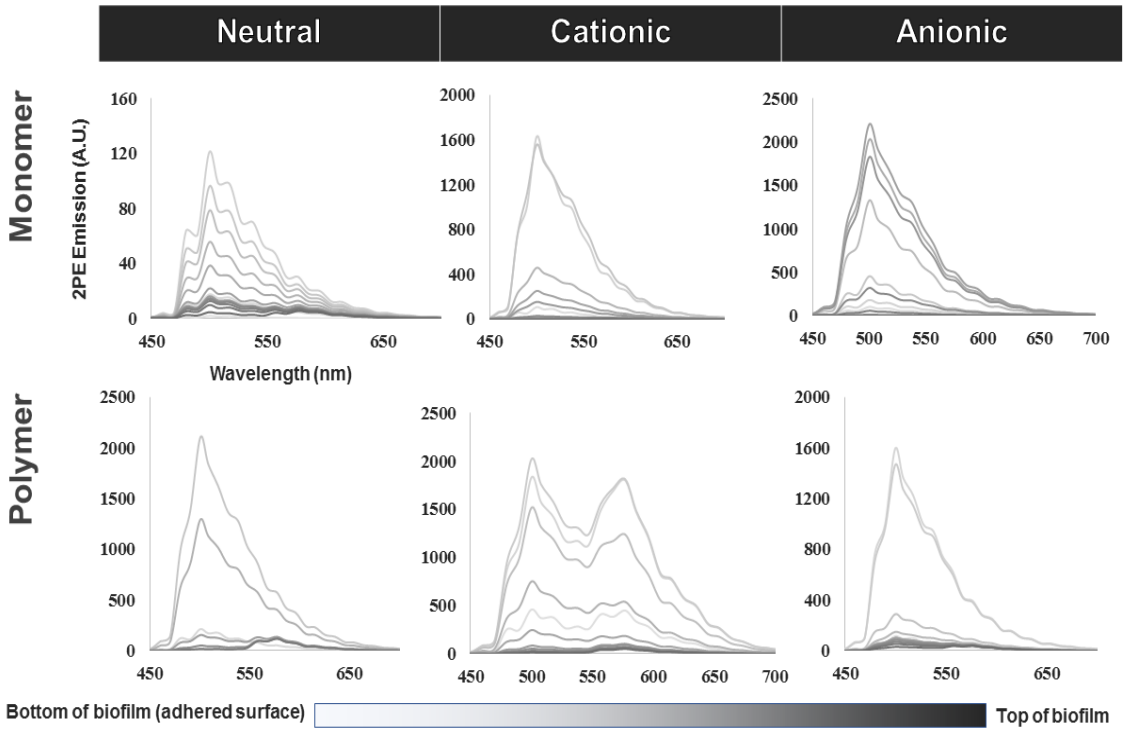

Figure 28. Two photon emission spectra of rhodamine labelled cyclodextrin (RB-CD) monomers and polymers after incubation with *S. epidermidis* biofilm. Spectral data was extracted from spectral imaging of biofilms with excitation of 860 nm. Neutral/cationic/anionic charged RB-CDs were measured. Signal from rhodamine emission is seen from cationic polymer cyclodextrins, whereas monomer cyclodextrins show minimal emission when incubated with the biofilm.

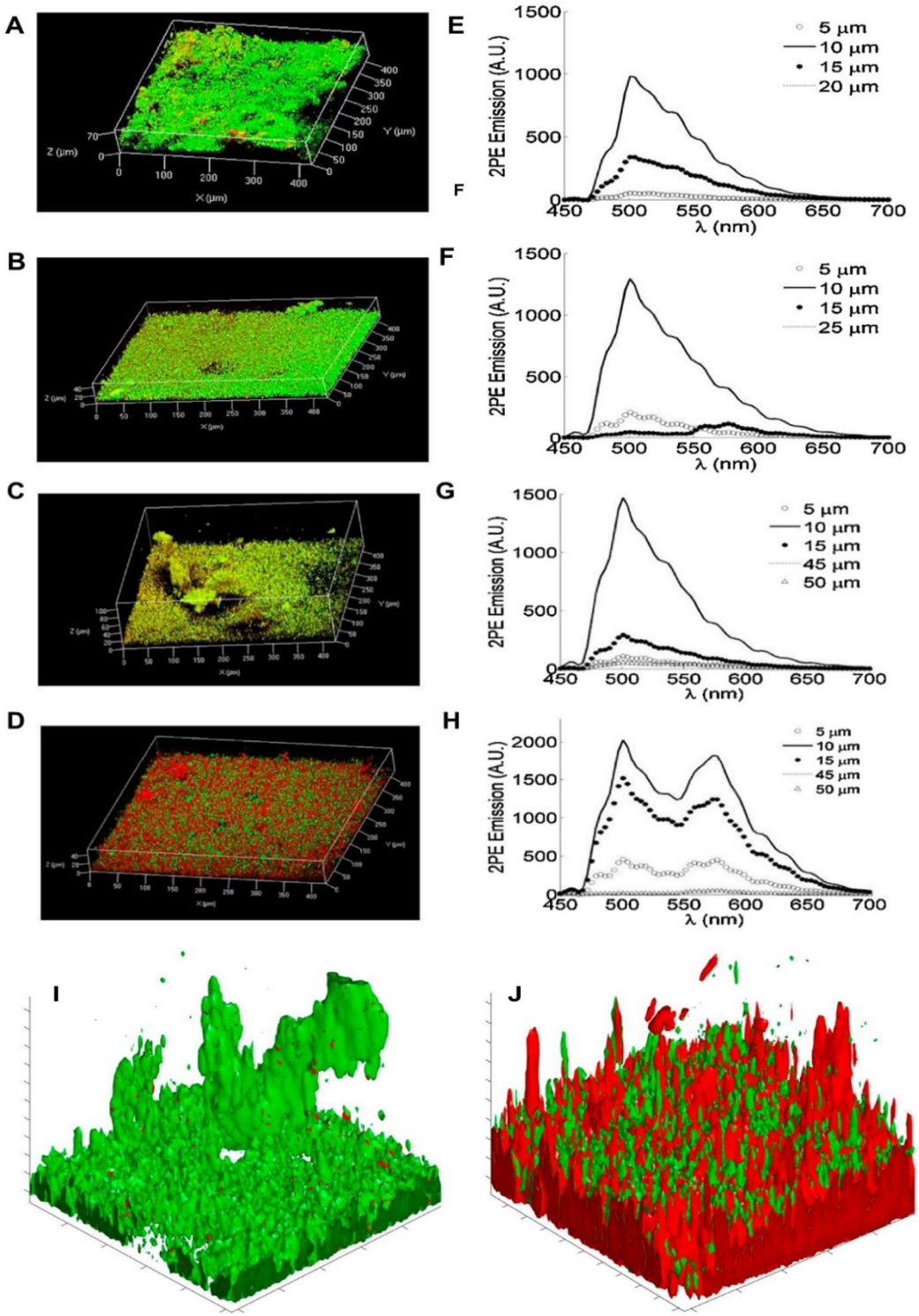

Figure 29. Multiphoton microscopy (MPM) data of S. *epidermidis* biofilms after incubation with rhodamine labelled cyclodextrin polymers (RB-CD). Green corresponds to SYTO9 staining (453-549 nm) and red corresponds to the RB-CD (562-718 nm). Field of view of 3D volumes corresponds to 424x424xz µm where z represents height from the adhered surface of the biofilms. (A) control biofilm, (B) Neutral charged RB-CD, (C) negatively charged RB-CD, (D) positively charged RB-CD. (E-H) corresponding 2PE emission spectra for A-D, respectively. (I,J) 3D surface rendering corresponding to C and D. A thresholding algorithm was implemented to asses ratio of SYTO9 (bacteria) to RB-CD signal. Images used with permission from [15].

5.5 Paper V

In paper IV, it was shown that positively charged cyclodextrin (CD) polymers most efficiently penetrate and localize within 3D biofilm structure. In this study, positively charged cyclodextrins are loaded with antibiotic and measured for efficacy against *S. epidermidis* biofilms. γCD labelled with fluorescein (γCD-FITC, section 4.3.2) was first monitored for localization to a biofilm, and then loaded with oxacillin and rifampicin for further studies of antibiotic efficacy.

MPM and spectral analysis was used to monitor the localization of the antibiotic loaded CDs. Figure 30 shows MPM images of *S. epidermidis-BFP* (bacteria expressing blue fluorescence) incubated with γCD molecules. To evaluate colocalization of *S. epidermidis* with γ-CDs, a colocalization scatter plot of *S. epidermidis-BFP* vs. FITC was created. BFP and γCys appear to be colocalized, although this does not indicate if the CD was taken up internally in the bacteria. To better understand the subcellular localization γCys, Airyscan microscopy was used for higher resolution imaging, shown in figure 31. In the high-resolution images, it appears as if γCys is localized in the EPS surrounding the bacteria, rather than intracellularly. This could suggest that γCys could act to penetrate the biofilm, while the antibiotics are released prior to uptake into the bacteria.

To determine if the antibiotic activity was in fact increased by delivery with CDs, biofilm viability was measured using a microtiter plate assay with serial dilutions of CD-antibiotic complex, and complimented with 3D viability imaging to understand varying effect throughout the biofilm structure (figure 32). As can be seen in the figure, in which biofilms are stained with propidium iodide (PI) for membrane-compromised cells, increased PI signal can be seen for biofilms treated with γCys, indicating inherent antibacterial activity of the CD alone. Ethanol-killed biofilms were monitored for reference. Biofilm viability following treatment with γCys-rifampicin and γCys-oxacillin complexes, compared to free antibiotics, were measured using the resazurin microtiter plate assay. A statistically significant reduction in biofilm viability was found with γCys complexed with rifampicin (figure 32B).

This work demonstrates potential increased effect of antibiotics to a biofilm by complexation with CDs, and demonstrates complementary methods for monitoring drug delivery and toxicity using imaging, thus providing a better understanding of how drugs interact with the complex 3D structure of biofilms.

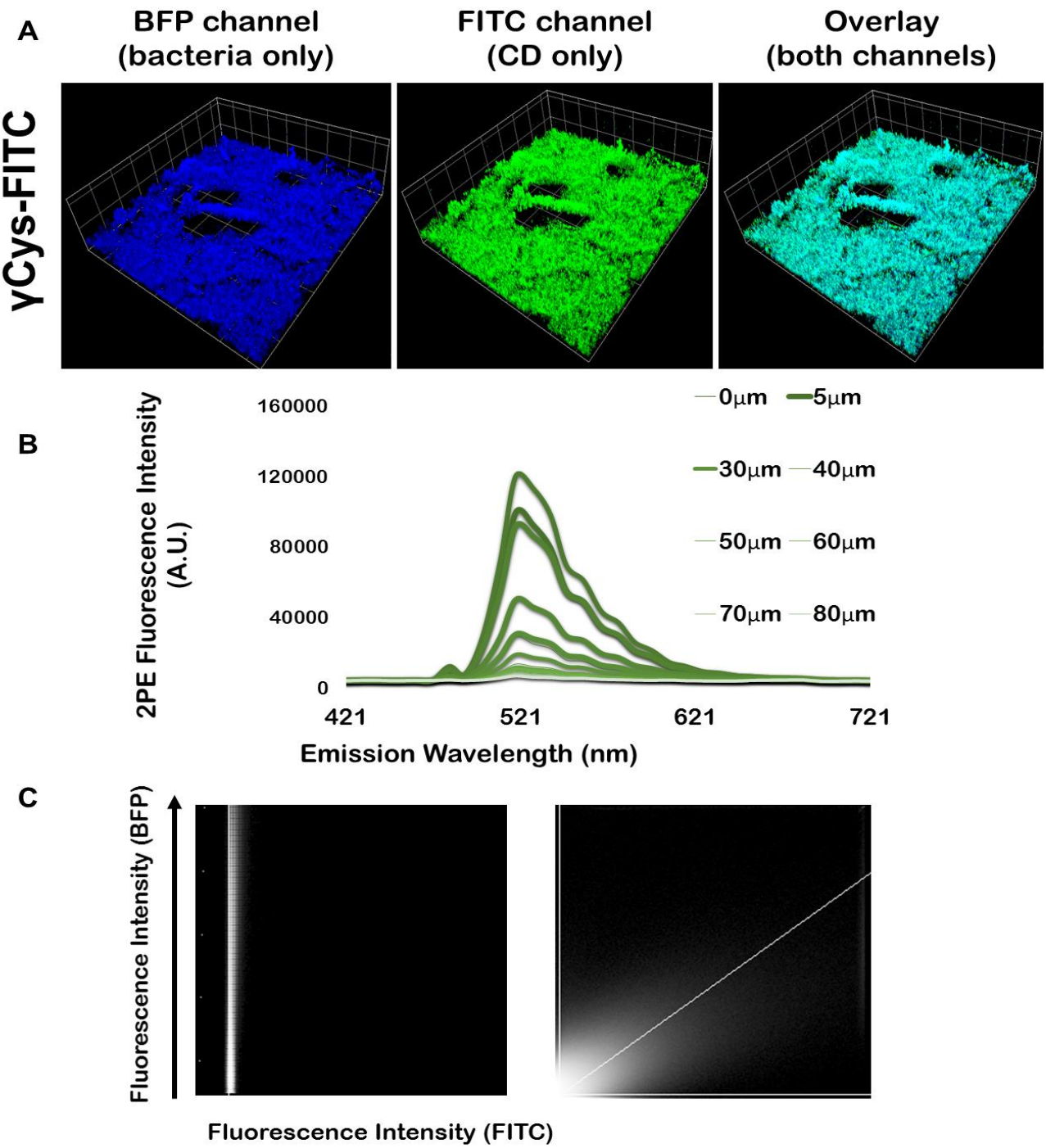

Figure 30. (A) Multiphoton microscopy images of *S. epidermidis* biofilms incubated with γCys-FITC (100 µM in PBS, pH 7.4, 30 min incubation). Fluorescence emission was collected in 2 channels corresponding to blue BFP emission of bacteria (λ = 399 – 493 nm) and green emission of FITC (λ = 504 – 659 nm), an overlay image is shown to demonstrate overlap of signal. 3D image stacks reconstructed from 80 1 µm image slices. Field of view 424 x 424 x z µm (B) Spectral profile of γCys-FITC within the biofilm corresponding to images in A. 2PE fluorescence emission intensity (A.U.) shown for z levels 0 – 80 µm collected at 10 nm increments. (C) Colocalization scatter plot corresponding to aimges in A. Colocalization was monitored by plotting fluorescence intensity in the BFP channel.

.

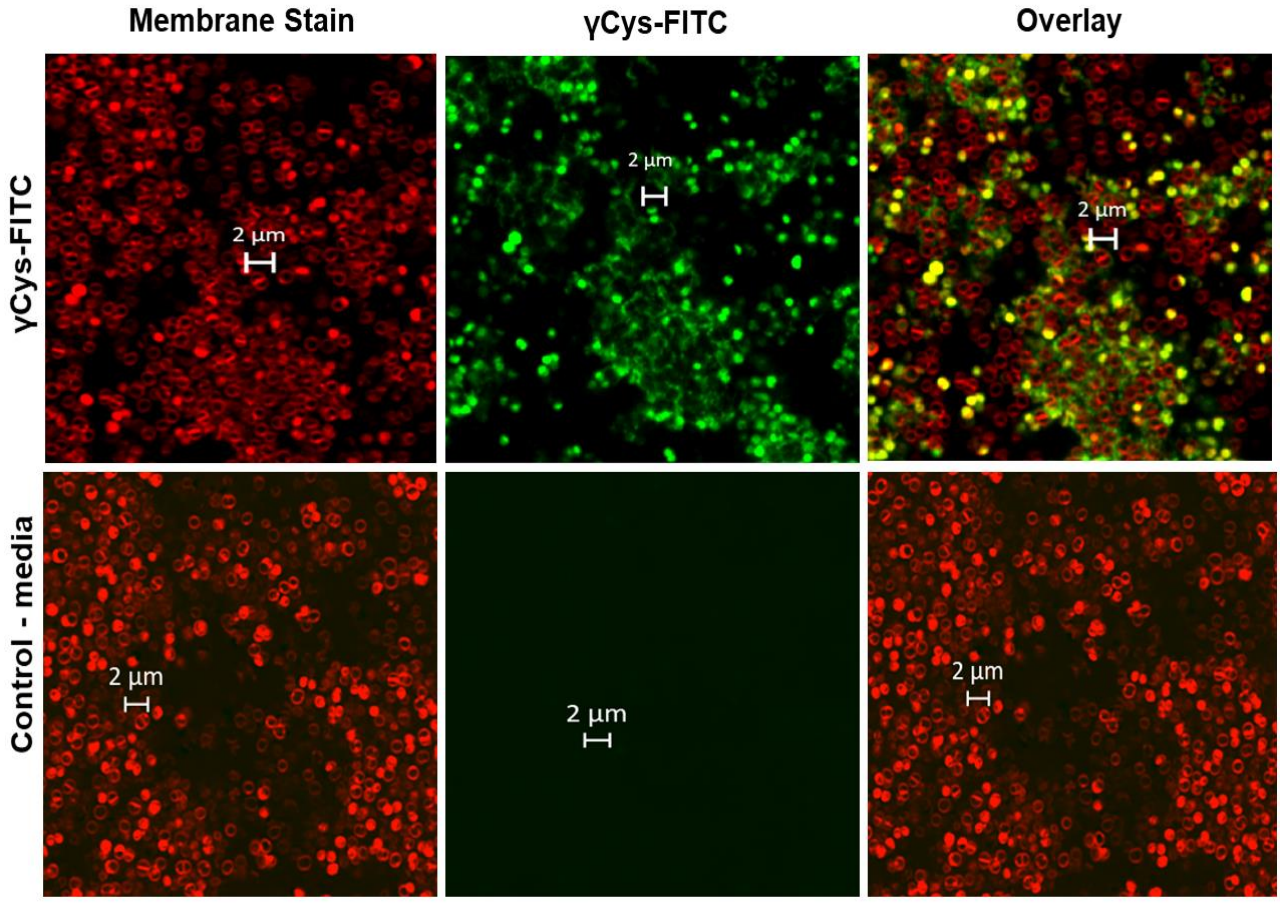

Figure 31. Airyscan confocal images of *S. epidermidis* biofilms incubated with γCys- FITC (100 µM in PBS, pH 7.4, 30 min incubation).

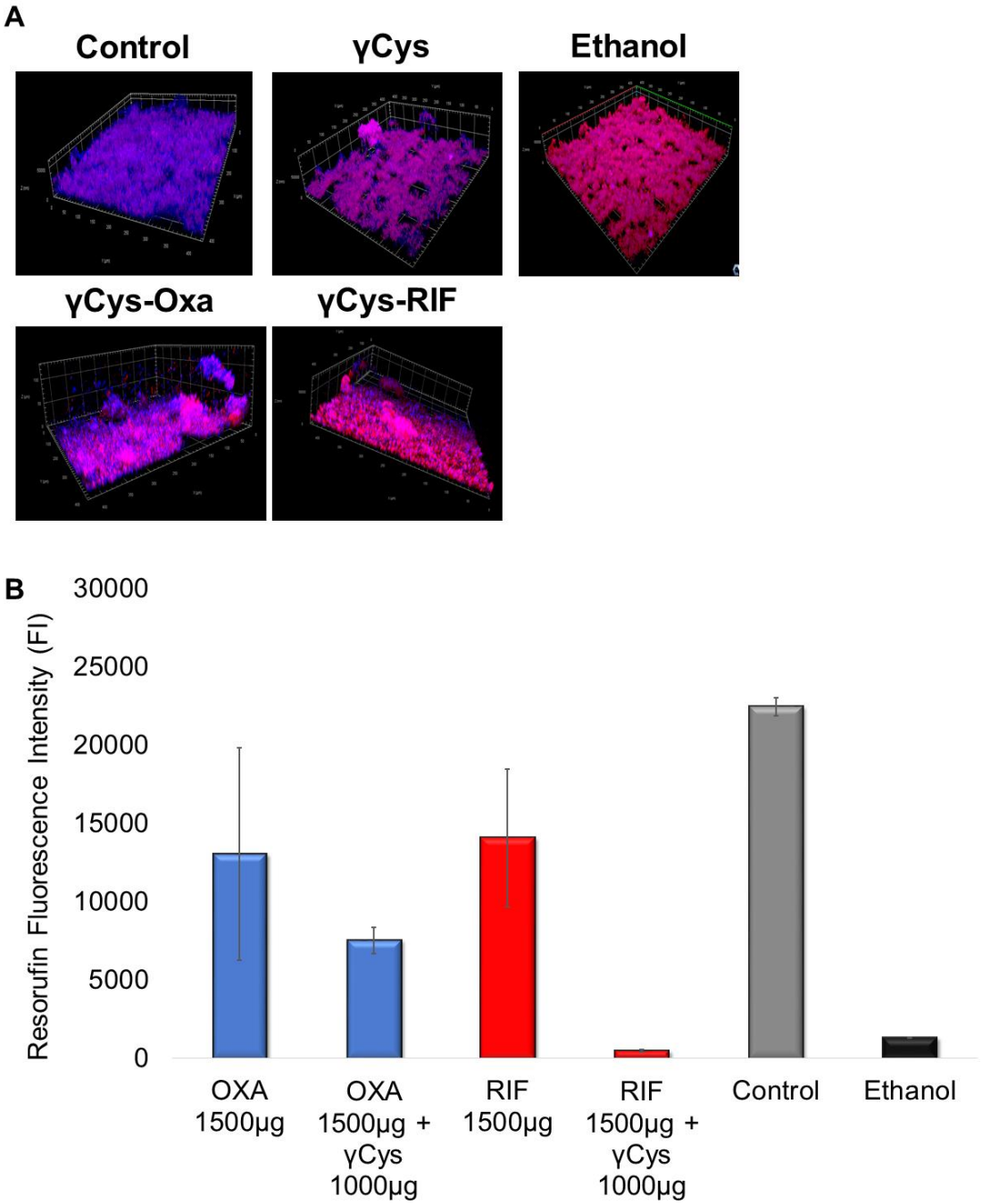

Figure 32. (A) MPM data of *S. epidermidis* biofilms (72 h growth) treated with γCys, media (control), γCys-oxacillin, γCys-rifampicin, or ethanol (99.9%). Blue fluorescence represents bacterial cells (*S. epidermidis-BFP)*, red fluorescence represents membrane-compromised cells (propidium iodide (PI) staining). Images were collected as Z-stacks of 1 µm and shown in the top panel as 3D representations of 70 µm stacks, with field of view 424 x 424 x 70 µm. (B) Biofilm bacterial viability measured via resazurin microtiter-plate assay; fluorescence intensity is represented on the y-axis; decreased fluorescence intensity is equivalent to a decrease in cell viability. Activity of oxacillin (oxa) and rifampicin (rif) were tested against biofilms both alone and complexed with γCys (1:1.5 ratio of γCys to antibiotic in phosphate buffered saline).

5.6 Paper VI

In this paper, photodynamic inactivation (PDI) of biofilms is demonstrated for use in studies of bacterial interactions with light, which could lead to using light to study more complex biofilm dynamics (figure 33) [138].

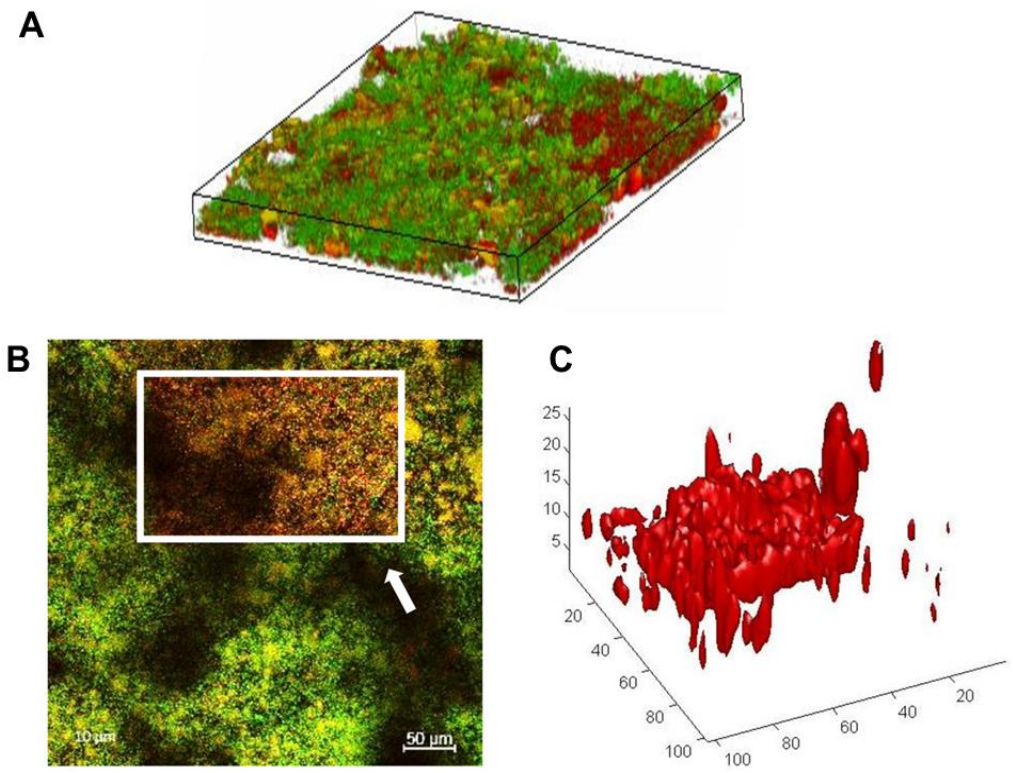

Figure 33. (A) MPM images reconstructed into a 3D representation of a *Staphylococcus epidermidis* biofilm stained with SYTO9 (green, stains cells with intact membranes) and PI (red, stains cells with compromised membranes). Field of view = 424 x 424 x 90 µm. (B) Results of photoinactivation of bacteria with curcumin (λ_{exc} = 950 nm). Boxed area and arrows demonstrate the region of interest irradiated. (C) Image analysis of image shown in B. A thresholding algorithm and 3D surface rendering of the PI-stained cells was implemented to demonstrate the specificity of the irradiated region. Imaged used with permission from [138].

2PE combined with photoinactivation using curcumin is optimized to selectively target and kill bacteria within a chosen region of interest as small as 1 µm. We show that we effectively eliminate chosen bacteria while keeping surrounding environment healthy, using the spatial confinement afforded by 2PE light. This conference proceedings focuses on one aspect of paper VII and is further developed therein.

5.7 Paper VII

Curcumin, and curcumin complexed with HPγCD ("curcumin-CD," described in section 4.3.2), were used for this proof-of-principle investigation in which three primary concerns surrounding the study and treatment of biofilms were addressed.

Penetration depth of drug compounds was determined using techniques described previously but further optimized with the use of inherently fluorescent bacteria, thus providing a control to accurately measure penetration. As seen in figure 34,

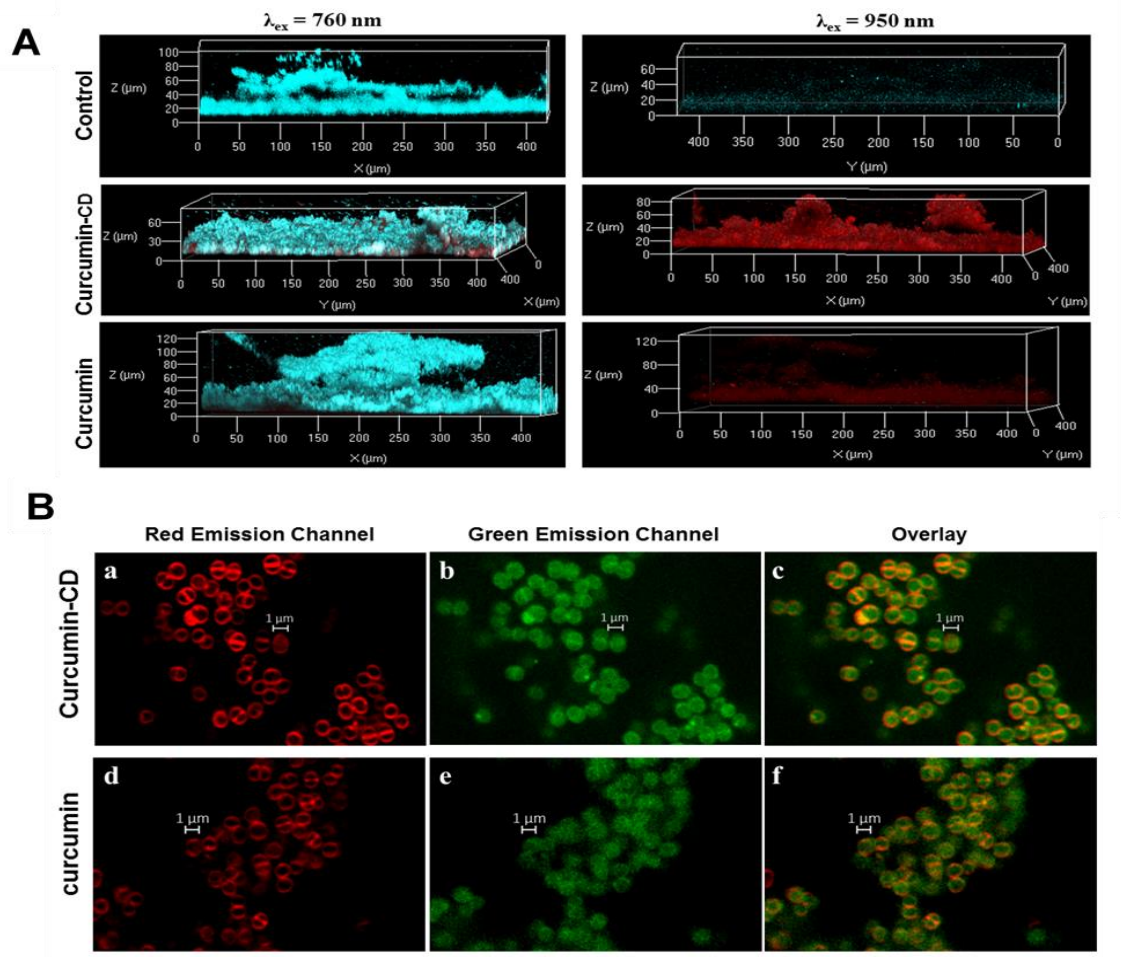

Figure 34. (A) Two photon microscopy images of *S. epidermidis* biofilms (blue) incubated with curcumin in PBS (bottom panel), curcumin-CD complex in PBS (mid panel) and control (top panel). Left column shows emission for bacteria only (388 – 493 nm) and right panel shows emission for curcumin (543 – 678 nm). Two photon excitation (λ = 950 nm) was used. z-stacks range from 60 to 120 µm using a z-step of 1 µm (B) Airyscan microscopy images of *S. epidermidis* biofilms incubated with curcumin or curcumin-CD, shown in the green channel. Bacteria are stained with FM4-64 membrane stain (λex/em = 515/640 nm) shown in the red channel. Emission was collected using a 570-620 nm bandpass with a 570 longpass filter combination and 495-550 nm bandpass filter. Images used with permission from [14].

curcumin complexed with a penetration enhancer appeared to distribute better within the 3D biofilm structure.

Airyscan confocal microscopy revealed the subcellular uptake of the PS (figure 34); both curcumin preparations (curcumin in PBS and curcumin-CD) appear to localize within bacteria cells.

In addition, a non-invasive method for monitoring treatment efficacy was presented. The biofilms were subjected to photodynamic inactivation (PDI) using curcumin and curcumin-CD and viability was measured in real-time using LIVE/DEAD fluorescence staining and 3D imaging and analysis (data in [15]).

Lastly, a novel method for eliminating adherent bacterial cultures was explored by using spatially confined 2PE. 800nm near infrared 2PE could excite the PS in confined regions as small as 1 µm to selectively eliminate bacteria in only the irradiated region while keeping surrounding bacteria healthy, demonstrated in figure 35.

This work presents a novel method for confined killing of bacteria through 2PE photoinactivation through proof-of-principle studies; although more experiments are required to expand and characterize this technique.

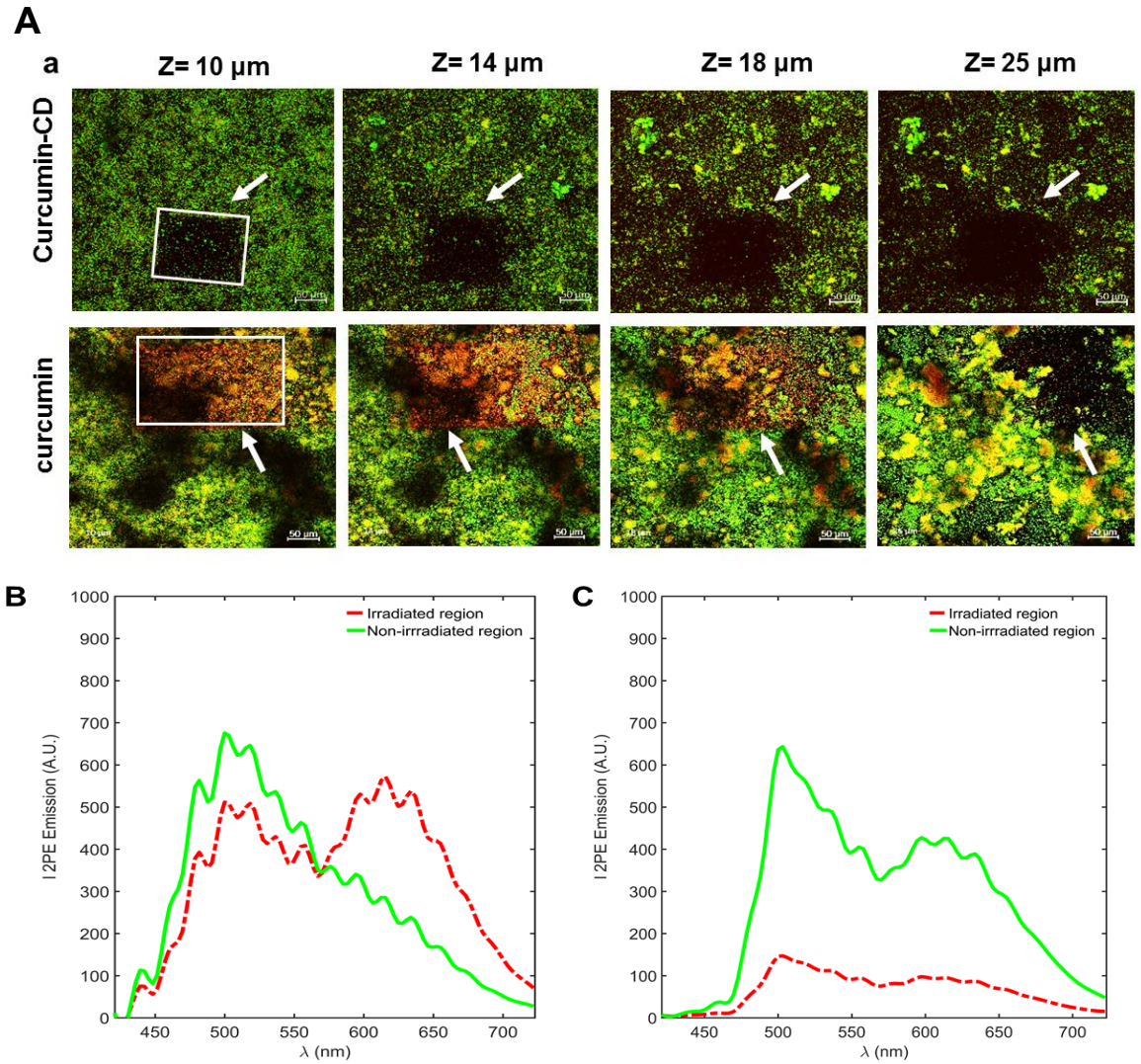

Figure 35. Two photon excited (2PE) photodynamic inactivation (PDI) of *S. epidermidis* with curcumin and curcumin-CD. (A) 2PM images collected in z-stacks of 1 µm, where "z" represents the height from the surface of the biofilm. Biofilms were irradiated with 2PE in the boxed regions only (λ_{exc} = 950 nm). Green fluorescence represents intact cells (stained with SYTO9), red fluorescence represents membrane-compromised cells (stained with propidium iodide). (B) 2PM spectra corresponding to images of PDI with curcumin, spectra represent fluorescent signal from STYO9 and PI stains. (C) 2PM spectra corresponding to images of PDI with curcumin-CD. Images used with permission from [14].

Chapter 6. Concluding Remarks

6 Concluding Remarks

The overall aim of this thesis was to develop biophotonics approaches for studying delivery of photopharmaceuticals and antimicrobials to biological systems. The approaches developed focused on use of MPM, spectral detection, and Airyscan microscopy to monitor delivery and interaction, while the pharmaceutical compounds studied have been based on fluorescent-reporting nanoparticles designed to release toxic species or carry drug compounds through an inclusion complex, as in the case of the cyclodextrins.

The delivery of fluorescent-reporting photoactivatable compounds was explored as a method to monitor potential toxicity in paper I. In addition, the NO photoreleasing system could successfully signal release of NO species, but with minimal toxicity using 2PE compared to 1PE. This opens new possibilities for tracking NO and drug delivery in cells without associated cellular toxicity and adds evidence to the theory of the NO cytotoxicity mechanism [139]. While the results may support the theory that peroxynitrite is required for NO-mediated cytotoxicity, this mechanism is still under debate. Thus, these experiments should be further optimized in experimental design as well as repeated with other systems.

The tissue imaging advantages of MPM were employed to monitor nanoparticle delivery in skin. A novel approach for non-invasively studying drug release in tissue using FRET-reporting nanoparticles was presented. Although, the nanoparticle system did not uphold the requirements necessary for quantifiable FRET studies, the approach holds promise for tracking drug release in tissues, and should be subject to further improvements in future study.

Nanoparticles expressing inherent luminescence were monitored to determine depth of localization in skin using MPM and spectral imaging. It was shown that penetration is size-dependent and the particles accumulate primarily in the skin furrows (up to 25 μm in depth). Spectral characterization of the nano-systems also demonstrated excitation-dependent luminescence; providing evidence of the formation of carbon nanodots within the particles developed, in agreement with earlier reports [140, 141].

An *in vitro* biofilm model of *S. epidermidis* was developed for MPM imaging and inherently fluorescent strains of *S. epidermidis* were created for studies of compound penetration in biofilms, eliminating the need for external staining. With the use of MPM spectral imaging, it was found that positively charged β-cyclodextrins show improved accumulation within the 3D biofilm structure

compared to negative or neutral charged, supported by literature [15]. This method provides details regarding how compounds spatially interact with biofilms. Future studies should focus on the mechanism of interaction of β-cyclodextrin within the biofilm, *i.e.*, investigate if it is sequestered by the EPS or binding to cells, and if this changes the efficacy of drug delivery.

Using these same methods, it was also shown that complexation of curcumin within cyclodextrin enhances distribution of the compound in the biofilm. To answer questions of biofilm viability, a non-invasive diagnostic method for monitoring viability as a 3D "map" was presented using LIVE/DEAD staining with MPM spectral imaging. Quantification of fluorescence signal within each depth layer of biofilms was performed as a complementary approach to traditional biological assays in which the 3D information from biofilm bacteria may be lost.

Curcumin was further monitored for potential toxicity using 2PE PDI, shown for the first time in biofilms. It was demonstrated that curcumin-mediated 2PE PDI can selectively inactivate confined regions as small as 1x1x1 μm within biofilms. This experiment was particularly challenging with the systems used; real-time measurements of LIVE/DEAD stained biofilms was time and cost-intensive, thus to be studied in detail as a potential translational method, a more systematic approach to this experiment should be developed.

Subcellular localization of two different antimicrobial systems, a β-cyclodextrin-curcumin complex and a FITC-tagged γ-cyclodextrin, were determined using high resolution Airyscan confocal microscopy; in one case it was found that the photosensitizer curcumin appears to localize intracellularly in *S. epidermidis* bacteria while γ-cyclodextrin (tagged with FITC for fluorescence tracking) appears to localize primarily surrounding the bacteria, perhaps in the EPS. The results here are an interesting approach to understanding single-bacteria interactions with drug carriers, but complementary biological studies should be added for a better understanding. Additionally, image analysis would expand on the interpretation of these results.

The γCD studied for subcellular localization was also monitored for toxicity. The γCD was loaded with the antibiotics oxacillin and rifampicin and increased efficacy of these two CD-antimicrobial complexed was measured, compared to antibiotic alone, in *S. epidermidis* biofilms, continuing from earlier reports on γCD-antibiotic complexes [134]. It was found that the CD-rifampicin complex significantly decreased bacterial viability compared to free antibiotic. Combined with the results that γCD does not localize subcellularly, this suggests that γCD is able to act as a carrier for antibiotics to be more efficiently delivered to bacteria in the biofilm format. These results are promising for future work in delivering

antibiotics to biofilm infections but should be expanded to further characterize the release mechanism of antibiotics from CDs as well as measuring the system on different bacterial strains and with different antibiotics for a more robust study.

In conclusion, this work resulted in multiple findings of importance in development of pharmaceutical systems and applications of biophotonics techniques to study delivery. But there is more work to be done. Continuing research can be done to strengthen these findings, which will be discussed next in chapter 7.

Chapter 7. Future Outlook

7 Future Outlook

A large portion of the research presented in this thesis, undertaken in the last four years, was focused on method development before any experiments could be performed. Thus, future work could be focused on applying the methods that have been developed in a more systematic and quantitative perspective.

Further evidence could help elucidate the mechanism of peroxynitrite and cell toxicity in paper I. It was shown that NIR 2PE photorelease of NO may not produce the same effect as traditional 1PE photorelease. Although initial studies to demonstrate that peroxynitrite may be the underlying cause of NO toxicity, supported previously in literature [139], this is still at the hypothesis stage and further control studies should be undertaken to answer this. Furthermore, NO release was monitored in direct relation to 1PE excitation; measuring NO release in cells simultaneous to 2PE excitation would be an important complement to this study. This measurement is very challenging *in vitro* but could be done with the use of an additional fluorescence reporter, although the challenge then becomes overlap in signal of a potential NO cross-stain and the test compound (CPA).

In paper II, qualitative monitoring of FRET efficiency did demonstrate proof-of-concept but to quantitatively measure NO release *via* FRET efficiency, a new nanoparticle system should be developed. The 2PE spectrum of the acceptor fluorophore, rhodamine, is broadened compared to 1PE, so creating a FRET pair in which the acceptor would not be excited by the donor excitation wavelength is a challenge. With a better design, accurate quantitative assessments of resonance energy transfer *via* equation 4 in section 2.1.6 could be performed and potentially connected to NO release.

Further experimentation to elucidate the mechanistic reasoning that positively charged cyclodextrins interact better with gram-positive biofilms, as shown in paper IV and paper V, should be performed, such as investigations into the interaction of CDs and CD-antibiotic complexes with the EPS, biofilm matrix, and effects of CDs when loaded with a wider range of antibiotics and applied against more challenging bacterial systems such as *Staphylococcus aureus* and gram-negative bacteria. In addition, paper V could be complimented with further studies such as measuring the inherent antibiotic effect of γCD; this was monitored *via* MPM imaging but should be measured with a standard biological assay, and monitoring the difference in biofilm viability in different z levels of

the biofilm when treated with free antibiotic compared to γCD-complexed antibiotic.

In papers VI and VII, spatially confined photodynamic inactivation of bacteria with 2PE was performed for the first time. This study could be complimented with investigations of the photosensitizer mode of action and toxicity to bacteria monitored with comparative biological assays. In addition, feasibility in a translational setting is an issue that could be addressed by considering the most recent developments in clinical NIR light delivery to complex disease target sites. The biggest challenge with this study was monitoring the viability of the biofilm in a very confined region. The goal was to demonstrate that bacteria were targeted in a very small area, in 3D, but to do this, viability staining was used combined with sensitive imaging techniques. To reproduce these results was very cost- and time-consuming, thus to make this technique widely available would require further optimization.

In all, this work contributes to the field of biophotonics by developing and applying methods for studying the delivery of new photopharmaceuticals and antimicrobials to a range of biological systems. It has been shown here that the interaction of light with biology can provide information on drug delivery and localization, and structural integrity of complicated tissue and biological matter, and the information collected was used to characterize novel photopharmaceutical and antimicrobial compounds. My understanding of the future of the field is that these techniques will be moved towards more quantitative measurements. Imaging and spectral detection are useful compliments in most *in vitro* and *in vivo* studies today, but to use this information to measure physiological indicators in-clinic seems to be the next step. This is seen in current efforts to move forward in *e.g.*, optical clinical diagnostics [142] and fluorescence-guided surgery [143], or in-clinic theragnostic approaches of light-emitting and light-excited pharmaceutics [2]. In terms of bacterial infections, quickly diagnosing and monitoring infection, with 3D assessment in the body, could provide major improvements in treatment [144]. In addition, the path forward of photoantimicrobials applied to antibacterial resistant infections might also be focused on optical development, *i.e.* clinical light technology, in tandem with pharmaceutical and biophotonics techniques, to produce translational research in this relatively new field [145, 146].

Chapter 8. Acknowledgments

8 Acknowledgments

First, I would like to thank my advisor, Marica Ericson, for her expert guidance throughout these four years. You were always available for discussion, always positive, and enabled me every day to grow as a researcher. Thank you!

Many thanks to my co-advisor Anne Farewell who has been of great help with biological knowledge and feedback, discussion, and consistent support.

There are many people without whom this work would not have been possible: former and current members of the biomedical photonics group: Vladimir Kirejev, thank you for patiently answering my millions of questions both during and after your time in the group. Johan Borglin and Danni Wang, thanks for your work in the laser lab and thank you for being overall great people to work with. Jeemol and Monika, I'm glad I got to work with you guys for this brief period – thanks for the talks, laughs, input, and cover-judging. Looking forward to watching your research progress. I had the pleasure of working with a few talented and engaged students throughout these years: Friederike Gerken aided in cell experiments and was a wonderful addition to the group, Joakim Zaar's LabView skills were a huge help in the first paper, Owens Uwangue (Anne Farewell lab) expertly performed the biological experiments in paper 5, and Rasmus Björk, Vicotria Tran, and Melina Möchel all contributed to a great group environment.

The last paper would not have been finished without the work of Fabrice Graf. Fabrice, thank you for making bacteria blue.

To all in the CyclonHIT project, thank you for the shared travels, stories, and collaboration. Special thanks to Marco Agnes, Sabrina Valetti, Gabor Benkovics, and Milo Malanga from the CyclonHIT group for your great collaboration and sharing your cyclodextrins and particles.

Many thanks to Maria Pihl and Mats Hulander of Martin Andersson's group (Chalmers University of Technology) for your guidance and use of the bacteria lab, as well as for the donation of my first bacteria strain.

Thank you to Carolina Tängemo, Julia Fernandez-Rodriguez, and Maria Smedh at the Center for Cellular Imaging for sharing your knowledge of all things microscopy!

Financial support and research funding for this research was provided by Marie Curie Program # 608407 CYCLONHIT (FP7-PEOPLE-ITN-2013) and the Swedish Research Council (621-2011-5189).

8. Acknowledgements

Finally, my biggest thanks of all to my friends and family: Nana and papa – how lucky I am to have your support. I wouldn't have made it here without you. Mom – thank you for being you! Dad and Sally, thank you for your stability and positivity. To my big brother, my forever idol. Trevor and Ashley, what would I have done if I hadn't met you guys? Thank you for being my science library family and forever horseman. Christina, thank you for being a constant source of sunshine here in rainy Gothenburg. Sophie, celebrating with you is the best end to this work I could have imagined. and to Marco, for your patience, kindness, encouragement, and travel booking skills. You helped make these last few months of writing not only doable, but enjoyable.

Chapter 9. References

8 References

1. Nurunnabi, M., et al., *Photoluminescent graphene nanoparticles for cancer phototherapy and imaging.* ACS Applied Materials and Interfaces, 2014. **6**(15): p. 12413-12421.
2. Ryu, J.H., et al., *Tumor-targeting multi-functional nanoparticles for theragnosis: New paradigm for cancer therapy.* Advanced Drug Delivery Reviews, 2012. **64**(13): p. 1447-1458.
3. Benninger, R.K.P. and D.W. Piston, *Two-Photon Excitation Microscopy for the Study of Living Cells and Tissues.* Current protocols in cell biology / editorial board, Juan S. Bonifacino ... [et al.], 2013. **0 4**: p. Unit-4.1124.
4. Helmchen, F. and W. Denk, *Deep tissue two-photon microscopy.* Nature Methods, 2005. **2**(12): p. 932-940.
5. Konig, K., *Multiphoton microscopy in life sciences.* Journal of Microscopy, 2000. **200**(2): p. 83-104.
6. Rai, P., et al., *Development and applications of photo-triggered theranostic agents.* Advanced Drug Delivery Reviews, 2010. **62**(11): p. 1094-1124.
7. Dougherty, T.J., et al., *Photodynamic therapy.* Journal of the National Cancer Institute, 1998. **90**(12): p. 889-905.
8. Goldberg, M. and I. Gomez-Orellana, *Challenges for the oral delivery of macromolecules.* Nature Reviews Drug Discovery, 2003. **2**: p. 289.
9. Organization, W.H., *Antimicrobial resistance: global report on surveillance*. 2014: World Health Organization.
10. Hamblin, M.R. and T. Hasan, *Photodynamic therapy: A new antimicrobial approach to infectious disease?* Photochemical and Photobiological Sciences, 2004. **3**(5): p. 436-450.
11. Wainwright, M., *Photodynamic antimicrobial chemotherapy (PACT).* Journal of Antimicrobial Chemotherapy, 1998. **42**(1): p. 13-28.
12. Conte, C., et al., *Monitoring the release of a NO photodonor from polymer nanoparticles via Forster resonance energy transfer and two-photon fluorescence imaging.* Journal of Materials Chemistry B, 2018. **6**(2): p. 249-256.
13. Thomsen, H., Marino, N., Conoci, S., Sortino, S., Ericson, M.B. , *Confined photo-release of nitric oxide with simultaneous two-photon fluorescence tracking in a cellular system.* Scientific Reports, 2018.
14. Thomsen H., G., F.E., Farewell, A., Ericson, M.B. , *Exploring photoinactivation of microbial biofilms using laser scanning microscopy and confined two-photon excitation.* Journal of Biophotonics, 2018.
15. Thomsen, H., et al., *Delivery of cyclodextrin polymers to bacterial biofilms — An exploratory study using rhodamine labelled cyclodextrins and multiphoton microscopy.* International Journal of Pharmaceutics.
16. Marcu, L., et al., *Biophotonics: the big picture*. J Biomed Opt, 2017. **23**(2): p. 1-7.
17. Lakowicz, J.R., *Principles of Fluorescence Spectroscopy*. 2006, New York, New York: Springer Science + Business Media. 954.
18. Monici, M., *Cell and tissue autofluorescence research and diagnostic applications.* Biotechnology annual review, 2005. **11**: p. 227-256.
19. Andersson, H., et al., *Autofluorescence of living cells.* Journal of microscopy, 1998. **191**: p. 1-7.
20. Hawe, A., M. Sutter, and W. Jiskoot, *Extrinsic fluorescent dyes as tools for protein characterization.* Pharmaceutical research, 2008. **25**(7): p. 1487-1499.
21. Neyfakh, A.A., *Use of fluorescent dyes as molecular probes for the study of multidrug resistance.* Experimental cell research, 1988. **174**(1): p. 168-176.
22. Jakobs, S., et al., *EGFP and DsRed expressing cultures of Escherichia coli imaged by confocal, two-photon and fluorescence lifetime microscopy.* FEBS letters, 2000. **479**(3): p. 131-135.
23. Tsien, R.Y., *The green fluorescent protein*. 1998, Annual Reviews 4139 El Camino Way, PO Box 10139, Palo Alto, CA 94303-0139, USA.

24. Boulos, L., et al., *LIVE/DEAD® BacLight™: application of a new rapid staining method for direct enumeration of viable and total bacteria in drinking water.* Journal of microbiological Methods, 1999. **37**(1): p. 77-86.
25. Bolte, S., et al., *FM-dyes as experimental probes for dissecting vesicle trafficking in living plant cells.* Journal of microscopy, 2004. **214**(2): p. 159-173.
26. Lichtman, J.W. and J.-A. Conchello, *Fluorescence microscopy.* Nature Methods, 2005. **2**: p. 910.
27. Shotton, D.M., *Confocal scanning optical microscopy and its applications for biological specimens.* Journal of Cell Science, 1989. **94**(2): p. 175-206.
28. White, J., W. Amos, and M. Fordham, *An evaluation of confocal versus conventional imaging of biological structures by fluorescence light microscopy.* The Journal of cell biology, 1987. **105**(1): p. 41-48.
29. Conchello, J.A. and J.W. Lichtman, *Optical sectioning microscopy.* Nature Methods, 2005. **2**(12): p. 920-931.
30. Paddock, S.W., *Principles and practices of laser scanning confocal microscopy.* Molecular Biotechnology, 2000. **16**(2): p. 127-149.
31. Kino, G.S. and T.R. Corle, *Confocal scanning optical microscopy and related imaging systems*. 1996: Academic Press.
32. Cox, G., et al., *3-dimensional imaging of collagen using second harmonic generation.* Journal of structural biology, 2003. **141**(1): p. 53-62.
33. Rowlands, C.J., et al., *Wide-field three-photon excitation in biological samples.* Light: Science & Applications, 2017. **6**(5): p. e16255.
34. Diaspro, A., et al., *Multi-photon excitation microscopy.* BioMedical Engineering Online, 2006. **5**.
35. Xu, C., et al., *Multiphoton fluorescence excitation: New spectral windows for biological nonlinear microscopy.* Proceedings of the National Academy of Sciences of the United States of America, 1996. **93**(20): p. 10763-10768.
36. Denk, W., *Two-photon excitation in functional biological imaging.* Journal of Biomedical Optics, 1996. **1**(3): p. 296-304.
37. Piston, D.W., *Imaging living cells and tissues by two-photon excitation microscopy.* Trends in Cell Biology, 1999. **9**(2): p. 66-69.
38. So, P.T.C., et al., *Two-photon excitation fluorescence microscopy*, in *Annual Review of Biomedical Engineering*. 2000. p. 399-429.
39. Zipfel, W.R., R.M. Williams, and W.W. Webb, *Nonlinear magic: Multiphoton microscopy in the biosciences.* Nature Biotechnology, 2003. **21**(11): p. 1369-1377.
40. Denk, W., J. Strickler, and W. Webb, *Two-photon laser scanning fluorescence microscopy.* Science, 1990. **248**(4951): p. 73-76.
41. Hecht, E., *Optics*. 2016: Pearson Education.
42. Kobayashi, H., et al., *New Strategies for Fluorescent Probe Design in Medical Diagnostic Imaging.* Chemical Reviews, 2010. **110**(5): p. 2620-2640.
43. Hsu, L.L., et al. *Two-photon 3-D mapping of ex vivo human skin endogenous fluorescence species based on fluorescence emission spectra*. 2005. SPIE.
44. Theer, P., M.T. Hasan, and W. Denk, *Two-photon imaging to a depth of 1000 µm in living brains by use of a Ti: Al 2 O 3 regenerative amplifier.* Optics letters, 2003. **28**(12): p. 1022-1024.
45. Bender, J., et al., *Lipid cubic phases in topical drug delivery: Visualization of skin distribution using two-photon microscopy.* Journal of Controlled Release, 2008. **129**(3): p. 163-169.
46. Ericson, M.B., et al., *Two-photon laser-scanning fluorescence microscopy applied for studies of human skin.* Journal of Biophotonics, 2008. **1**(4): p. 320-330.
47. Piston, D.W., B.R. Masters, and W.W. Webb, *Three-dimensionally resolved NAD(P)H cellular metabolic redox imaging of the in situ cornea with two-photon excitation laser scanning microscopy.* Journal of Microscopy, 1995. **178**(1): p. 20-27.
48. De Giorgi, V., et al., *Combined non-linear laser imaging (two-photon excitation fluorescence microscopy, fluorescence lifetime imaging microscopy, multispectral multiphoton*

microscopy) in cutaneous tumours: First experiences. Journal of the European Academy of Dermatology and Venereology, 2009. **23**(3): p. 314-316.
49. Huang, B., M. Bates, and X. Zhuang, *Super resolution fluorescence microscopy.* Annual review of biochemistry, 2009. **78**: p. 993-1016.
50. Gustafsson, M.G.L., *Surpassing the lateral resolution limit by a factor of two using structured illumination microscopy.* Journal of Microscopy, 2000. **198**(2): p. 82-87.
51. Schermelleh, L., R. Heintzmann, and H. Leonhardt, *A guide to super-resolution fluorescence microscopy.* Journal of Cell Biology, 2010. **190**(2): p. 165-175.
52. Huang, B., M. Bates, and X. Zhuang, *Super-Resolution Fluorescence Microscopy.* Annual Review of Biochemistry, 2009. **78**(1): p. 993-1016.
53. Diaspro, A., *Confocal and two-photon microscopy: foundations, applications and advances.* Confocal and Two-Photon Microscopy: Foundations, Applications and Advances, by Alberto Diaspro (Editor), pp. 576. ISBN 0-471-40920-0. Wiley-VCH, November 2001., 2001: p. 576.
54. Huff, J., *The Airyscan detector from ZEISS: confocal imaging with improved signal-to-noise ratio and super-resolution.* Nature Methods, 2015. **12**.
55. Jares-Erijman, E.A. and T.M. Jovin, *FRET imaging.* Nature Biotechnology, 2003. **21**(11): p. 1387-1395.
56. Wu, P. and L. Brand, *Resonance energy transfer: Methods and applications.* Analytical Biochemistry, 1994. **218**(1): p. 1-13.
57. Ishikawa-Ankerhold, H.C., R. Ankerhold, and G.P.C. Drummen, *Advanced fluorescence microscopy techniques-FRAP, FLIP, FLAP, FRET and FLIM.* Molecules, 2012. **17**(4): p. 4047-4132.
58. Ventola, C.L., *The Antibiotic Resistance Crisis: Part 1: Causes and Threats.* Pharmacy and Therapeutics, 2015. **40**(4): p. 277-283.
59. Stewart, P.S. and J. William Costerton, *Antibiotic resistance of bacteria in biofilms.* The Lancet, 2001. **358**(9276): p. 135-138.
60. Davies, J. and D. Davies, *Origins and Evolution of Antibiotic Resistance.* Microbiology and Molecular Biology Reviews, 2010. **74**(3): p. 417-433.
61. Hawkey, P.M., *The origins and molecular basis of antibiotic resistance.* BMJ : British Medical Journal, 1998. **317**(7159): p. 657-660.
62. Costerton, J.W., et al., *Microbial biofilms*, in *Annual Review of Microbiology*. 1995. p. 711-745.
63. Costerton, J.W., P.S. Stewart, and E.P. Greenberg, *Bacterial biofilms: a common cause of persistent infections.* Science, 1999. **284**(5418): p. 1318-22.
64. Donlan, R.M., *Biofilms: Microbial life on surfaces.* Emerging Infectious Diseases, 2002. **8**(9): p. 881-890.
65. Flemming, H.-C., T.R. Neu, and D.J. Wozniak, *The EPS matrix: the "house of biofilm cells".* Journal of bacteriology, 2007. **189**(22): p. 7945-7947.
66. Donlan, R.M., *Biofilms: microbial life on surfaces.* Emerging infectious diseases, 2002. **8**(9): p. 881.
67. Sutherland, I.W., *Biofilm exopolysaccharides: a strong and sticky framework.* Microbiology, 2001. **147**(1): p. 3-9.
68. Martin, C., et al., *Strategies for antimicrobial drug delivery to biofilm.* Curr Pharm Des, 2015. **21**(1): p. 43-66.
69. Stewart, P.S. and J.W. Costerton, *Antibiotic resistance of bacteria in biofilms.* The lancet, 2001. **358**(9276): p. 135-138.
70. Anderl, J.N., M.J. Franklin, and P.S. Stewart, *Role of Antibiotic Penetration Limitation in Klebsiella pneumoniae Biofilm Resistance to Ampicillin and Ciprofloxacin.* Antimicrobial Agents and Chemotherapy, 2000. **44**(7): p. 1818-1824.
71. Donlan, R.M. and J.W. Costerton, *Biofilms: Survival mechanisms of clinically relevant microorganisms.* Clinical Microbiology Reviews, 2002. **15**(2): p. 167-193.
72. James, G.A., et al., *Biofilms in chronic wounds.* Wound Repair and Regeneration, 2008. **16**(1): p. 37-44.
73. Otto, M., *Staphylococcus epidermidis – the "accidental" pathogen.* Nature reviews. Microbiology, 2009. **7**(8): p. 555-567.

74. Bryers, J.D., *Medical Biofilms.* Biotechnology and bioengineering, 2008. **100**(1): p. 1-18.
75. Mack, D., *Molecular mechanisms of Staphylococcus epidermidis biofilm formation.* Journal of Hospital Infection, 1999. **43**(SUPPL. 1).
76. O'Gara, J.P. and H. Humphreys, *Staphylococcus epidermidis biofilms: Importance and implications.* Journal of Medical Microbiology, 2001. **50**(7): p. 582-587.
77. Spikes, J.D., *The origin and meaning of the term "photodynamic" (as used in "photodynamic therapy", for example).* Journal of Photochemistry and Photobiology B: Biology, 1991. **9**(3): p. 369-371.
78. Henderson, B.W. and T.J. Dougherty, *How does photodynamic therapy work?* Photochemistry and Photobiology, 1992. **55**(1): p. 145-157.
79. Dolmans, D.E.J.G.J., D. Fukumura, and R.K. Jain, *Photodynamic therapy for cancer.* Nature Reviews Cancer, 2003. **3**(5): p. 380-387.
80. Abrahamse, H. and Michael R. Hamblin, *New photosensitizers for photodynamic therapy.* Biochemical Journal, 2016. **473**(4): p. 347-364.
81. Klán, P. and J. Wirz, *Photochemistry of organic compounds: from concepts to practice*. 2009: John Wiley & Sons.
82. Hamblin, M.R. and T. Hasan, *Photodynamic therapy: a new antimicrobial approach to infectious disease?* Photochemical & photobiological sciences : Official journal of the European Photochemistry Association and the European Society for Photobiology, 2004. **3**(5): p. 436-450.
83. HSIEH, C.-Y., *Phase I clinical trial of curcumin, a chemopreventive agent, in patients with high-risk or pre-malignant lesions.* Anticancer research, 2001. **21**: p. 2895-2900.
84. Sharma, R.A., et al., *Phase I clinical trial of oral curcumin: biomarkers of systemic activity and compliance.* Clinical Cancer Research, 2004. **10**(20): p. 6847-6854.
85. Jurenka, J.S., *Anti-inflammatory properties of curcumin, a major constituent of Curcuma longa: a review of preclinical and clinical research.* Alternative medicine review, 2009. **14**(2).
86. Araújo, N.C., et al., *Overall-mouth disinfection by photodynamic therapy using curcumin.* Photomedicine and Laser Surgery, 2012. **30**(2): p. 96-101.
87. Haukvik, T., et al., *Photokilling of bacteria by curcumin in different aqueous preparations. Studies on curcumin and curcuminoids XXXVII.* Pharmazie, 2009. **64**(10): p. 666-673.
88. Haukvik, T., et al., *Photokilling of bacteria by curcumin in selected polyethylene glycol 400 (PEG 400) preparations: Studies on curcumin and curcuminoids, XLI.* Pharmazie, 2010. **65**(8): p. 600-606.
89. Hegge, A.B., et al., *Photoinactivation of Staphylococcus epidermidis biofilms and suspensions by the hydrophobic photosensitizer curcumin - Effect of selected nanocarrier: Studies on curcumin and curcuminoides XLVII.* European Journal of Pharmaceutical Sciences, 2012. **47**(1): p. 65-74.
90. Leite, D.P.V., et al., *Effects of photodynamic therapy with blue light and curcumin as mouth rinse for oral disinfection: A randomized controlled trial.* Photomedicine and Laser Surgery, 2014. **32**(11): p. 627-632.
91. Mahdi, Z., et al., *Lethal effect of blue light-activated hydrogen peroxide, curcumin and erythrosine as potential oral photosensitizers on the viability of porphyromonas gingivalis and fusobacterium nucleatum.* Laser Therapy, 2015. **24**(2): p. 103-111.
92. Gao, D., et al., *Nanoparticles for two-photon photodynamic therapy in living cells.* Nano letters, 2006. **6**(11): p. 2383-2386.
93. Wilson, M. and C. Yianni, *Killing of methicillin-resistant Staphylococcus aureus by low-power laser light.* Journal of medical microbiology, 1995. **42**(1): p. 62-66.
94. Allison, R.R., et al., *Photosensitizers in clinical PDT.* Photodiagnosis and Photodynamic Therapy, 2004. **1**(1): p. 27-42.
95. Dolmans, D.E., D. Fukumura, and R.K. Jain, *Photodynamic therapy for cancer.* Nature reviews cancer, 2003. **3**(5): p. 380.
96. Castano, A.P., T.N. Demidova, and M.R. Hamblin, *Mechanisms in photodynamic therapy: part one—photosensitizers, photochemistry and cellular localization.* Photodiagnosis and Photodynamic Therapy, 2004. **1**(4): p. 279-293.

97. Chignell, C.F., et al., *SPECTRAL AND PHOTOCHEMICAL PROPERTIES OF CURCUMIN.* Photochemistry and Photobiology, 1994. **59**(3): p. 295-302.
98. Tønnesen, H.H., M. Másson, and T. Loftsson, *Studies of curcumin and curcuminoids. XXVII. Cyclodextrin complexation: solubility, chemical and photochemical stability.* International Journal of Pharmaceutics, 2002. **244**(1–2): p. 127-135.
99. Dahl, T.A., et al., *Photocytotoxicity of curcumin.* Photochem Photobiol, 1994. **59**(3): p. 290-4.
100. Chen, Q., et al., *Curcumin induces apoptosis in human lung adenocarcinoma A549 cells through a reactive oxygen species-dependent mitochondrial signaling pathway.* Oncology Reports, 2010. **23**(2): p. 397-403.
101. Cheng, A.L., et al., *Phase I clinical trial of curcumin, a chemopreventive agent, in patients with high-risk or pre-malignant lesions.* Anticancer Res, 2001. **21**(4b): p. 2895-900.
102. Paschoal, M.A., et al., *Longitudinal effect of curcumin-photodynamic antimicrobial chemotherapy in adolescents during fixed orthodontic treatment: a single-blind randomized clinical trial study.* Lasers in Medical Science, 2015. **30**(8): p. 2059-2065.
103. Kumar, A., et al., *Two-photon fluorescence properties of curcumin as a biocompatible marker for confocal imaging.* Applied Physics Letters, 2012. **100**(20): p. 203701.
104. Hou, Y., et al., *Targeting nitric oxide to cancer cells: cytotoxicity studies of glyco-S-nitrosothiols.* Bioorg Med Chem Lett, 1999. **9**(15): p. 2255-8.
105. Coleman, J.W., *Nitric oxide in immunity and inflammation.* International Immunopharmacology, 2001. **1**(8): p. 1397-1406.
106. Fang, F.C., *Mechanisms of nitric oxide-related antimicrobial activity.* Journal of Clinical Investigation, 1997. **99**(12): p. 2818-2825.
107. Fraix, A., N. Kandoth, and S. Sortino, *Nitric oxide photoreleasing nanoconstructs with multiple photofunctionalities*, in *Photochemistry*. 2013. p. 302-318.
108. Hirst, D. and T. Robson, *Targeting nitric oxide for cancer therapy.* Journal of Pharmacy and Pharmacology, 2007. **59**(1): p. 3-13.
109. Xu, L., K. Xie, and I.J. Fidler, *Therapy of human ovarian cancer by transfection with the murine interferon beta gene: role of macrophage-inducible nitric oxide synthase.* Hum Gene Ther, 1998. **9**(18): p. 2699-708.
110. Lala, P.K. and C. Chakraborty, *Role of nitric oxide in carcinogenesis and tumour progression.* Lancet Oncology, 2001. **2**(3): p. 149-156.
111. Mocellin, S., V. Bronte, and D. Nitti, *Nitric oxide, a double edged sword in cancer biology: Searching for therapeutic opportunities.* Medicinal Research Reviews, 2007. **27**(3): p. 317-352.
112. Rose, M.J. and P.K. Mascharak, *Fiat Lux: selective delivery of high flux of nitric oxide (NO) to biological targets using photoactive metal nitrosyls.* Current Opinion in Chemical Biology, 2008. **12**(2): p. 238-244.
113. Rose, M.J., et al., *Sensitization of ruthenium nitrosyls to visible light via direct coordination of the dye resorufin: Trackable NO donors for light-triggered NO delivery to cellular targets.* Journal of the American Chemical Society, 2008. **130**(27): p. 8834-8846.
114. Sortino, S., *Light-controlled nitric oxide delivering molecular assemblies.* Chemical Society Reviews, 2010. **39**(8): p. 2903-2913.
115. Rapozzi, V., et al., *Nitric oxide-mediated activity in anti-cancer photodynamic therapy.* Nitric Oxide - Biology and Chemistry, 2013. **30**: p. 26-35.
116. Dutta, R.C., *Drug carriers in pharmaceutical design: promises and progress.* Curr Pharm Des, 2007. **13**(7): p. 761-9.
117. Montagna, W., *The structure and function of skin*. 2012: Elsevier.
118. Elias, P.M. and D.S. Friend, *The permeability barrier in mammalian epidermis.* The Journal of cell biology, 1975. **65**(1): p. 180-191.
119. Prausnitz, M.R. and R. Langer, *Transdermal drug delivery.* Nature Biotechnology, 2008. **26**: p. 1261.
120. Bronaugh, R.L. and R.F. Stewart, *Methods for in vitro percutaneous absorption studies IV: The flow-through diffusion cell.* Journal of pharmaceutical sciences, 1985. **74**(1): p. 64-67.

121. Bronaugh, R.L., R.F. Stewart, and M. Simon, *Methods for in vitro percutaneous absorption studies VII: use of excised human skin.* Journal of pharmaceutical sciences, 1986. **75**(11): p. 1094-1097.
122. Kuchler, S., K. Struver, and W. Friess, *Reconstructed skin models as emerging tools for drug absorption studies.* Expert Opin Drug Metab Toxicol, 2013. **9**(10): p. 1255-63.
123. Lipinski, C., *Poor aqueous solubility—an industry wide problem in drug discovery.* Am Pharm Rev, 2002. **5**(3): p. 82-85.
124. Benson, H.A., *Transdermal drug delivery: penetration enhancement techniques.* Current drug delivery, 2005. **2**(1): p. 23-33.
125. Rajendran, L., H.-J. Knölker, and K. Simons, *Subcellular targeting strategies for drug design and delivery.* Nature reviews Drug discovery, 2010. **9**(1): p. 29.
126. Davis, M.E. and M.E. Brewster, *Cyclodextrin-based pharmaceutics: Past, present and future.* Nature Reviews Drug Discovery, 2004. **3**(12): p. 1023-1035.
127. Hirayama, F. and K. Uekama, *Cyclodextrin-based controlled drug release system.* Advanced Drug Delivery Reviews, 1999. **36**(1): p. 125-141.
128. Challa, R., et al., *Cyclodextrins in drug delivery: an updated review.* AAPS PharmSciTech [electronic resource]. 2005. **6**(2).
129. Loftsson, T. and D. Duchene, *Cyclodextrins and their pharmaceutical applications.* Int J Pharm, 2007. **329**(1-2): p. 1-11.
130. Zhou, J. and H. Ritter, *Cyclodextrin functionalized polymers as drug delivery systems.* Polymer Chemistry, 2010. **1**(10): p. 1552-1559.
131. Vittorino, E., E. Cicciarella, and S. Sortino, *A "dual-function" photocage releasing nitric oxide and an anthrylmethyl cation with a single wavelength light.* Chemistry - A European Journal, 2009. **15**(28): p. 6802-6806.
132. Malanga, M., et al., *New synthetic strategies for xanthene-dye-appended cyclodextrins.* Beilstein J Org Chem, 2016. **12**: p. 537-48.
133. Malanga, M., L. Jicsinszky, and É. Fenyvesi, *Rhodamine-labeled cyclodextrin derivatives.* Journal of Drug Delivery Science and Technology, 2012. **22**(3): p. 260-265.
134. Agnes, M., et al., *Designed positively charged cyclodextrin hosts with enhanced binding of penicillins as carriers for the delivery of antibiotics: The case of oxacillin.* International Journal of Pharmaceutics, 2017. **531**(2): p. 480-491.
135. L., C.M., et al., *PHOTOSENSITIZED PRODUCTION OF SUPEROXIDE ANION BY MONOCHROMATIC (290–405 nm) ULTRAVIOLET IRRADIATION OF NADH and NADPH COENZYMES.* Photochemistry and Photobiology, 1985. **42**(2): p. 125-128.
136. Pacher, P., J.S. Beckman, and L. Liaudet, *Nitric oxide and peroxynitrite in health and disease.* Physiol Rev, 2007. **87**(1): p. 315-424.
137. van Dam, B., et al., *Excitation-Dependent Photoluminescence from Single-Carbon Dots.* Small, 2017. **13**(48).
138. Thomsen, H., James, Jeemol., Farewell, Anne., Ericson, Marica B., *Spatially confined photoinactivation of bacteria: towards novel tools for detailed mechanistic studies.* Proc. SPIE 10498, Multiphoton Microscopy in the Biomedical Sciences XVIII, 2018(1049825).
139. Pacher, P., J.S. Beckman, and L. Liaudet, *Nitric oxide and peroxynitrite in health and disease.* Physiological Reviews, 2007. **87**(1): p. 315-424.
140. Chen, H., et al., *Label-free luminescent mesoporous silica nanoparticles for imaging and drug delivery.* Theranostics, 2013. **3**(9): p. 650-7.
141. Valetti, S., et al., *Mesoporous silica particles as a lipophilic drug vehicle investigated by fluorescence lifetime imaging.* Journal of Materials Chemistry B, 2017. **5**(17): p. 3201-3211.
142. Smith, B.R. and S.S. Gambhir, *Nanomaterials for in Vivo Imaging.* Chemical Reviews, 2017. **117**(3): p. 901-986.
143. Low, P.S., S. Singhal, and M. Srinivasarao, *Fluorescence-guided surgery of cancer: applications, tools and perspectives.* Current Opinion in Chemical Biology, 2018. **45**: p. 64-72.
144. Jain, S.K., *The Promise of Molecular Imaging in the Study and Treatment of Infectious Diseases.* Molecular Imaging and Biology, 2017. **19**(3): p. 341-347.

145. Wainwright, M., et al., *Photoantimicrobials—are we afraid of the light?* The Lancet Infectious Diseases, 2017. **17**(2): p. e49-e55.
146. Yun, S.H. and S.J.J. Kwok, *Light in diagnosis, therapy and surgery.* Nature Biomedical Engineering, 2017. **1**(1).